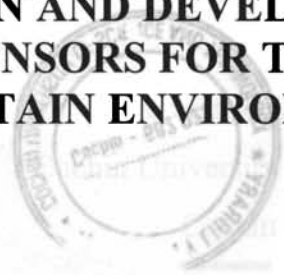


DESIGN AND DEVELOPMENT OF FIBER OPTIC SENSORS FOR TRACE DETECTION OF CERTAIN ENVIRONMENTAL POLLUTANTS



P. Suresh Kumar
International School of Photonics
Cochin University of Science and Technology
Cochin – 682 022, India

Ph D Thesis submitted to Cochin University of Science and Technology in
partial fulfillment of the requirements for the award of the Degree of
Doctor of Philosophy

October 2003

G9051

**Design and Development of Fiber Optic Sensors for Trace Detection of
Certain Environmental Pollutants
Ph D thesis in the field of Photonics**

Author

P. Suresh Kumar
International School of Photonics
Cochin University of Science and Technology
Cochin – 682 022
India
E mail: sureshmec@cusat.ac.in; sureshmec@email.com



Research Advisor

Dr. P. Radhakrishnan
Professor & Director
International School of Photonics
Cochin University of Science and Technology
Cochin – 682 022
India
E mail: radhak@cusat.ac.in

**International School of Photonics, Cochin University of Science and Technology
Cochin – 682 022, India
URL: www.photonics.cusat.edu**

October 2003



International School of Photonics
Cochin University of Science and Technology
Cochin – 682 022, India

CERTIFICATE

Certified that the work presented in this thesis entitled **“DESIGN AND DEVELOPMENT OF FIBER OPTIC SENSORS FOR TRACE DETECTION OF CERTAIN ENVIRONMENTAL POLLUTANTS”** based on the bonafide research work done by Mr. P. Suresh Kumar is an authentic record of research work done by him under my guidance in the International School of Photonics, Cochin University of Science and Technology, Cochin-682022, India and has not been included in any other thesis submitted previously for the award of any degree

Cochin – 22
22nd October 2003

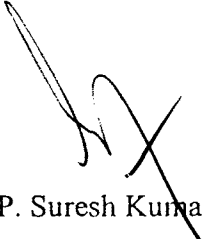
Prof. P. Radhakrishnan
(Supervising Guide)
International School of Photonics
CUSAT

DECLARATION

I hereby declare that the work presented in this thesis entitled “**DESIGN AND DEVELOPMENT OF FIBER OPTIC SENSORS FOR TRACE DETECTION OF CERTAIN ENVIRONMENTAL POLLUTANTS**” is based on the original work done by me under the guidance of Prof. P. Radhakrishnan, International School of Photonics, Cochin University of Science and Technology, Cochin- 682022, India and it has not been included in any other thesis submitted previously for the award of any degree

Cochin – 22

22nd October 2003



P. Suresh Kumar

CONTENTS

Preface

Words of gratitude

List of publications

Chapter1 INTRODUCTION TO FIBER OPTICS AND FIBER OPTIC SENSORS

1.1	Introduction	3
1.2	Why optical fibers?	3
1.3	Propagation of light within a fiber	4
1.4	Modes in an optical fiber	6
1.5	Classification of fibers	6
	1.5.1 Refractive index profile	7
	1.5.2 Core diameter	9
	1.5.3 Cladding and core materials	9
1.6	Fiber characteristics	9
	1.6.1 Attenuation in fiber	9
	1.6.2 Dispersion in fiber	10
1.7	Optical sources	10
	1.7.1 Incandescent lamps	11
	1.7.2 Discharge lamps	11
	1.7.3 Lasers	11
	1.7.4 Semiconductor sources	12
1.8	Detectors	12

1.9	Fiber optic sensors	13
1.9.1	Intensity modulated FOS	13
1.9.2	Phase modulated FOS	15
1.9.3	Polarization modulated FOS	17
1.9.4	Frequency modulated FOS	17
1.9.5	Wavelength modulated FOS	18
1.9.6	Fiber optic chemical sensors	19
1.9.6.1	Advantages of FOCS	20
1.9.6.2	Classification of FOCS	21
1.9.6.2.1	Direct spectroscopic sensors	21
1.9.6.2.2	Reagent mediated sensors	22
1.9.6.2.3	Porous glass sensor	22
1.9.7	Distributed optical fiber sensors (DOFS)	23
1.9.8	Bio sensors	24

**Chapter 2 EVANESCENT WAVE FIBER OPTIC SENSORS:
TRACE DETECTION OF CERTAIN WATER
CONTAMINANTS**

2.1	Introduction	31
2.2	Pollutants in water	31
2.3	Role of evanescent wave fiber optic sensors(EWFS) in water pollution monitoring	33
2.4	Theoretical outline	34
2.5	Detection of dissolved ammonia in water	39
2.5.1	Chemistry	39
2.5.2	Experimental	
2.5.2.1	Preparation of the sensing element	41
2.5.2.2	Sensor cell	41
2.5.2.3	Experimental set-up	41

2.5.3	Design of LED based EWFS	
2.5.3.1	Electronic components	42
2.5.3.2	Characterization of LED	42
2.5.3.3	Block diagram	43
2.5.3.4	Electronic circuitry	43
2.5.4	Preparation of test solutions	44
2.5.5	Results and discussions	46
2.6	Detection of nitrites in water	51
2.6.1	Chemistry	52
2.6.2	Experimental	52
2.6.3	Preparation of test solutions	53
2.6.4	Results and discussions	53
2.7	Detection of chromium in water	58
2.7.1	Experimental	59
2.7.2	Results and discussions	60
2.8	Simultaneous detection of nitrite and chromium content in water	
2.8.1	Design	63
2.8.2	Results and discussions	67
2.9	An alternate design of LED based EWFS	68

Chapter 3 TRACE DETECTION OF CERTAIN WATER POLLUTANTS USING MICROBENT OPTICAL FIBERS

3.1	Introduction	75
3.2	Theoretical background	77
3.3	Experimental	
3.3.1	Preparation of permanent microbent fiber	80
3.3.2	Experimental set-up	80
3.4	Results and discussions	82

Chapter 4 APPLICATION OF LONG PERIOD GRATING IN WATER POLLUTION MONITORING

4.1	Introduction	91
4.2	Short Period Gratings	92
4.3	Long Period Gratings	95
4.4	Grating fabrication Techniques	96
	4.4.1 Holographic Technique	97
	4.4.2 Phase Mask Technique	98
	4.4.3 Point-by-Point Fabrication Technique	99
	4.4.4 Amplitude mask technique	100
4.5	Fiber Grating Sensors	100
4.6	LPG Sensor for Detecting Chemical Species	101
	4.6.1 Experimental details	101
	4.6.2 Results and Discussion	104
4.7	Fuel level indicator using LPG in multimode optical fibers	109

Chapter 5 FIBER OPTIC EVANESCENT WAVE SENSORS FOR AMMONIA GAS SENSING

5.1	Introduction	117
5.2	Sol-gel technology	120
	5.2.1 Sol-gel chemistry	121
	5.2.2 Sol-gel coating methods	122
	5.2.2.1 Dip-coating	122
	5.2.2.2 Spin coating	123
	5.2.3 Dye encapsulation in sol-gel matrix	124
5.3	Unclad EWFS for Ammonia gas detection	
	5.3.1 Introduction	125
	5.3.2 Experimental	

	5.3.2.1	Preparation of the sensing Element	126
	5.3.2.2	Optical arrangement for sensor- Characterization	128
	5.3.3	Results and discussions	129
5.4		LPG in multimode fiber for Ammonia gas detection	134
Chapter 6		CONCLUSIONS	143

PREFACE

Besides the field of Optical communication, optical fibers have also drawn considerable attention in the field of transducing technology for fulfilling the ever-increasing need for fast, sensitive and reliable sensors. The conventional wisdom of optical fiber sensors points towards medical and biomedical engineering, the electrical power industry, structural monitoring and specialized industrial sectors as the principal users of OFS technology. However, theoretically, there exist no limits to the diverse areas of Fiber optic sensors, where accurate measurements of different parameters are required. Several meritorious features as well as attractive capabilities of fiber optic sensors have brought them to the forefront of other sensing methods. The unique features of the optical fiber that make them highly desirable for sensing applications include immunity to electromagnetic interference, compactness and light weight, low cost, reliability, short response time etc. With the growing environmental concern, such sensors have acquired a wide interest for realizing sensor systems for accurate detection and analysis of different environmental pollutants. Compared to other methods, fiber optic sensors are highly sensitive and can be used to perform accurate absorption measurements on highly absorbing or scattering media due to small effective path length.

A fiber optical sensor (FOS) is a transducer that converts a change in the parameter to be detected into a corresponding variation on any one of the five parameters, intensity, phase, polarization, wavelength or frequency of the light transmitted through the fiber. However, fiber optic sensors based on variations of the intensity of the light propagating in the fiber are of considerable interest in sensing applications because of their simple design, low cost and good sensitivity. The present thesis describes the design, fabrication and characterization of some intensity modulated FOS for the trace

detection of certain environmental pollutants in water as well as in air. The thesis is organized into five chapters and brief summaries of each chapter are given below.

Chapter 1 gives a general understanding of the characteristics of optical fibers, various light sources etc and how they are used in the development of various sensors. It also discusses the basic theory, design and applications of different classes of optical fiber based sensors. Necessary mathematical treatment of light propagation is used wherever needed and emphasis is given on the physical understanding of the various properties of optical fibers.

Chapter 2 describes the theory, design, fabrication and characterization of unclad evanescent wave fiber optic sensors (EWFS) and its application for trace detection of certain pollutants like ammonia, nitrites and chromium content in water. The superior performance of these sensors are established by comparing its performance in terms of sensitivity, lower detection limit, dynamic range etc with that of the existing spectrophotometric method. Efforts are made to reduce the size and cost of the sensors by using super bright light emitting diodes (LED) and hence different LED modulating and detecting schemes are included in this chapter along with the concept of reference arm to eliminate the ill effects due to power supply fluctuations, thermal noise etc. The capacity to make distributed measurement is one of the principle features of fiber optic technology and hence a novel cost effective technology for simultaneous detection of different contaminants in water is discussed at the end of this chapter.

Permanently bent plastic fibers with cladding are found to be a possible substitute for unclad fibers in chemical sensing applications for absorption measurements. **Chapter 3** deals with the theory, design, fabrication and characterization of Microbend EWFS and its application in water pollution monitoring. The performances of this class of sensors are compared with unclad EWFS and standard spectrophotometric method.

Long period gratings (LPGs) are a relatively new class of fiber optic devices that act to couple light from the propagating fiber mode to cladding modes, producing a series of attenuation bands in the fiber transmission spectrum. The resonance wavelengths of the attenuation are sensitive to local environment experienced by the fiber. LPGs are normally fabricated in single mode fibers but LPGs in multimode fibers also have some applications. **Chapter 4** presents theory, design, fabrication and characterization of LPG in multimode fiber for chemical sensing application like water pollution monitoring. Moreover, a sensitive, reliable and compact Fuel level indicator using LPG in multimode fiber for detecting fuel levels in motor vehicles is also included in this chapter.

In **chapter 5**, presents the details of the design and characterization of two different types of FOS, unclad EWFS and multimode long period grating EWFS for the detection of ammonia gas. Sol-gel technology is used in both of these sensors for immobilizing ammonia sensitive dye on the unclad or LPG region of the fiber. Hence, a brief introduction of this technology is included in this chapter along with the details like reversibility, response time, reusability etc of the sensor.

The thesis is concluded with a summary and an overall conclusion of the work presented in the previous chapters. Future prospects of FOS are also addressed.

WORDS OF GRATITUDE

I would like to express my sincere gratitude to my guide, Prof. P. Radhakrishnan, for his invaluable guidance and constant support. His brother cum friendly approach and constant enquiries about my research always be a source of inspiration for me.

Right from the beginning, with invaluable suggestions and encouragement, Prof. V. P. N. Nampoori was always with me. The fruitful discussions with him have resulted in exposure to different areas related to my research work.

I also thank Dr. C. P. Girijavallabhan for the invaluable discussions, especially on the technical aspects of the experimental setup. His critical evaluation and analysis on the manuscript that I have written played a vital role in all my international journal publications.

The outstanding classes from Dr. V. M. Nandakumaran helped me a lot in understanding the physical aspect of light propagation through fibers and related fields. I thank him for his constant support and friendly nature.

I thank Mr. Kailasnath for his friendly nature as well as for the support and help that he rendered while he was in the charge of Photonics library

I am lucky enough to work with a young and enthusiastic scientist Mr. Thomas Lee, who always inspired me with his innovative ideas. The intellectual discussions with him played a major role in my research activities.

I would like to express my sincere gratitude to Mr. Sajan D George for the various helps rendered by him throughout my work. His hard working nature and smiling face had made a deep impression in me.

The help rendered by Dr. Shelly John, who introduced this field to me, is worth to mention. Although I came up from an engineering background, the discussions with Mr. K. P. Unnikrishnan helped me a lot in understanding the basics of lasers as well as

handling of various equipments in the lab. I remember with a great sense of gratitude for the support given by Mr. Abraham V.S, especially on the final phase of my work.

I thank Dr. Sivasankara Pillai of Enviromental Studies, CUSAT for giving me a clear understanding about the different aspects about the enviornmental pollutants. I thank Dr. Sugunan of Chemistry Department, CUSAT for the invaluable discussions, which played a key role in my research activities. I also thank all research scholars of chemistry department for their timely help and support.

It is worth to remember the help rendered by Dinesh Kumar in directing me in the field of Fiber Gratings. The collaborative work with him helped me a lot, not only in my research activities but also in understanding the various aspects of grating.

Help and support provided by Aneesh and Praśanth are really great, especially on literature collection. I thank them for their friendly and supportive attitude.

I also thank my colleagues in Fiber lab Ms. Geetha and Mr. Rajesh M for the constant support and encouragement that they provided in all my activities.

Dr. Nibu A George has helped me a lot in preparing the manuscripts for international journals, especially on early stages of my research. I thank Dr. Achamma Kurian, Mr. Jibu Kumar and Dr. A. Deepthy for their support and friendly attitude.

Eventhough she belongs to Physics department, Ms. Jyotsna Ravi always showed keen interest in my research activities.

I am very much enjoyed the funny moments with Pramod, Binoy, Vinu, Manu, Jijo and making my life at ISP as a wonderful thing to remember.

I also thank my colleagues Dilna.S, Sr. Ritty Nedumapara, Sreeja, Rekha, Rajesh, Pravitha and Santhi for their support.

The support given by nonteaching staff of ISP was very important. I thank them for that. I also thank various library staffs and people of Instrumentation Department for their timely help.

I remember with gratitude the fruitful discussions with Prof. T K Mani regarding the various aspect of opto-electronic circuit design.

I thank all the teaching and non-teachings staffs in Model Engineering College, Ernakulam for their c-operation.

I thank IHRD for providing me a chance to do Ph.D by choosing me as a sponsored candidate. I also thank AICTE for the instruments that used in the present work through a research project to Dr. P. Radhakrishnan.

I thank all the M.Tech and M.Phil students who have collaborated with me either in the form of projects or discussions.

I thank each and all of CUSAT campus who added flavors to my days in this campus.

It is beyond words to express my gratitude to my family, Viji, Paru and Appu for all the support and encouragement that they have provided me. I am sure that I could not accomplish this task without their supportive attitude.

P. SURESH KUMAR

LIST OF PUBLICATIONS,

In International Journals

1. **P Suresh Kumar**, C P G Vallabhan, V P N Nampoori, V N Sivasankara Pillai and P Radhakrishnan, 'A fibre optic evanescent wave sensor used for the detection of trace nitrites in water' Journal of Optics A: Pure and Applied Optics, Page no.247-250, Volume4, November3, May 2002.
2. **P Suresh Kumar**, Thomas Lee S, C P G Vallabhan, V P N Nampoori and P Radhakrishnan, 'Design and development of an LED based fiber optic evanescent wave sensor for simultaneous detection of chromium and nitrite traces in water' Optics Communication, vol 214/1-6 pp 25-30 Dec 2002.
3. **P. Suresh Kumar**, Dinesh Kumar. R, C. P. G. Vallabhan, V.P.N. Nampoori and P. Radhakrishnan 'Trace Detection of Nitrites in water using Long Periodic Grating in multimode optical fiber' Asian Journal of Physics, vol 12, Nos 2&3 pp 233-236(2003).
4. Thomas Lee S, R Dinesh Kumar, **P Suresh Kumar**, P Radhakrishnan, C P G Vallabhan & V P N Nampoori, Long period gratings in multimode fibers: application in chemical sensing, Optics Communication, vol 224 pp 237-241 (2003)
5. Thomas Lee S, **P Suresh Kumar**, K P Unnikrishnan, V P N Nampoori, C P G Vallabhan, S Sugunan and P Radhakrishnan, Evanescent Wave Fiber Optic Sensors for Trace Analysis of Fe^{3+} in water, Meas. Sci. and Technol., vol 14 pp 858-861(2003).
6. Thomas Lee S, Nibu A George, **P Suresh Kumar**, P Radhakrishnan, C P G Vallabhan and V P N Nampoori, Chemical sensing with microbent optical fiber, Opt. Lett. 20,1542-1543(2001)

Papers presented in conferences/ seminars

1. P. Suresh Kumar, V S Abraham, C P G Vallabhan, V P N Nampoori and P. Radhakrishnan, Fiber Optic Evanescent Wave Sensor for Ammonia Gas Detection, APOC 2003, Wuhan, China.
2. P. Suresh Kumar, V S Abraham, C P G Vallabhan, V P N Nampoori and P. Radhakrishnan, Long Period Grating in Multimode Fiber for Ammonia Gas Detection, APOC 2003, Wuhan, China.
3. P Suresh Kumar, C P G Vallabhan , V P N Nampoori and P Radhakrishnan, Long periodic grating in multimode fiber for measuring traces of chromium in water, SPIE Conference on Smart Sensors, Actuators, and MEMS, Canary Island, SPAIN, May 18-20 (2003).
4. P Suresh Kumar, C.P.G. Vallabhan, V.P.N. Nampoori and P. Radhakrishnan, Fibre Optic Evanescent Ammonia Sensor, SPIE Conference on Transducing Materials and Devices, Brugge, Belgium, Oct 28-Nov 1(2002).
5. P Suresh Kumar, C.P.G. Vallabhan, V.P.N. Nampoori and P. Radhakrishnan, Fibre Optic Evanescent Chromium Sensor, APOC-2002, Shanghai; China, Oct 14-18 (2002).
6. P Suresh Kumar, C.P.G. Vallabhan, V.P.N. Nampoori and P. Radhakrishnan, An LED based Fibre Optic Evanescent Wave Sensor for Simultaneous Detection of Chromium and Nitrate Traces in Water, Photonics- 2002, TIFR, Mumbai, India, Dec 16-18 (2002).
7. P Suresh Kumar, C.P.G. Vallabhan, V.P.N. Nampoori and P. Radhakrishnan, Fibre Optic Evanescent Wave Sensor for Nitrites in Water, OPTONICS 2001,

Science and Technology Museum, Thiruvananthapuram, India, Aug27-29, (2001).

8. P Suresh Kumar, Dinesh Kumar. R, Jibukumar G, C. P. G. Vallabhan, V.P.N. Nampoori, and P. Radhakrishnan, Fuel level indicator using long periodic grating in multimode optical fibers, National Laser Symposium (NLS-2002), SCTIMST, Thiruvananthapuram, Nov 14-16 (2002).
9. P. Suresh Kumar, C. P. G. Vallabhan, V.P.N. Nampoori, and P. Radhakrishnan, An LED Based Fibre Optic Evanescent Wave Sensor for the Detection of Trace Nitrites in Water, DAE- BRNS, National Laser Symposium (NLS-2001), CAT, Indoor, India, Dec 19-21(2001) (**Got best poster award**)
10. Suresh Kumar, S. Thomas Lee, C.P.G.Vallabhan, V.P.N. Nampoori and P. Radhakrishnan, Fibre Optic Ammonia Sensor, SPENDE 2001, Kerala University, Kariavattom Campus, Thiruvananthapuram, May 25-26 (2001).



Chapter1

INTRODUCTION TO FIBER OPTICS AND FIBER OPTIC SENSORS

The present chapter gives a general overview of the characteristics of optical fibers, various light sources, detectors etc and how they are used in the development of various fiber optic sensors. It also discusses the basic principles and applications of different classes of optical fiber based sensors. Emphasis is given on the physical understanding rather than on the mathematical treatment.

1.1. Introduction

The dramatic reduction in transmission loss of optical fibers coupled with equally important developments in the area of light sources and detectors have brought about a phenomenal growth of the fiber optic industry during the past two decades [1-16]. Although the major application of optical fibers has been in the area of telecommunications, optical fibers have drawn considerable attention in the field of transducing technology for fulfilling the ever-increasing need for fast, sensitive and reliable sensors. Fiber optic sensors find applications in wide range of areas like biomedicine, aviation, surgery, pollution monitoring, etc., apart from areas in basic science. However, theoretically, there exist no boundaries to the diverse areas of fiber optic sensors, where accurate measurements of different parameters are required.

1.2. Why optical fibers?

The optical fibers are widely used in all realms of industry due to its superior properties and characteristics over conventional data transmission and light transmission systems. It offers widest bandwidth till today and allows wavelength division multiplexing. Communication through optical fibers is free from electromagnetic interference and allows the simultaneous transmission of several light waves through a single fiber. It is also free from microwave and radio frequency interference. As the materials used for the fabrication of optical fibers are dielectric in nature, it is immune to electrical conductivity and hence provide higher safety. These cables have very small diameter and are lightweight in nature. It can withstand relatively higher temperature and can be used in remote sensing applications. The optical fiber confines energy into it and thus offers a high degree of security and privacy.

The unique features of the optical fiber that make them highly desirable for sensing applications include immunity to electromagnetic interference, compactness and light weight, low cost, reliability, short response time etc. With the growing environmental concern, such sensors have acquired a wide interest and acceptance for

realizing sensor systems for accurate detection and analysis of different environmental pollutants. Compared to other methods, fiber optic sensors are highly sensitive and can be used to perform accurate absorption measurements on highly absorbing or scattering media due to small effective path length.

1.3. Propagation of light within a fiber

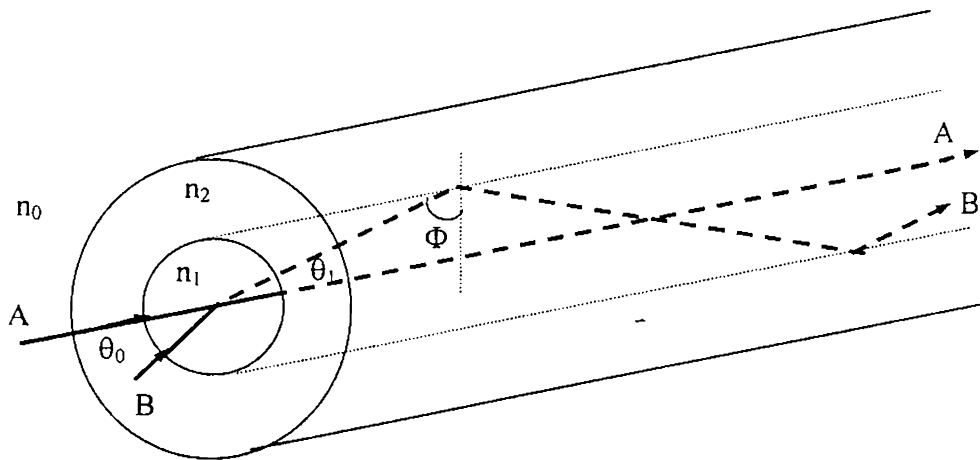


Figure 1.1: Propagation of light through an optical fiber

An optical radiation entering one end of a fiber at a slight angle to its axis follows a zigzag path through a series of total internal reflections (TIR) at the core cladding interface and propagates to the other end of the fiber. The following two conditions must be satisfied for the total internal reflection of light through the fiber. Firstly, the fiber core must have slightly higher index of refraction (n_1) than the index of refraction (n_2) of the material (cladding) surrounding the fiber core. Secondly, the incident angle Φ (between the ray path and the normal to the fiber wall) must be greater than the critical angle Φ_c , which is defined as $\sin \Phi_c = n_2/n_1$. Any radiation incident at angles less than the critical angle undergoes refraction and these radiations penetrate the cladding and are lost. The refraction phenomena in fibers

follow the well-known Snell's law, $n_0 \sin \theta_0 = n_1 \sin \theta_1$, where θ_0, θ_1 are the incident and refraction angle and n_0, n_1 are the index of refraction of launch region and core, respectively. It is seen from the figure 1.1 that the internal incidence angle and refraction angle are related by the expression $\theta_1 = (90 - \Phi)$, so that, Snell's law becomes $n_0 \sin \theta_0 = n_1 \cos \Phi$. As long as the light enters the fiber at an incident angle such that the internal reflection angle Φ is not less than the critical angle Φ_c , the light will be contained within the fiber and will propagate to the far end by a series of reflections. Thus by using the expression for critical angle, the maximum value of incidence angle for which light will propagate through the fiber is given by

$$\theta_0 (\text{max}) = \sin^{-1} [(n_1^2 - n_2^2)^{1/2} / n_0] \quad (1.1)$$

This maximum angle is called the acceptance angle or the acceptance cone half angle. The sine of maximum acceptance angle is used as the figure of merit of the fiber and is called numerical aperture (NA)

$$NA = \sin \theta_0 (\text{max}) = [(n_1^2 - n_2^2)^{1/2} / n_0] \quad (1.2)$$

If the light is launched from air, $n_0=1$, the numerical aperture NA becomes

$$NA = (n_1^2 - n_2^2)^{1/2} \quad (1.3)$$

In terms of the normalized difference (Δ) between the indices of the core and cladding and for $n_1 \approx n_2$, expression 1.2 becomes

$$NA = n_1 (2\Delta)^{1/2} / n_0 \quad (1.4)$$

$$\text{where } \Delta = (n_1 - n_2) / n_1 \quad (1.5)$$

If the light is launched from air, the expression 1.4 becomes

$$NA = n_1 (2\Delta)^{1/2} \quad (1.6)$$

From this equation, it is evident that, NA of a fiber is effectively dependent only on the refractive indices of the core and cladding materials and is not a function of fiber dimensions.

1.4. Modes in an optical fiber

The propagation of light in an optical fiber is characterized by a set of guided electromagnetic waves called the modes. Each guided mode is a pattern of electric or magnetic field distribution that is repeated along the fiber at equal intervals. A monochromatic electromagnetic radiation at an angular frequency ω traveling along the z - direction (i.e, along the fiber axis) is represented by the expression $e^{i(\omega t - \beta z)}$, where the factor β is the z component of the wave propagation constant

$k = \frac{2\pi}{\lambda}$. For guided modes, β can assume only certain discrete values in the limit of $n_1 \gg \beta \gg n_2$. A guided mode traveling along the axis of a fiber is the superposition of plane waves whose phases change at each reflection at the core-cladding interface. In planar waveguides, the solution of Maxwell's equation at the boundary yields transverse electric and transverse magnetic modes. However, in the case of cylindrical fibers, the boundary conditions lead to the coupling between electric and magnetic field components to produce hybrid modes such as HE and EH modes depending on the magnitude of electric and magnetic field. Although, the theory of light propagation is well understood, a complete description of the guided radiation modes that correspond to rays not satisfying total internal reflection condition becomes rather complex. However, a further simplification is possible by using weakly guiding approximation i.e. $(n_1 - n_2) \ll 1$, which gives linearly polarized (LP) modes.

1.5. Classification of fibers

Fibers can be classified into various classes depending on the refractive index profile of the core and the cladding medium, core diameter as well as the materials used for the core and cladding. Each of these fibers have their own advantages and disadvantages.

1.5.1. Refractive index profile

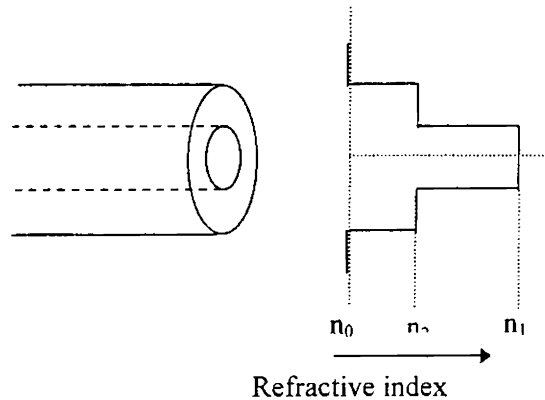
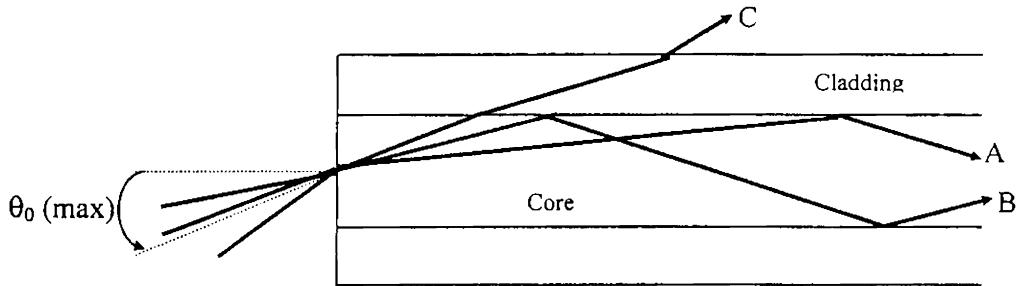


Figure 1.2: Refractive index profile of a step index fiber



A & B: Light rays launched within the acceptance cone
 C: Light rays launched outside the acceptance cone

Figure 1.3: Light ray propagation in a step index fiber

Based on the refractive index of the core material, optical fibers are mainly classified as step index fibers and graded index fibers. In the case of step index fibers, the core refractive index remains uniform and the core cladding interface is characterized by an abrupt change in the refractive index as shown in figure 1.2. The light propagation through the core of this type of fiber is characterized by the light rays following the zigzag path of straight line segments as depicted in figure 1.3.

However, in the case of graded index fibers, there is gradual change in refractive index within the core as shown in figure 1.4. These fibers allow light in the

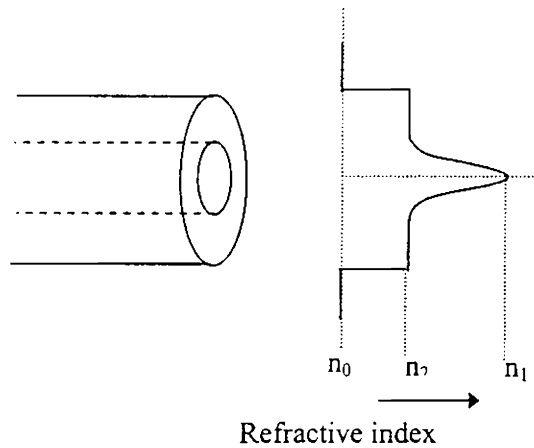
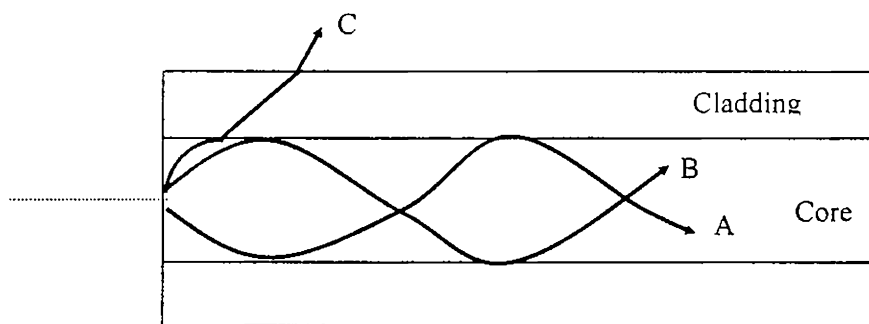


Figure 1.4: Refractive index profile of a graded index fiber

longer modes to travel faster than light in shorter modes and hence reduce the modal dispersion of the fiber. In this case, light rays periodically diverge and converge along the length of the fiber as shown in figure 1.5. This fiber allows somewhat larger acceptance cone than step index fiber and the rays outside the acceptance cone will escape through the cladding.



A & B: Light rays launched within the acceptance cone
C: Light rays launched outside the acceptance cone

Figure 1.5: Light ray propagation in a graded index fiber

1.5.2. Core diameter

The reduction in size of the core results in the reduction of the number of modes that can propagate through the fiber. In a single mode fiber the core diameter is so small that only one mode propagates through the fiber. The typical size of the core in a single mode fiber is of the order of a few micrometers. Hence, it is very difficult to launch light into the tiny core of the fiber. As a result, the installation and operation cost increases and it outweighs the advantages for short distance fiber applications. However, for long distance applications the single mode fiber is used because of its advantages. Multimode fibers have relatively larger core diameter and allows easier operation.

1.5.3. Cladding and core materials

Based on the material used for the fabrication of core and cladding there are variety of optical fibers such as silica fibers, plastic clad silica fibers and plastic fibers. The losses in the propagation of light radiation are affected by the material used. With the introduction of proper dopants into the core material, the characteristics of optical fiber, for example Er doped fibers, can be changed. In recent years, considerable efforts have been made for the fabrication of various low cost fibers with core as polymers.

1.6. Fiber Characteristics

The research on the design and fabrication of optical fibers is focused on the development of fibers with minimal attenuation and dispersion. Decreasing the attenuation is to bring as much of the light originally launched in the fiber to the other end. Reducing the dispersion limits the amount of distortion in the signal carried by the light through the fiber.

1.6.1. Attenuation in fiber

The attenuation occurs mainly due to absorption and scattering of light that occurs within the fiber during its propagation. Depending on the wavelength used and the impurities present in the fiber, the absorption losses can be significant. The

impurities and imperfections in the fiber can cause the scattering of light and result in the scattering loss and this loss mechanism is wavelength dependent. This scattering is called Rayleigh scattering and it is inversely proportional to fourth power of wavelength used. In addition to these mechanisms, the variation in the smooth surface of the core can result in loss of light propagating through the fiber and this mechanism is called bending loss. The variation on the surface of the core or bumps, changes the angle at which light strikes the core to cladding interface and can cause the light to refract into the cladding rather than reflect into the core. Microbends can occur during the manufacturing of the fiber cable or during the handling of the fiber.

1.6.2. Dispersion in fiber

Mainly there are three mechanisms, which can cause distortion to the signals that, propagate through a fiber. They are modal dispersion which occurs in fibers having more than one mode, material or chromatic dispersion which is a wavelength based effect caused by the glass of which the fiber is made and waveguide dispersion which has a greater concern for single mode fibers. The modal dispersion occurs due to difference in path length of the different modes propagating through the fiber. As a result, some modes will travel faster than the other and consequently the pulse of light containing data gets stretched so that at the output of the fiber the data obtained is distorted. Like modal dispersion, material dispersion causes the pulses in the signal to stretch out due to the propagation of different wavelengths of light travelling at different speeds in the glass that makes up the fiber core. As the core diameter of single mode fibers is very small, some portion of the incoming radiation will travel through the cladding of the fiber. The cladding has a different index of refraction and light traveling through it will reach the end of the fiber sooner than the light traveling through the core.

1.7. Optical Sources

The selection of optical sources is extremely important in devices and sensors based on optical fibers. The parameters like spectral output, intensity, stability, ease of modulation, predicted lifetime, cost and power consumption, size etc. of optical

sources have to be considered during their selection. In general, the incandescent lamps, discharge lamps, lasers (non semiconductor) and semiconductor sources (LEDs and laser diodes) are utilized as the optical sources in fiber based systems.

1.7.1. Incandescent lamps

Incandescent filament bulbs (such as tungsten halogen lamps) emit over a broad spectral range (Vis, IR). They are relatively inexpensive and are available in compact sizes. However, they are not suited for modulation and the operational lifetime of these sources are less compared to LEDs. In addition, these sources dissipate large amount of heat and the alignment using these sources are rather difficult.

1.7.2. Discharge lamps

The UV range (200 nm – 400 nm) is an important range of electromagnetic radiation, especially for the absorption as well as for the fluorescence studies. Deuterium lamps are the best available sources in the range 200 nm – 300 nm. However, these lamps are generally bulky, consume more power and hence expensive power supplies are required for their operation. Xenon flash lamps provide a broadband output in the 200 nm – 1000 nm range, but demand a power source regulation and suffer from pulse to pulse variation in output intensity.

1.7.3. Lasers

Apart from semiconductor lasers, the 488nm and 514 nm output radiations of Argon laser, 633 nm of He- Ne laser and 325 nm of He – Cd laser are the commonly used wavelengths for the fiber based systems. The advantage of laser as source of optical radiation is that it offers monochromatic output (obviating the need for a spectral selection filter), high intensity and directionality (facilitating easy launching

into the fiber). Nevertheless, these systems are highly expensive and are fragile in nature.

1.7.4. Semiconductor sources

Semiconductor solid state sources, which include laser diodes and LEDs, are the most attractive option for fiber based systems because of their low power consumption, high stability, long lifetime, robustness and compact size. These sources are inexpensive and the laser diode provides intense collimated beam that can be easily modulated. However, unlike LEDs, laser diodes operating below 630 nm are highly expensive. The laser diodes are commonly available in the wavelength range, 630 – 670 nm, 750- 830 nm and the ‘Telecom windows’ (1330nm and 1550 nm). In recent years, most of the academic as well as industrial researches on this area are focused on developing blue laser diode-source based on GaN and ZnSe materials with sufficient operational time. Availability of a blue laser diode will be a major stimulus to the fluorescence based chemical sensor and biosensors and it will facilitate the development of both compact and remote systems. In addition to the advantages of semiconductor sources already given, LEDs are particularly attractive sources for optical sensing because of their low cost, ease of modulation and ease of coupling to multimode fibers. Unlike lasers, they are not sensitive to back reflection and have low coherence.

1.8. Detectors

Silicon photodiodes are the commonly used detectors with a spectral response that spans the visible range but falls sharply above 1000nm and these are relatively inexpensive. Avalanche photodiodes (APDs) are employed in systems where the gain is the prime concern. Photomultiplier tubes (PMTs) are more expensive than photodiodes, but offer greater sensitivity and can be operated even at very low light levels. In the IR range, photothermal and pyroelectric detectors find some

applicability. However, photoconductive detectors based on PbS, PbSe, InSb and HgCdTe are commonly employed in the IR range.

1.9. Fiber optic sensors

In addition to the major role played in the modern communication systems, optical fibers find wide applicability in other realms of Photonics industry especially in the fabrication of Fiber Optic Sensors (FOS) [17-33]. The applicability of FOS is facilitated by many of the unique features of fibers. These FOS offers high sensitivity, durability and reliability and allows the direct and remote measurements. Many of the FOSs are based on monitoring the variation in one of the principal parameters that characterizes the light beam in accordance with the variation in physical or chemical parameters to be measured. The principal parameters of light utilized for the fabrication of FOS are intensity, phase, polarization and frequency. Free from electromagnetic interference and radio frequency interference and low losses gives FOS a unique place in the sensor technology. In FOSs, the light may be modulated either inside or outside the fiber and correspondingly it can be classified as intrinsic sensors and extrinsic sensors. In intrinsic sensors, the physical parameter to be sensed modulates the transmission properties of the sensing fiber. Hence, one of the physical properties of the guided light like intensity, phase, polarization etc is modulated by the measurand. In the case of extrinsic FOS, the modulation takes place outside the fiber. Based on the modulation technique employed, the FOS can be classified into different groups such as Intensity modulated FOS, Phase modulated FOS, Polarization modulated FOS, Frequency modulated FOS and Wavelength modulated FOS.

1.9.1. Intensity modulated FOS

In a simple and inexpensive intensity modulated FOS, the measurand modulates the intensity of transmitted light through the fiber and these variations in

output light is measured using a suitable detector. These FOSs offer the easiest method of implementation and compatible with multimode fiber technology. Intensity modulation can take place through light interruption due to the displacement of one fiber relative to another or misalignment of one fiber with respect to another fiber. The misalignment can take place in three different ways viz. axial (longitudinal) misalignment, transverse misalignment and angular misalignment. Among these methods, FOS based on the transverse misalignment is more sensitive. The sensitivity of FOS can be enhanced by cleaving and polishing the two ends at a slant angle and keeping the slant face of the two fibers sufficiently close as shown in figure 6. In this case, the power will get couple to the receiving fiber through the slant face due to frustrated total internal reflection.

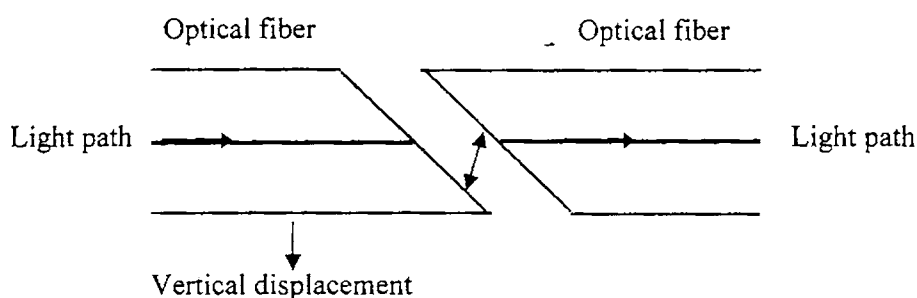


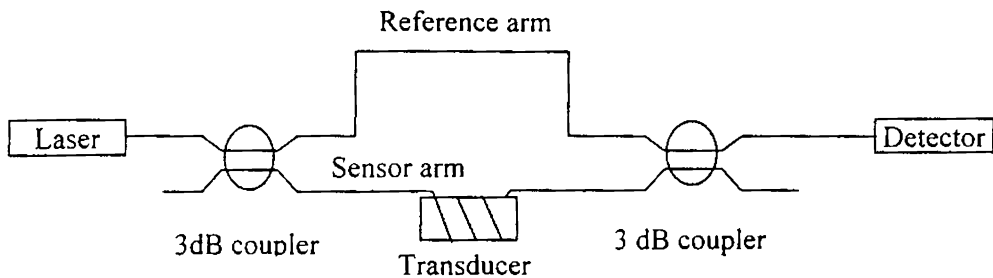
Figure 1.6: Intensity modulated sensor based on frustrated total internal reflection

In another class of intensity modulated FOS, the measurand modulates the light reflected from a reflecting surface. The reflective FOSs can be used to measure displacement, pressure etc and is widely used in medical field as inter-cardiac pressure transducer. A certain class of intensity modulated FOSs are working on the basis of transmission loss occurring due to microbending of the optical fiber and it is widely used for the measurement of acoustic pressure, strain, temperature, displacement and recently in chemical sensing applications which is described in detail in chapter 3.

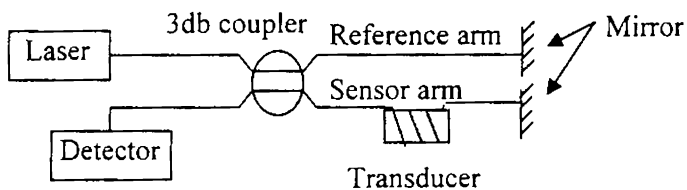
The evanescent waves are the electromagnetic field that penetrates into the cladding of an optical fiber as the optical radiation propagates through the fiber. A class of intensity modulated FOSs utilizes these waves for sensing different physical and chemical parameters, especially for sensing different environmental pollutants. The forthcoming chapters of this thesis discuss the design and development of different forms of fiber optic evanescent wave sensors in detail.

1.9.2. Phase modulated FOS

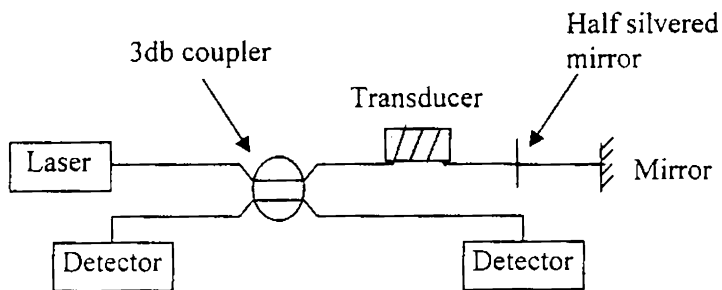
The most sensitive fiber optic sensing methods is based on the optical phase modulation. The total phase of the light along an optical fiber depends on the properties such as physical length of the fiber, transverse geometrical dimension of the guide, refractive index and the index profile of the waveguide. If the index profile remains a constant with environmental variations, then the depth of phase modulation depends on the other remaining parameters. The total physical length of an optical fiber may be modulated by the perturbations like thermal expansion, application of hydrostatic pressure causing expansion via Poisson ratio etc. The refractive index varies with temperature, pressure and longitudinal strain via photo elastic effect. Waveguide dimensions vary with radial strain in pressure field, longitudinal strain in a pressure field and by thermal expansion. The phase change occurring in an optical fiber is detected using optical fiber interferometric techniques that convert phase modulation into intensity modulation. There are a variety of fiber optic interferometers such as Mach-Zehnder, Michelson, Sagnac and Fabry Perot as shown in figure 1.7.



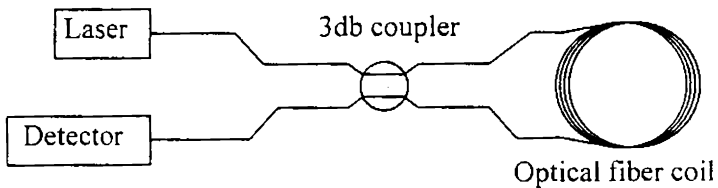
(a) Mach-Zehnder



(b) Michelson



(c) Fabry-Perot



(d) Sagnac

Figure 1.7: Optical fiber interferometric sensors

1.9.3. Polarization modulated FOS

Polarization properties of fibers are utilized for the measurement of a range of parameters. The action of any given external field on the polarization properties of an optical fiber normally modifies either the linear or the circular birefringence component. Thus, the measurand modulates the state of polarization in a fiber polarimetric sensor. A variety of physical phenomena such as optical activity, Faraday rotation, electro-gyration, electro-optic effect, Kerr effect, photoelastic effect etc can influence the polarization of light and can result in birefringence. A typical example of Polarization modulated FOS based on Faraday rotation is shown in figure

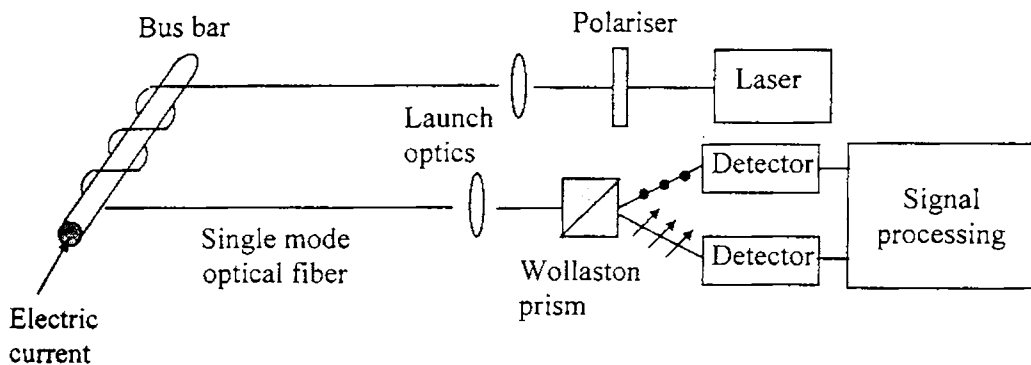


Figure 1.8: Fiber optic Polarization modulation sensor based on Faraday rotation for current monitoring

1.8. This system is highly useful for high tension lines, where current and voltage measurements using conventional techniques are both expensive and difficult to implement.

1.9.4. Frequency modulated FOS

Frequency modulation of light occurs under a limited range of physical conditions. Different effects like Doppler effect, Brillouin scattering, Raman scattering etc. are made use of in these types of FOS. A typical example of Frequency modulated FOS used for the sensitive detection of the motion of scattering bodies in a transparent medium is shown in figure 1.9. This frequency modulated FOS is based

on Doppler effect. In Doppler effect, if a radiation at a frequency f is incident on a

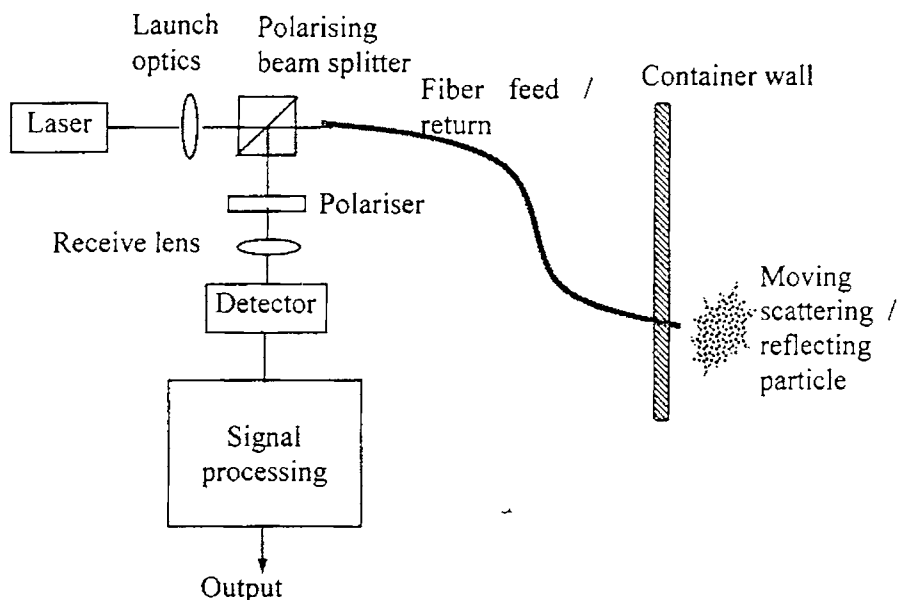


Figure 1.9: Frequency modulated FOS based on Doppler effect

moving body with a velocity v , then the radiation reflected from the body appears to have frequency f_1 , where

$$f_1 = \frac{f}{1 - v/c} = (1 + v/c)f \tag{1.7}$$

This fiber optic probe is readily suited to the detection of moving targets or to the detection of mobile bodies in suspension and it will detect velocities as low as one micron per second and up to meters per second or above depending on the detection electronics, corresponding to frequency offsets ranging from a few hertz to tens of megahertz.

1.9.5. Wavelength modulated FOS

In this type of sensors, a change in the value of the measurand is converted to a variation in wavelength of the transmitted light. There are numerous physical phenomena, which influence the variation of reflected or transmitted light intensity

principal areas. These are in chemical analysis using indicator solutions, in the analysis of phosphorescence and luminescence, in the analysis of black body radiation and in Fabry Perot, Lyot or similar optical filters in which transmission characteristics of the filters are made to be a function of an external physical parameter. A general block diagram of a wavelength modulated FOS is shown in figure 1.10.

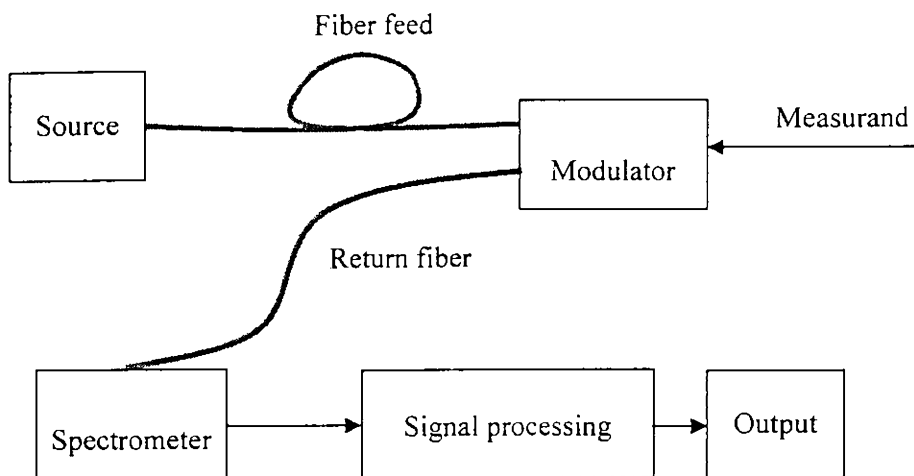


Figure 1.10: Wavelength modulated FOS

1.9.6. Fiber optic chemical sensors

Chemical sensors are a particular class of FOS, which is used to measure the concentration or activity of a chemical species present in the specimen. In addition to earlier mentioned qualities of optical fibers, its inertness towards chemical reaction makes it a promising candidate for the fabrication of chemical sensors. All the chemical sensors can be categorized according to their transduction mechanism; that is, the principle upon which the detection is based such as electrochemical, optical, thermal and mass transduction mechanisms. Electrochemical sensors can be based on a variety of different phenomena including amperometric, potentiometric, and conductimetric mechanisms. All of these sensors have electrodes and the nature of

the electrochemical phenomenon observed is dependent on the electrodes configuration. In some systems, an electrochemical potential is measured, whereas in others redox reaction takes place, generating a current due to the reaction of the intended species.

In temperature based sensors the uptake or release of heat caused by specific chemical reactions is measured by a thermistor. The amount of heat taken up or released is correlated with the concentration of the analyte. Mass based sensors are extremely diverse in their mechanism, but typically employ piezoelectric substrates for implementation. These sensors have a piezoelectric substrate coated with a polymeric material. Selective absorption or adsorption of the analyte alters the mass of the polymer layer coating the substrate. This mass change is detected as a change in the resonant frequency of the piezoelectric substrate. Other methods of mass detection employ chemical reactions, which generate precipitates, thereby altering the resonant frequency of the substrate on which the precipitate deposits.

The optical transduction allows a wide variety of chemical detection schemes that were previously impossible using conventional potentiometric and amperometric electrochemical devices. Fiber optic chemical sensors (FOCS) can be based on absorbance, fluorescence, polarization, Raman effect, refraction or reflection. The species or group specific chemistry can be selected from organics, inorganics, metals, enzymes, mono and polyclonal antibodies and polymers. Interaction of the analytes with the sensing reagents produces a change in one of the above mentioned spectroscopic parameters. The readout device electronically converts light flux into voltage. Modulation in the voltage reading directly correlates with the analyte concentration.

1.9.6.1. Advantages of FOCS

Chemical sensing based on optical fiber has several attractive features, which may be summarized as follows

- 1) No coupling optics are required in the sensing region because the interrogating light remains guided

- 2) The low attenuation of optical fibers enables remote *in situ* monitoring of species in difficult or hazardous locations.
- 3) No reference electrode is required.
- 4) Enhanced sensitivity.
- 5) Considerable miniaturization is possible.
- 6) Significant cost reduction.
- 7) Since the reagent phase need not be in physical contact with the optical fiber, it is easy to change the reagent phase.
- 8) No electrical interference.
- 9) Can be used for accurate absorption measurements.
- 10) Distributed sensing is possible.
- 11) It can exploit the high quality components like fibers, sources, detectors, connectors, etc. developed for the more mature fiber optic telecommunication technology.

1.9.6.2. Classification of FOCS

FOCS can be classified conventionally into two categories namely direct spectroscopic sensors and reagent mediated sensors.

1.9.6.2.1. Direct spectroscopic sensors

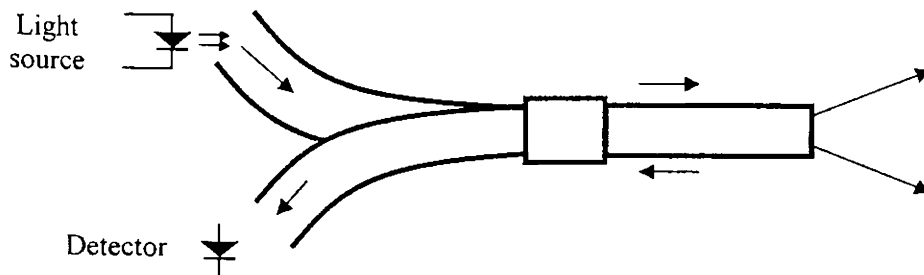


Figure 1.11: Direct spectroscopic sensor

In direct spectroscopic sensors, the fiber acts as a simple light guide, which separates the sensing location from the monitoring instrumentation as shown in

figure 1.11. In an alternate design, the evanescent wave of the transmitted light directly interacts with the targeted analyte via the optical fiber. Both sensor schemes identify optical modulation by changes in absorption or fluorescence properties, which correspond to the analyte concentration.

1.9.6.2.2. Reagent mediated sensors

In the case of reagent-mediated FOCS, analyte-sensitive material is attached to the tip of the fiber or its side as shown in figure 1.12(a & b). This material is often an indicator fixed to a polymeric substrate, which reacts reversibly with a component

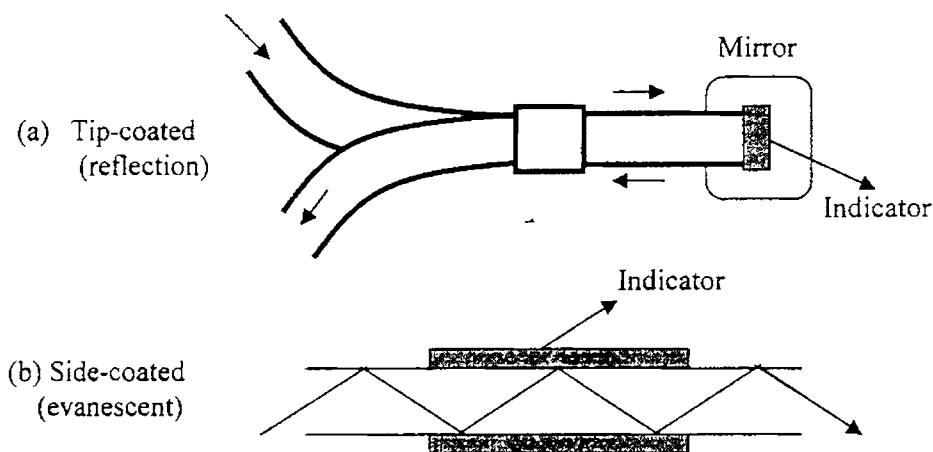


Figure 1.12 Reagent-mediated FOCS

of the solution. Light sent down to the fiber interacts with this indicating layer and modifies the light. The modified light collected by the detector correlates the change in concentration of the species being measured. Optical mechanisms include absorbance, fluorescence, polarization and luminescent lifetime changes with the indicating species.

1.9.6.2.3. Porous glass sensor

Another class of FOCS makes use of porous glass fiber as the sensing element. Since the porous fiber is an integral part of the waveguide, an intrinsic sensor is developed by coating or impregnating a porous section with an appropriate

indicator. As a result of the porosity, the analyte penetrates the fiber and reacts with the indicator, providing an in-line absorption or luminescence monitoring. The high surface area of the porous fiber enhances the sensitivity of the device since the light interaction is markedly increased. Depending upon the demands of the sensor, the depth of the porous layer may be varied from tens of micrometers to hundreds of micrometers and the depth of porosity influences sensing properties such as sensitivity, response time and dynamic range. Moreover, porous substrate have been combined with sol-gel immobilization for making a variety of chemical sensors including pH sensing, gas sensing, etc. Chapter 5 of this thesis explains this technique in detail for the detection of ammonia gas sensing.

1.9.7. Distributed Optical Fiber Sensors (DOFS)

Distributed Optical Fiber Sensors (DOFS) utilize the very special properties of the optical fiber to make simultaneous measurement of both the spatial and temporal behavior of the measurand field. This technique provides a new level of understanding, especially in the case of large structures and leads to a finer monitoring of the behavior of measurand. Using DOFS, we can measure the spatial distribution with resolution of 0.1-1 m over a distance of 100 m and to an accuracy of 1%. With the aid of these sensors, it becomes possible to determine the value of a desired measurand continuously as a function of position, along the length of a suitably configured fiber having arbitrary large spatial resolution. The temporal nature is determined simultaneously from the time dependence of the signal. Thus, this technique offers many attractive possibilities for industrial and research applications. It is very important and necessary to get accurate information of the spatial/temporal behavior of strain and temperature from the point of view of both safety monitoring and improved understanding of the behavior under anomalous conditions in dams, bridges, multi-storied buildings, air crafts, space crafts, boilers, chemical pressure vessels, electrical generators etc. The flexibility of the fiber makes it relatively easy to install over the chosen measurement path and thus allows

retrospective fitting unlike other sensor systems. Distributed sensing has also potential application in the field of chemical sensing for detecting a number of chemical species simultaneously.

1.9.8. Biosensors

In recent times, considerable efforts have been going for the development of an important class of FOS namely biosensors. Biosensors employ a biological recognition element to impart selectivity. An important application of the biosensors is for the detection of glucose, in which, an oxygen sensor is employed in conjunction with an enzyme. The sensing element is comprised of an immobilized enzyme attached or trapped within a polymer layer. When glucose encounters the enzyme, glucose oxidizes in the presence of oxygen, oxidation of the glucose to gluconic acid occurs and hydrogen peroxide is released as a byproduct. The uptake of oxygen is monitored with an oxygen sensor such as oxygen-sensitive electrode or optical sensor. In this way, the degree of oxygen depletion can be correlated directly to the concentration of glucose. However, there are several disadvantages with enzyme biosensors. First, the enzyme activity changes with time because of enzyme denaturation. Second, the concentration of co-reactant, in this case oxygen, must be kept in excess or must be measured independently. A second type of biosensor employs antibody molecules as the recognition element. These sensors are complex because they need to couple the signal to the binding event and the antibodies, unlike enzymes, do not transform the analyte. Consequently, complicated schemes for ascertaining the degree of binding must be employed. The selectivity of antibodies for their antigen-binding partners is extremely high, making antibodies attractive recognition elements for sensors. A major disadvantage of antibodies is their extremely high affinity for antigen, which results in binding such a way that it is irreversible. Sensors, based on antibodies, therefore, are only useful for extremely limited periods of time, as antibody binding sites become saturated and cannot be recovered except by exposure to rather harsh conditions. FOS used in biomedical

applications are mostly of the intensity modulated type, which employs optical spectroscopy as the basic tool.

The following chapters describe the design and fabrication of some fiber optic sensors for the trace detection of some pollutants in air and water using techniques such as evanescent waves, microbending and long period grating.

REFERENCES

1. A. K. Ghatak and M. R. Shenoy, *Fiber Optics through Measurements*, Viva Books, New Delhi (1994)
2. G. P. Agarwal, *Nonlinear Fiber Optics (II Ed.)* Academic Press, San Diego (1995)
3. A. K. Ghatak and K. Thyagarajan, *Introduction to Fiber Optics*, Cambridge University Press, New Delhi (1999)
4. G. Keiser, *Optical Fiber Communications (II Ed.)* Mc-Graw Hill, Boston (2000)
5. A. K. Ghatak, A. Sharma and R. Tewari, *Fiber Optics on a PC*, Viva Books, New Delhi (1994)
6. C. R. Pollock, *Fundamentals of Optoelectronics*, IRWIN, Chicago (1995)
7. I. P. Kamikov and T. L. Koch, *Optical Fiber Communications III B*, Academic Press, San Diego (1997)
8. J. Wilson and J F B Hawkes, *Optoelectronics*, Prentice Hall India, New Delhi (1996)
9. S. D Personick, *Fiber Optics – Technology and Applications*, Plenum Press, New York (1988)
10. J. M. Senior *Optical Fiber Communications (II Ed.)* Prentice Hall India, New Delhi (2001)
11. J. Powers, *Fiber Optic Systems*, Mc Graw Hill, Singapore (1999)
12. P. Diament, *Wave Transmission and Fiber Optics*, Macmillan Publishing, New York (1990)
13. A, H, Cherin, *An Introduction to Optical Fibers*, Mc Graw Hill, Auckland (1983)
14. J. Hecht, *Understanding Fiber Optics*, Prentice Hall, New Jersey (1993)
15. D. Derickson, *Fiber Optic Test and Measurement*, Prentice Hall, New Jersey (1998)
16. J. C. Palais, *Fiber Optic Communications (IV Ed.)*, Pearson Education, New Delhi (2001)
17. K TV Grattan and B T Meggitt, *Optical Fiber Sensor Technology*, Kluwer Academic Publishers, London (1998)
18. I. P. Kaminow, *IEEE J. Quantum Electron.* QE 17, 15 (1981)
19. B. P. Pal, *Fundamentals of Fiber Optics in Telecommunications and Sensor Systems*, New Age International, New Delhi (1992)
20. J. P. Dakin and B. Culshaw, *Optical Fiber Sensors – Vol IV*, Artech House, Boston (1996)
21. D. A. Krohn, *Fiber Optic Sensors – Fundamentals and Applications*, Instrument Society of America (1988)
22. O. S Wolfbeis, *Anal. Chem.* 74, 2663 (2002)
23. D. A Jackson and J. D. C. Jone, *Opt. Laser Technol.* 18, 199 (1986)
24. A. F. Mignani and F. Baldini, *IEEE J. Lightwave Technol.*, 13, 1396 (1995)

25. F de Fornel, *Evanescent wave from Newtonian Optics to Atomic Optics*, Springer (1997)
26. B. Culshaw, *Optical Fiber Sensing and Signal Processing*, Peter Peregrinus, London (1984)
27. B. Culshaw and J. P. Dakin, *Optical Fiber Sensors Vol.III*, Artech House, Boston (1996)
28. P. A. Payne, *J. Phys. E. Sci. Instrum.* 16, 947 (1983)
29. D. A. Jackson, *Meas. Sci. Technol.*, 5, 621 (1994)
30. Y. N. Ning, Z. P. Wang, A. W. Palmer and K. T.V. Grattan. *Rev. Sci. Instrum.*, 66, 3097 (1995)
31. F. Ansari, *Cement and Concrete Composites*, 19, 3 (1997)
32. D. A. Jackson, *J. Phys. E. Sci. Instrum.*, 18, 981 (1985)
33. E. Udd, *Fiber Int. Opt.*, 11, 319 (1992).



Chapter 2

EVANESCENT WAVE FIBER OPTIC SENSORS: TRACE DETECTION OF CERTAIN WATER CONTAMINANTS

This chapter describes the necessary theoretical background, design, fabrication and characterization of unclad evanescent wave fiber optic sensors (EWFS) and their application for trace detection and measurement of certain pollutants in water such as ammonia, nitrites and chromium. The superior performance of these sensors is established by comparing their performance in terms of lower detection limit, dynamic range etc, with that of the conventional spectrophotometric method. Efforts are made to reduce the size and cost of the sensors by using super-bright light emitting diodes (LED). Moreover, a novel cost effective technology for simultaneous detection of different contaminants in water is discussed at the end of this chapter.

2.1. Introduction

A detailed account of the various FOSs based on intensity modulation, phase modulation and polarization modulation and their application have been described in the previous chapter. Among the various FOSs, the intensity modulated sensors are easy to design and develop. In this chapter, the necessary theory, design, fabrication and characterization of novel intensity modulated evanescent wave fiber optic sensors (EWFS), and their applicability in monitoring the water contaminants such as ammonia, nitrites and chromium are discussed in detail.

2.2. Pollutants in water

Increasingly, ground water supplies are affected by the intrusion of toxic chemicals from industrial discharge, agricultural run-off, chemical spills, and leachate from landfills and leaking underground storage tanks. Moreover, the steep rise in the growth of various industries, with no regard for the environment, has resulted in pollution of every kind, which have become a major health hazard. In recent years, however, there is a growing concern regarding the pollution of our natural resources and efforts are being made to analyse and reduce the ill-effects of pollution.

The pollutants in water may be of different forms, which include organic content, phosphates, nitrogen compounds, heavy metal ions, complex anions, etc [1]. Organic contaminants (e.g. Biological oxygen demand, pesticides, etc.) enter water supplies through run off of precipitation, introduction of sewage and industrial waste, and accidental spills of industrial organic materials. Many organic species, including pesticides are very stable but they do not last forever. However, spillages of polychlorinated biphenyl (used in plastic, paints, rubbers, waxes) create problems to human beings because of the toxicity of these materials.

One of the many factors to be taken into account in considering the possibility of reclaiming water for industrial or portable use is the phosphate content. The phosphate content can arise from industrial effluents or from domestic sewage. Phosphates are a normal constituent of human excreta and not all is removed during

sewage treatment. Other sources are soaps, detergents and fertilizers. The phosphates can be present in several forms, the main classifications being orthophosphates, condensed phosphates and organically bound phosphates.

The total nitrogen content of water can be present in many chemical forms like ammonia, nitrite, nitrate, etc. Nitrogen is a constituent of proteins, chlorophyll and many other biological compounds. Upon the death of plants or animals, complex organic matter is broken down to simple forms like ammonia, nitrite, nitrate, etc. by bacterial decomposition. Other sources of nitrogen in aquatic systems include animal waste, fertilizer industries and waste water discharges. Nitrogen from these sources may be discharged directly into streams or may enter waterway through surface runoff or ground water discharge and cause serious problems to human health.

Sources of metal ion in natural water include effluent discharge from industry, oxidation and leaching of mine dumps, corrosion of metal surfaces, discharges from domestic and agricultural waste water, etc. All metals are soluble to some extent in water. While excessive amounts of any metal may present health hazards, only those metals that are harmful in relatively small amounts are labeled toxic; other metals fall into the nontoxic group. Toxic metals that may be dissolved in water include arsenic, barium, cadmium, chromium, lead, mercury, and silver. The nontoxic group includes iron, calcium, magnesium, sodium, manganese, aluminum, copper, zinc, etc.

The anions that may be dissolved in water are cyanides, chlorides, fluorides, sulphides, NTA (nitrilotriacetate), etc.

As explained, the ever-expanding industrialization and concomitant domestic waste generation causes the release of steadily growing number of pollutants into the environment. Therefore, a great deal of attention must be paid to the pollution of natural fresh water and seawater reserves. Standards for drinking water have evolved over the years as knowledge of the nature and effects of various contaminants have grown. It is considered desirable that drinking water be free of suspended solids and turbidity. In addition, it should be tasteless, odourless and dissolved inorganic solids

be in moderate quantities, and toxic substances and pathogens be absent. With further improvements in water quality standards, additional requirements may be added to this list, making drinking water quality requirements even more stringent.

2.3. Role of Evanescent wave Fiber Optic Sensors (EWFS) in water pollution monitoring

Pollutants in water present a major health hazard and their accurate estimation is very important in the process of pollution monitoring. Detection of these chemicals in water is usually made by atomic absorption spectrophotometry or colorimetric method. The procedure used in these methods is generally based on the formation of a colored complex species on the addition of specific chemical reagents corresponding to the required contaminant and by comparison of the intensity of color thus formed (which is related to concentration) [2]. However, this has many difficulties such as complex procedures required for measuring chemicals and the need for large and delicate instruments. Moreover, these techniques are not sensitive to lower concentrations of the contaminant, especially in the range of parts per billion (ppb).

In recent years, there has been a significant progress in the field of fiber optic sensors for the detection of various chemical species [3-7] and hence it is worthwhile to investigate the feasibility of this method to the above problem. Although most optical chemical sensors rely on conventional geometrical configurations, whereby light is incident directly on a miniature cell or on a layer of immobilized reagent located in free space or at the distal end of an optical fiber, significant advantages can be obtained by adopting an alternative approach based on evanescent wave interactions. Optical waveguide sensors for chemical and biological species based on such evanescent wave (EW) interactions have attracted considerable research interest. Compared to other sensing methods, evanescent wave sensing technique offers a number of advantages especially in chemical sensing applications [8-13].

1. Because the interrogating light remains guided, no coupling optics is required in the sensor region and an all fiber approach is feasible. Considerable

miniaturization possible with EW interaction has wide applicability in integrated optics.

2. The surface and bulk effects can be discriminated by using proper launch optics and thereby confining the EW field to the short distance from the guiding interface.
3. Fiber optic EW absorption devices are more sensitive than bulk-optic ATR (attenuated total reflection) crystals by virtue of the greater number of reflections per unit length.
4. Fiber Optic EW sensors is the most suitable to perform accurate absorption measurements on highly absorbing and highly scattering media because of the small effective path length.
5. If an optical fiber is configured to be sensitive to EW interactions all along its length or at discrete zones, then fully or quasi-distributed sensing is possible which allows the monitoring of spatial profile of an analyte concentration over substantial distances.
6. In contrast with conventional distal-face optrodes, the EW approach affords the sensor designer greater control over interaction parameters such as interaction length, sensing volume and response time.
7. By the invention of super bright light emitting diodes (LED) and highly sensitive photo detectors, EWFS offers significant cost reduction

2.4. Theoretical outline

Even though electromagnetic wave incident at the core-cladding interface of a multimode fiber at an angle greater than the critical angle undergoes total internal reflection, a small portion of the incident field penetrates into the cladding of the fiber. This field is called evanescent wave, which decays exponentially from the core-cladding interface and propagates parallel to the fiber axis as shown in figure 2.1. These waves can interact with chemical species surrounding the core region in which the cladding was removed. The absorption of evanescent wave by the chemical species surrounding the core region gives rise to a phenomenon called

attenuated total internal reflection (ATR) which in turn results in the reduction of the output power from the fiber.

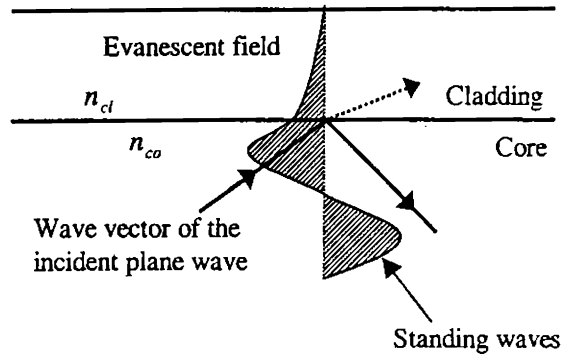


Figure 2.1 Illustration of exponentially decaying evanescent wave

In order to evaluate the expression for evanescent wave absorption, consider a cylindrical optical fiber of core radius a and diameter d having core refractive index n_{co} and cladding refractive index n_{cl} and the light radiation propagating along z -direction. Define the parameter U and W such that [14-16,38,39,40,41]

$$U = a(k^2 n_{co}^2 - \beta^2)^{1/2} \quad (2.1)$$

$$W = a(\beta^2 - k^2 n_{cl}^2)^{1/2} \quad (2.2)$$

where, β , is the propagation constant of any mode of the fiber which is limited within the interval $n_{co}k \geq \beta \geq n_{cl}k$ where $k = 2\pi/\lambda$. Thus, any mode can be expressed by a Bessel function $J(Ur/a)$ inside the core and a modified Hankel function $K(Wr/a)$ in the cladding. The quadratic summation [39]

$$V^2 = U^2 + W^2 \quad (2.3)$$

leads to a third parameter

$$V = (\pi d / \lambda)[n_{co}^2 - n_{cl}^2]^{1/2} \quad (2.4)$$

which is defined as the normalized frequency. By matching the fields at the core-cladding interface, the characteristic functions $U(V)$ or $W(V)$ for all the modes can be obtained and consequently the propagation constant and all other parameters of interest can be determined. The evaluation of exact solution of Maxwell's equation for the light propagation through a dielectric cylinder is complicated even with a simplified assumption of infinitely thick cladding. Hence a weakly guiding approximation is considered in which the parameter, $\Delta = \frac{(n_{co} - n_{cl})}{n_{cl}}$, is assumed to be much less than 1 so that Maxwell's equations are solvable in an optical fiber. Under such an approximation the various HE modes and EH modes can be considered as linearly polarized (LP) modes.

The transverse field components of light inside the fiber with respect to Cartesian co-ordinate system is given by

$$E_y = H_x \left\{ \begin{array}{l} Z_0/n_{co} \\ Z_0/n_{cl} \end{array} \right\} = E_l \left\{ \begin{array}{l} J_l(Ur/a) / J_l(U) \\ K_l(Wr/a) / K_l(W) \end{array} \right\} \cos l\phi \quad (2.5)$$

Here, as well as in the following equations the upper line holds for the core and lower line holds for the cladding: Z_0 is the plane wave impedance in vacuum and E_l is the strength of the electric field component at the interface. Since we have the freedom of choosing either $\sin l\phi$ or $\cos l\phi$ along with the choice of two orthogonal states of polarization, the construction of four modes for every l is possible as long as $l > 0$. For $l = 0$, only two orthogonally polarized modes are allowed.

The longitudinal field components can be obtained as

$$E_z = \frac{iZ_0}{k} \left\{ \frac{1/n_{co}^2}{1/n_{cl}^2} \right\} \frac{\partial H_x}{\partial y} \quad (2.6a)$$

$$\text{and } H_z = \left(\frac{i}{kZ_0} \right) \left(\frac{\partial E_y}{\partial x} \right) \quad (2.6b)$$

By substituting the values of H_x and E_y from (2.5), the expression for E_z and H_z are obtained in terms of Bessel and Henkel functions multiplied by factors U/ak and W/ak , respectively. However, from equation 2.1 and 2.2 it is clear that both U/ak and W/ak are of the order of $\Delta^{1/2}$, i.e., the longitudinal field components are negligibly small in comparison with transverse components. Hence it is approximated that the field inside an optical fiber are transverse with linearly polarized (LP) modes.

The characteristic equation, which matches all the tangential components at the interface of LP modes, is given by [40]

$$U \frac{J_{l-1}(U)}{J_l(U)} = -W \frac{K_{l-1}(W)}{K_l(W)} \quad (2.7)$$

The Bessel functions $J_l(U)$ are similar to harmonic functions since they exhibit oscillatory behavior for real k values. Hence, there will be m roots for a given l value and each value is representing an LP_{lm} mode.

The integration of the Poynting vector calculated from the cross product of transverse fields given in (2.5), over the cross-section of core and cladding leads to the power in the core and cladding as [37]

$$P_{core} = \left[1 + \left(\frac{w^2}{u^2} \right) \left(\frac{1}{k_l} \right) \right] \left(\frac{\pi a^2}{2} \right) \left(\frac{Z_0}{n_{co}} \right) E_l^2 \quad (2.8)$$

$$P_{clad} = \left[\left(\frac{1}{k_l} \right) - 1 \right] \left(\frac{\pi a^2}{2} \right) \left(\frac{Z_0}{n_{co}} \right) E_l^2 \quad (2.9)$$

$$\text{where } k_l = \frac{K_l^2(W)}{K_{l+1}(W)K_{l-1}(W)} \quad (2.10)$$

By ignoring the small difference between n_{co} and n_{cl} , the total power in a certain mode is given by

$$P_{total} = P_{core} + P_{clad} = \left(\frac{u^2}{v^2} \right) \left(\frac{1}{k_l} \right) \left(\frac{\pi a^2}{2} \right) \left(\frac{Z_0}{n_{co}} \right) E_l^2 \quad (2.11)$$

The fraction of the power flowing in the cladding for a linearly polarized (LP) mode of a step index optical fiber under the weakly guiding approximation

$$\eta_{lm} = \left(\frac{P_{clad}}{P_{total}} \right)_{lm} = \left(\frac{U^2}{V^2} \right) (1 - k_l) \quad (2.12)$$

where

$$(1 - k_l) \cong (V^2 - U^2 + l^2 + 1)^{-1/2} \quad (2.13)$$

A simple estimate of the fraction of the power flowing in the cladding, η , can be provided by considering a step-index fiber with a large V number. With the total number of modes given by $N \propto V^2/2$, equation (2.12) can be integrated to yield [38]

$$\eta = \frac{4\sqrt{2}}{3V} = \left(\frac{4}{3} \right) N^{-1/2} \quad (2.14)$$

For a fiber with $V = 100$, approximately 2% of the total power flows in the cladding and is therefore available for evanescent wave absorption, which occurs when the medium forming the cladding of the fiber absorbs light at the wavelength being transmitted. If the imaginary parts of the core and cladding refractive indices are small compared to the real parts, the power attenuation coefficient is given by

$$\alpha = (1 - \eta)\alpha_{co} + \eta\alpha_{cl} \quad (2.15)$$

where η is the fraction of power flowing in the cladding, α_{co} is the core bulk

absorption coefficient, and α_{cl} is the cladding bulk absorption coefficient. If the range of α_{cl} is small, then the power transmission through an optical fiber, having a lossy cladding can be approximated by the modified Beer-Lambert's law [37]

$$P(L) = P_0 \exp(-\gamma CL) \quad (2.16)$$

where L is the length of the lossy cladding or unclad portion of the fiber, P_0 is the power transmitted in the absence of an absorbing species, C is the concentration of the absorbing medium and γ is the evanescent wave absorption coefficient. Since $\gamma = \eta\alpha$, the above equation can be written as,

$$P(L) = P_0 \exp(-\eta\alpha CL) \quad (2.17)$$

where η is the fraction of the power transmitted through the cladding and α is the bulk absorption coefficient. The last equation is the basis of EWFS and since $\alpha = \alpha(\lambda)$, spectroscopic measurements using evanescent waves are possible.

2.5. Detection of dissolved ammonia in water

Free ammonia (i.e., ammonium salts) invariably originates from animal wastes and the amount detected can range from 0.02ppm (surface water) to 100ppm (in sewage discharge). Detection of these chemicals in water is usually made by atomic absorption spectrophotometry. However, there are so many other methods to find out the ammonia concentration in water as well as in air [17-29]. But, all these methods are not sensitive at lower concentrations of the contaminant, especially in the parts per billion (ppb) range. In recent years, there has been a significant progress in the field of fiber optic sensors for the detection of various chemical species and hence it is worthwhile to investigate the feasibility of this method to the above problem.

2.5.1. Chemistry

The same reaction that is used in colorimetric or spectrophotometric determination of ammonia [2] is employed in EWFS for measuring ammonia content in water. When Nessler's reagent ($K_2 [Hg L_4]$) is added to ammonia contained water,

the liberated ammonia reacts with the reagent fairly rapidly, but not instantaneously, to form an orange brown product, amido tri iodo dimercury(11), and the depth of colour of this colloidal solution is directly proportional to the ammonia concentration in water. The reaction may be represented as

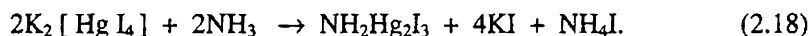


Figure 2.2 shows the absorption spectra of water samples containing different ammonia concentrations, in the wavelength range 400-700nm, recorded using a commercial Spectrophotometer (Jasco V -570). It can be seen that the absorption starts nearly at 700nm and peaks near the UV range. So light sources like lasers or LEDs having light emission in this range (eg: green or blue LEDs or laser) can be used to power the sensor.

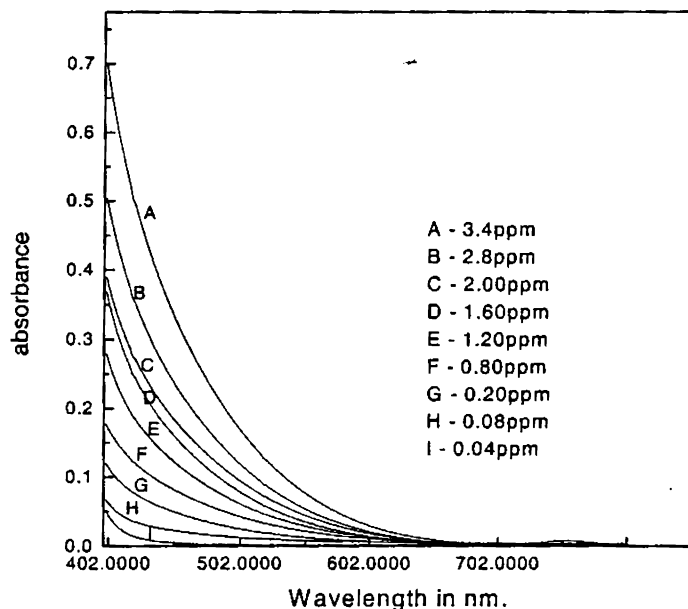


Figure 2.2. The absorption spectra of test solutions containing various concentrations of ammonia

2.5.2. Experimental

2.5.2.1. Preparation of the sensing element

Multimode, plastic clad silica fiber (200/380 μ m) is used for making the sensor element. In order to exploit the evanescent wave phenomenon in the multimode fiber, a known length (12cm) of the cladding at the middle portion of the fiber is chemically removed and this region acts as the sensing region. To avoid vulnerability of the exposed silica to surface cracking and other damage phenomenon, the removal of cladding is performed carefully with acetone, since it reacts only with plastic and not with silica and hence we get a smooth silica core.

2.5.2.2. Sensor cell

A sensor cell of 15cm length is designed for taking the water samples containing ammonia. It is made of cylindrical glass tube having a diameter of 3cm with inlet and outlet provisions. The optical fiber is introduced into the glass tube through the holes provided at the sides so that the unclad portion of the fiber is within the glass tube and remains straight.

2.5.2.3. Experimental set-up

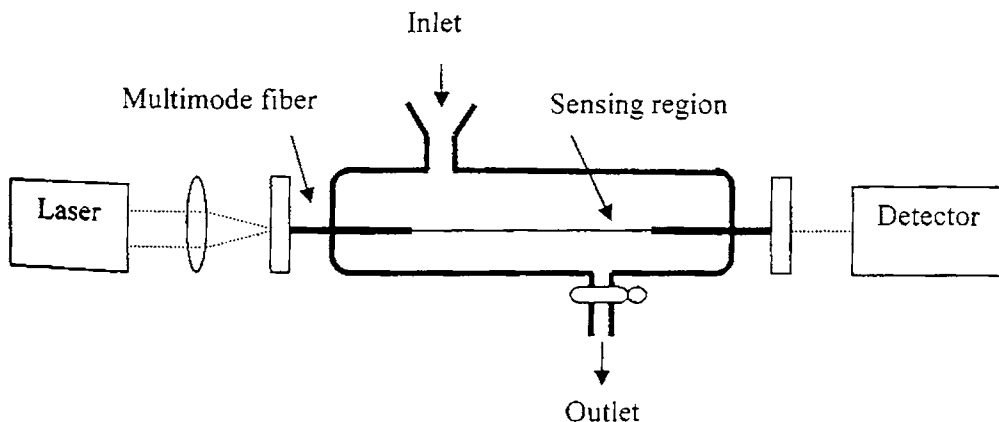


Figure2.3 Schematic diagram of the experimental set up

Schematic diagram of the experimental set-up is shown in fig.2.3. An Argon ion laser (Liconix 5000 series) emitting at 488nm is launched into one end of the fiber

using a short focal length lens. The light emerging from the farther end of the fiber is fed to a light detector unit (Digital Power Meter 45-545 , Metrologic make) which digitally displays the detected optical power. When the unclad portion of the fiber is immersed in test solution, the evanescent field penetrates into the liquid and interacts with it. Since the wavelength of light passing through the fiber is within the absorption band of the solution, evanescent wave absorption occurs and it increases with the increase in concentration of ammonia.

The laser provides a source of quasi-monochromatic, highly collimated, intense, coherent light but the overall system becomes bulky and expensive. However, in order to make the system more compact and cost effective, LED based EWFS has been designed using super bright blue LED and detectors employing pin photodiodes.

2.5.3. Design of LED based EWFS

2.5.3.1. Electronic Components:

The super-bright blue LEDs is purchased from RS Components, New Delhi and its dome is sword off and the remainder polished prior to use. The light source is modulated by using a standard 555 timer (NE 555). The pin photo detector, 13 DAH 001, is purchased from Melles Griot. The ICs 4016,4027 and 4017 are from Goldstar and the low noise operational amplifier (LF 356N) and monolithic sample and hold IC (LF398) are from National Semiconductors. The analogue divider AD 534JD is obtained from Analogue Devices.

2.5.3.2. Characterization of blue LED

The super-bright blue LED has a relatively wide emission band of about 80nm (full width at half maximum) and is centred at approximately 470nm. This wavelength is well suited for our experiment because the resultant solution of the chemical reaction between ammonia and Nessler's reagent has significant absorption at this wavelength. The output intensity of the LED is about two orders of magnitude higher than that of commonly used LEDs and is comparable to that of low intensity semiconductor lasers.

2.5.3.3. Block diagram

A schematic block diagram of the LED based experimental set up is shown in figure 2.4. The sensing element is fixed in the sensing arm and an identical piece of fiber is kept in the reference arm without removing the cladding. The square wave modulated light from the super bright blue LED is simultaneously guided through the sensing and reference arm fibers. Light from the two arms is detected separately by

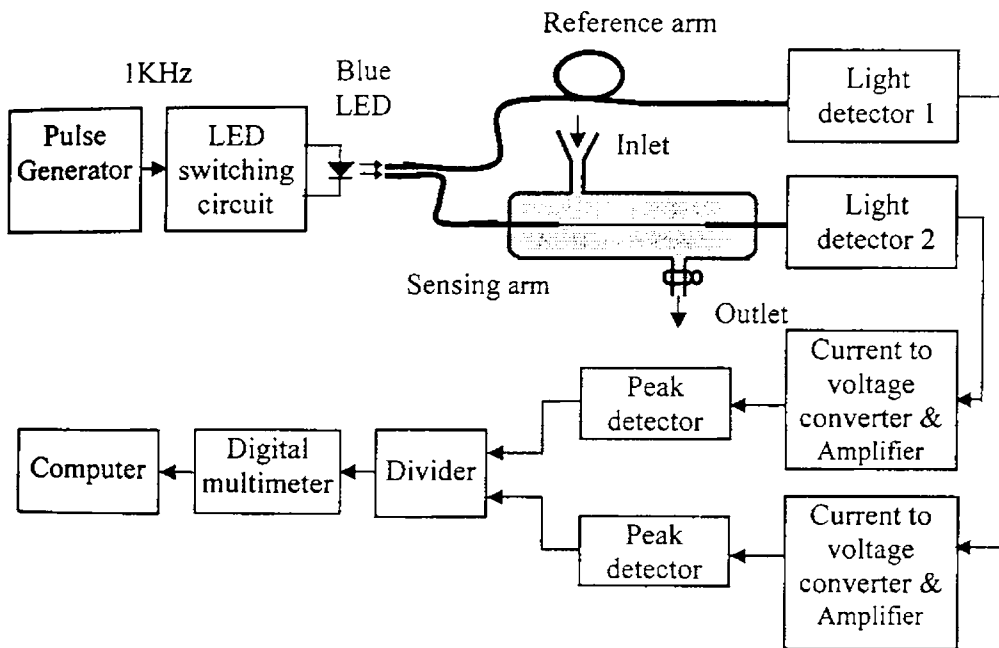


Figure 2.4. Schematic diagram of the LED based experimental set-up identical PIN photo detectors and the detected signals are processed separately. Finally, the ratio detector (divider) gives the ratio of the two processed signals. Since the two arms are driven from a single source, any power supply fluctuations or ambient variations cause equal effects on the sensing and reference arm signals and hence these effects will be nullified at the divider output.

2.5.3.4. Electronic circuitry

The electronic circuitry involved in the modulation as well as detection of light signals is shown in figure 2.5 and 2.6 respectively. The square wave modulator

for the LED is based on a standard NE 555 timer, which operates at 2KHz and its output is fed to a D flip flop 4027. Because of the frequency divided by two action of the D flip flop, we are getting a perfect 1KHz square wave signal with 50:50 duty cycle from its output. This signal is used to modulate the LED through a transistor (BD 139) switch.

The modulated light signals coming from the sensing and reference arms are detected separately using identical pin photo detectors. The outputs of each of the detectors are connected to operational amplifiers in the current to voltage converter mode followed by voltage amplification. In order to obtain the peak value of the amplified signals, the output of the amplifiers are fed to peak detectors whose outputs are the two inputs of the analogue divider AD534. The divider output gives the ratio of the signals coming from the sensing and reference arms. All the measurements are carried out using Lab VIEW. For this, the output of the analogue divider is connected to a digital multimeter (HP34410) which in turn is further interfaced to a computer loaded with Lab VIEW software using the GPIB (IEE488) cards.

2.5.4. Preparation of test solutions

Standard water samples having ammonia concentration ranging from 0.01ppm to 3.5ppm are prepared by dissolving ammonium chloride in ammonia free water [2], which is obtained by redistilling distilled water in a pyrex vessel containing one percentage each of potassium permanganate and anhydrous sodium carbonate. Standard ammonium chloride solution is prepared by dissolving 0.3141 gm of A.R. ammonium chloride dried at 100°C in ammonia free water and diluted to the required concentration with the same water. By adding suitable quantities of this stock solution in ammonia free water, test water samples with known concentration of ammonia are prepared. Then Nessler's reagent is added to each of these test samples (1ml. of Nessler's reagent to 50ml. of the test sample). Now, the colour of the samples become orange brown and the depth of colour varies with ammonia concentration in each of the water samples.

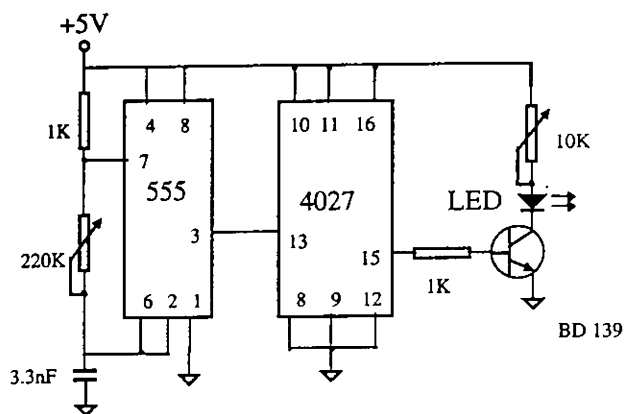


Figure 2.5. LED modulating circuit

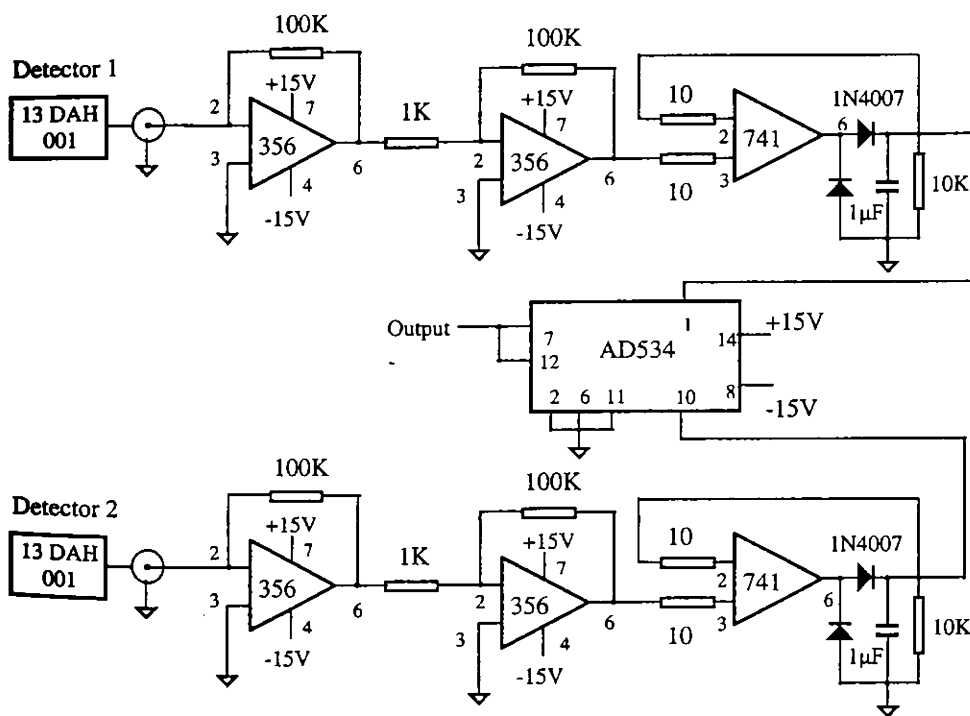


Figure 2.6. Light detection circuit

2.5.5. Results and Discussions

When the unclad portion of the fiber is immersed in the test solution, the evanescent field penetrates into the liquid and interacts with it. Since the wavelength

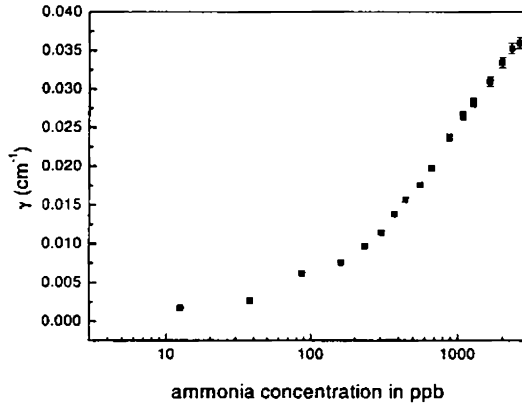


Figure 2.7 Variation of evanescent absorption coefficient on various ammonia concentrations at 488nm

of light passing through the fiber is within the absorption band of the solution, evanescent wave absorption occurs and it increases with the increase in concentration of ammonia. Figure 2.7 shows the variation of evanescent wave absorption coefficient with different ammonia concentrations in water at 488nm using Argon ion laser. It is evident from the plot that the present system can measure the dissolved ammonia content in water even from 0.01ppm. In addition, the sensor responds in a logarithmic fashion, which makes the device to cover a large dynamic range, though sacrificing its sensitivity at higher concentrations. The reason for the logarithmic response of the sensor is explained below.

The evanescent absorption coefficient in equation (2.17) can be rewritten as

$$\gamma = r_f \alpha_m \quad (2.19)$$

where r_f is the effective fraction of the total guided power in the sensing region and α_m is the bulk absorption coefficient of the absorbing species. The optical power transmitted through an optical fiber is distributed in different modes and hence r_f is proportional to the number of modes in the fiber. Since the different modal groups in a multimode fiber have different penetration depths, equation (2.17) can be modified as

$$P(L) = P(0)[\exp(-\gamma_1 CL) + \exp(-\gamma_2 CL) + \exp(-\gamma_3 CL) + \dots] \quad (2.20)$$

where γ_1, γ_2 and γ_3 are effective evanescent wave absorption coefficients corresponding to different modal groups having different penetration depths [31]. Fortunately, this kind of behavior makes it possible for the sensor to act in a logarithmic fashion with long dynamic range.

In order to evaluate the performance of the present EWFS system a standard spectrophotometer is employed (Model Jasco V -570). Figure 2.8 shows the variation

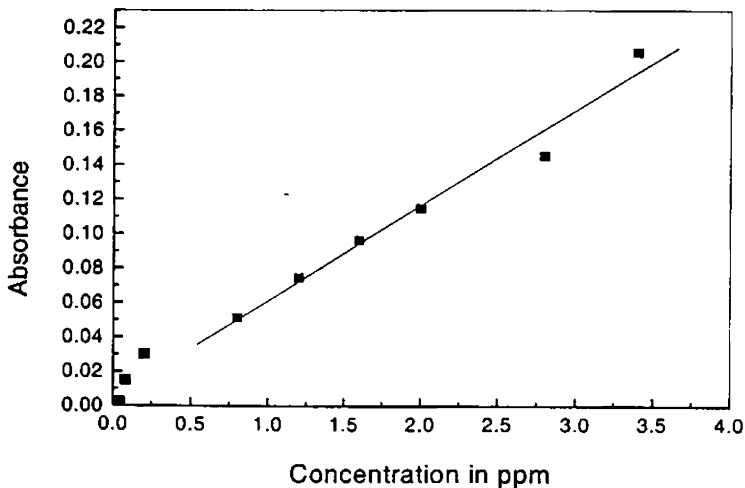


Figure 2.8 Variation of absorbance on ammonia concentrations at 488nm using standard spectrophotometer

of light absorbance with concentrations of ammonia recorded using spectrophotometer at 488nm wavelength. It is seen that the graph is linear only within the midrange of concentrations. At ammonia concentrations below 0.8ppm and above 3ppm, this method does not obey Beer – Lambert law. Comparison of figures 2.7 and 2.8 reveals that EWFS gives good linearity in the lower ranges of concentrations compared to the spectrophotometric method.

The experiment was repeated at 532 nm using Diode Pumped Solid State laser (DPSS - Nd: YVO₄, model BWT-50 of B&T TEK) and the sensor showed almost the same characteristic profile (figure 2.9) as shown at 488nm except for the reduced dynamic range. It is observed that, the lower limit of detection of the sensor

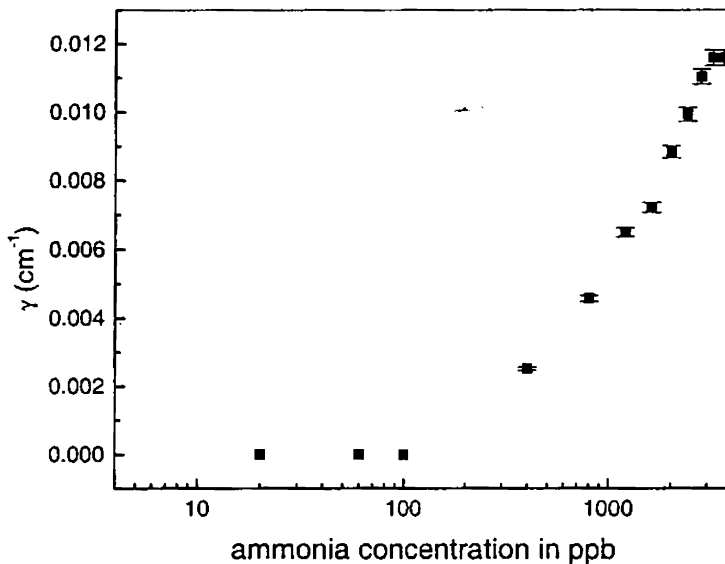


Figure 2.9. Variation of evanescent absorption coefficient on various ammonia concentrations at 532 nm

is shifted to 0.2 ppm at 532 nm instead of 0.01ppm at 488nm due to the lower absorption at 532nm compared to 488nm. Comparison of figure 2.7 and 2.9 shows that the value of evanescent absorption coefficient γ is lower at 532 nm, confirming the above observation.

In the case of LED based set up, the pin number 1 and 10 are respectively the denominator (X) and numerator (Z) inputs of the divider IC, AD 534 is designed in such a way that its out put (Y) from pin number 12 is $Y= Z / X$. As shown in the Figure 2.4 and 2.6, the peak detected signals corresponding to the sensing and reference arms are connected to denominator and numerator inputs respectively. Under idle condition (no samples in the sensing arm), the coupling between the LED and fibers is adjusted in such a way that almost equal amount of light passes through the sensing and reference arm fibers and the output is set to zero volt. During sample runs the output from the sensing arm decrease with increase in concentration of ammonia due to evanescent absorption in the unclad region and hence the output of the divider increases since the sensing arm is connected to the denominator input of the divider. Figure 2.10 shows the variation at the divider output with various concentrations of ammonia surrounding the unclad portion of the fiber in the sensor

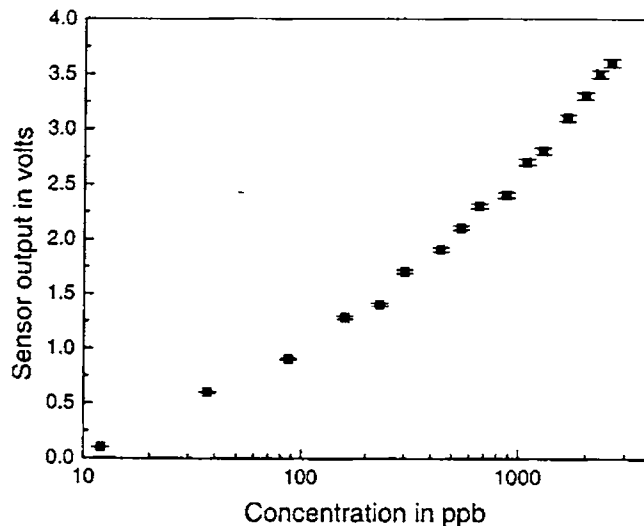


Figure 2.10. Variation of sensor output with various ammonia concentrations

arm. Comparison of figures 2.7, 2.9 and 2.10 shows that the sensor with LED and the inexpensive detector circuit is as sensitive as that obtained with the laser and an expensive detector. A comparative study of different ammonia sensing methods is shown in table 2.1.

It is also observed that after removing each of the standard ammonia samples from the sensor cell, the signal comes down almost to the initial values. This indicates the reversible nature of the sensing elements, which is an added advantage of the system because this eliminates the difficulty of replacing the sensor arm fiber after each measurement. The present EWFS also showed the same behavior after cleaning the unclad portion of the fiber with acetone for repeated measurements. Since evanescent field absorption is the key phenomenon in this setup, any minor changes to surface conditions of the fiber will affect the scale factor of the sensor. In order to avoid this, investigations are performed starting from low concentrations and the sensor cells are carefully cleaned between each sample run.

Sl. No.	Method		Lower detection limit	Dynamic range
1	Spectrophotometric method		800ppb	800-3000 ppb
2	Laser based FOEWS	Using Argon Iron laser emitting at 488nm	150ppb	10-2500ppb
		Using DPSS emitting at 532nm	400ppb	400-3000ppb
3	LED based EWFS		100ppb	100-2500 ppb

Table 2.1 Comparison of spectrophotometric & evanescent wave fiber optic method for measuring ammonia content in water

2.6. Detection of nitrites in water

Discharges from sewages, animal wastes and fertilizer industries lead to the accumulation of nitrogen compounds in water. The nitrogen content of water samples can be present in many chemical forms like nitrites, nitrates, ammonia etc. When nitrogenous matter is oxidized by the environment, the nitrogen remains mainly in the form of nitrite and nitrate. The presence of appreciable quantities of nitrite can be regarded as an indication of sewage contamination of recent origin. However, nitrite is oxidized to nitrate and hence the presence of large amount of nitrate points to an earlier sewage contamination [1]. Nitrite poisoning in infant animals including humans can cause serious problems and even death, because it has a greater affinity for hemoglobin than does oxygen and thus replaces oxygen in the blood complex. The body is denied essential oxygen and in extreme cases, the victim suffocates. Oxygen starvation results in a bluish discoloration of the body and hence, nitrite poisoning has been referred as blue body syndrome [31]. According to drinking water standards of World Health Organization, the drinking water should be free of nitrites. Hence, its accurate estimation is very important in the process of pollution monitoring.

The usual procedure used for the determination of nitrite in water is generally based on the formation of a colored complex species on the addition of specific chemical reagents and by comparison of the intensity of color thus formed, (which is related to concentration), with standards [2]. However, this has many difficulties such as complex procedures required for measuring chemicals and the need for large and delicate instruments. Moreover, these techniques are not sensitive to lower concentrations of the contaminant, especially in the range of parts per billion. However, evanescent wave fiber optic technology offers several advantages for chemical sensing over conventional methods and hence it is worthwhile to investigate the feasibility of this method to the above problem of nitrite pollution in water.

2.6.1. Chemistry

The same reaction, which is commonly used in colorimetric or spectrophotometric method, is employed in EWFS for measuring nitrite content in water [2]. In this reaction, the nitrite ion, under acidic conditions, causes diazotisation of sulphanilamide to occur, and the product is coupled with N- (1-naphthyl) ethylenediamine dihydrochloride to produce a violet coloration. The depth of color of this resultant solution is directly proportional to the nitrite concentration in water. Figure 2.11 shows the absorption spectra of water samples containing different nitrite concentrations in the wavelength range 400-800nm recorded using a commercial spectrophotometer (Jasco V-570). The absorption peak of the spectra is at around 545nm and the amount of absorption of light passing through the solution increases with the concentration of the colored constituent in the solution.

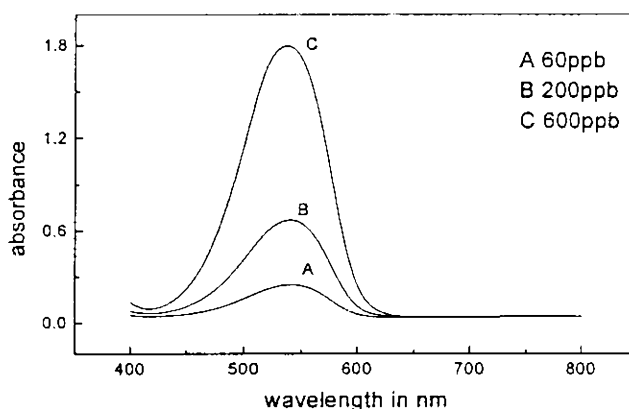


Figure 2.11. Absorption spectra of water samples containing various concentrations of nitrite

2.6.2. Experimental

Preparation of the sensing element, design of the sensor cell and the experimental set-up are the same as that of the evanescent wave fiber optic ammonia sensor already explained except the selection of light source. Since the absorption peak of the resultant solution of the chemical reaction between nitrite and the reagents

is around 545nm, the experiments are carried out using a He-Ne laser emitting at 543.5nm and super bright green LED emitting at around 558nm in laser and LED based EWFS respectively.

2.6.3. Preparation of test solutions

Standard water samples having nitrite concentration ranging from 1ppb to 1000ppb are prepared by dissolving sodium nitrite in water. Then sulphanilamide solution is added and after 5 minutes N- (1-naphthyl) ethylenediamine dihydrochloride solution is added to each of the prepared sample solutions such that the ratio is 50:1:1. Now, the color of the test solution becomes violet and its color intensity varies with nitrite concentration. These test samples are then allowed to remain for 10 minutes to complete the reaction after which the measurements are carried out. Standard nitrite solution, sulphanilamide solution and N- (1-naphthyl) ethylenediamine dihydrochloride solution are prepared by the same manner as in standard colorimetric or spectrophotometric method of detecting nitrites.

2.6.4. Results and Discussions

When the unclad portion of the fiber is immersed in the test solution, the evanescent field penetrates into the liquid and interacts with it. Since the wavelength of light passing through the fiber is almost close to the peak absorption wavelength of the solution, strong evanescent wave absorption occurs and it increases with the increase in concentration of nitrite. Figure 2.12 shows the light absorbance versus nitrite concentrations within the range 60ppb to 4000ppb at the peak absorption wavelength obtained from the spectrophotometer. It is clear that the graph is linear in the midrange of concentrations only. At nitrite concentration below 200ppb and above 1200ppb, the spectrophotometric plot does not show linear variation.

However, in the case of evanescent wave fiber optic sensor using a He-Ne laser emitting at 543.5nm as source, the variation of evanescent wave absorption coefficient is linear even from 1ppb to 1000ppb of nitrite concentration as shown in Figure 2.13. The sensor responds in a logarithmic fashion, which enables the device

to cover large dynamic ranges. Comparing figures 2.12 and 2.13, it is evident that the EWFS gives a good sensitivity and increased dynamic range in the lower range of concentrations compared to spectrophotometric method.

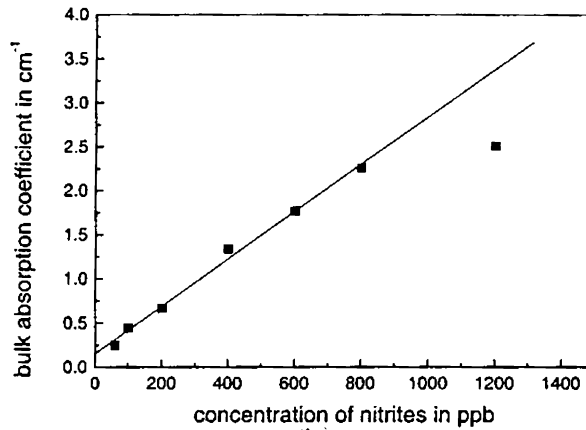


Figure 2.12. Variation of bulk absorption coefficient at the peak absorption wavelength (545nm) with respect to nitrite concentration using spectrophotometric method

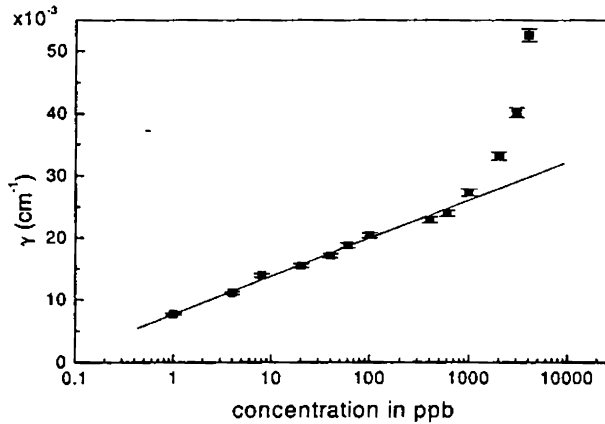


Figure 2.13. Variation of evanescent absorption coefficient nitrite concentration using a He-Ne Laser emitting at 543.

Figure 2.14 shows the variation of evanescent absorption coefficient with concentration using white light as the source instead of a laser. In this case, light from a 50W tungsten halogen lamp is coupled to one end of the fiber using a short focal length lens. At the farther end, the light from the fiber is focused to a monochromator (McPherson UV 275) tuned at 543.5nm and detected using a photomultiplier tube. Here, the nature of the graph is the same as that of figure 2.13, but the dynamic range is limited.

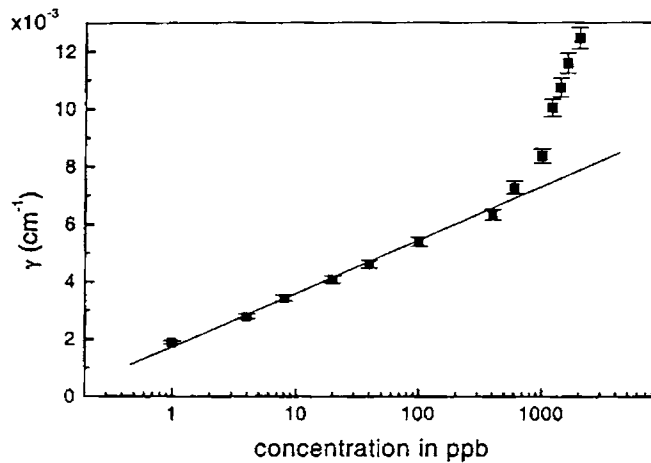


Figure 2.14 Variation of evanescent absorption coefficient with nitrite concentration using white light

Comparison of figure 2.13 and 2.14 reveals that the variation of γ is less when white light is used as the source. It is also observed that the linear range of the sensor is reduced to around 600ppb instead of 1000ppb when white light is used as the source. This is due to the fact that the deviation from perfect Beer- Lambert law increases as the bandwidth ($\Delta\lambda$) of the incident beam increases and is particularly severe when $\Delta\lambda$ is greater than the spectral width of the absorption band of the absorbing species. This results in a sensitivity, which falls off with concentration and

a consequent reduction in the useful measurement range [32,33]. To avoid this, the bandwidth of the incident beam should be very narrow, ideally approximating monochromatic radiation, which is justified by the results obtained using laser source (figure 2.13). It may be noted that in both cases the absorption increases steeply beyond 1000ppb, presumably due to the formation of strongly absorbing aggregates and complexes in the solution, which significantly alters the optical properties of the medium [32].

Figure 2.15 shows the variation of output voltage with concentration for various concentrations of nitrite surrounding the unclad portion of the sensing element in the case of LED based FWFS. Here in the detecting part of the electronic circuitry (figure 2.6), the peak detected signals corresponding to the sensing and reference arms are connected to numerator (Z) and denominator (X) inputs of the divider IC (AD 534) respectively. Since the out put (Y) from pin number 12 is $Y = Z/X$, the sensor outputs decrease with increase in concentration of nitrite. This sensor can measure nitrite concentration from 4 ppb to 1000 ppb, which is comparable with the existing detection limit of nitrite in water.

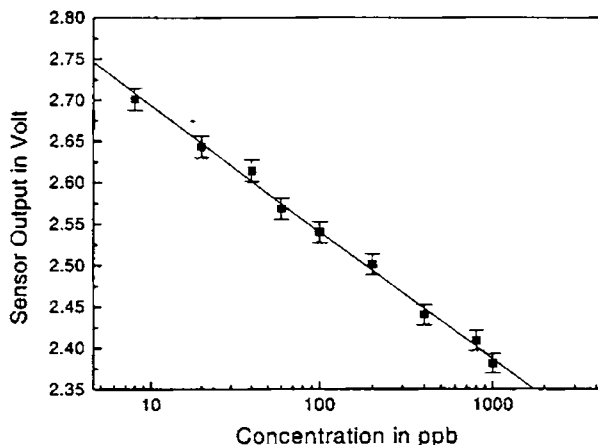


Figure 2.15 Variation of output voltage with nitrite concentration using green LED

The temporal response of the device to various concentrations of nitrite is measured by taking the readings continuously in block data collection mode of Lab VIEW as shown in figure 2.16. The valleys in the graph (k) correspond to the removal of test solutions from the sensor cell and shows that the signal has come down almost to the previous valley region after removing each of the standard test solutions from the sensor cells. This indicates the reversible nature of the sensing element [34]. In addition, the regions 'a' and 'i' of the plot indicate the signal strength corresponding to 4ppb concentration of nitrite sample, before and after a series of concentration measurements from lower to higher concentrations. It can be seen that the signal strengths are almost the same in both the cases. This reversible nature of the sensing element eliminates the difficulty of replacing the sensing fiber after each measurement. In order to avoid any minor changes to surface conditions of the fiber, investigations are performed starting from low concentrations and the sensor cell and the unclad portion of the fiber are carefully cleaned between each sample run.

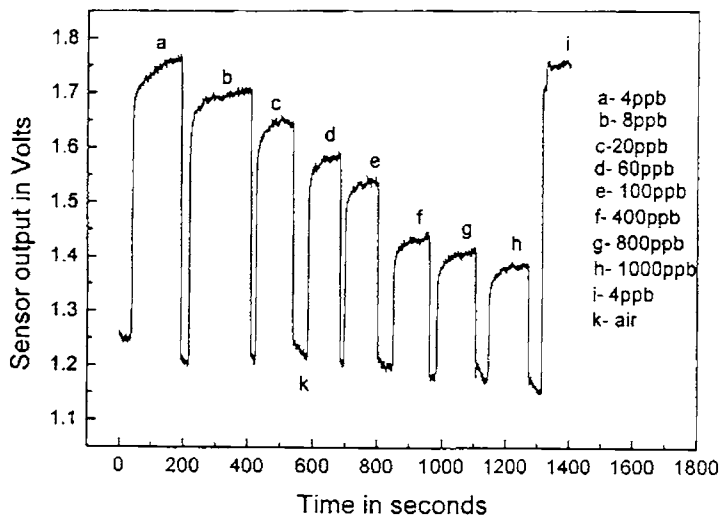


Figure 2.16 Response of LED based EWFS to different concentrations of nitrite

The response time, the time required for the readings to get stabilized, is also measured. To estimate the response time, the sensor is subjected to only one cycle of 100ppb of nitrite sample in the sensor cell and the responses are recorded separately on an extended time scale setting. It is observed that the response time is approximately 2 minutes. However, 3 seconds only are required to reach 90% of the stabilized reading.

Table 2.2 gives a comparative study of different nitrite sensing methods. From the table it is clear that LED based EWFS possesses almost same dynamic range as that of laser based EWFS and shows good performance in the lower ranges of concentration compared to spectrophotometric method. In addition, it is simple, compact and low cost as the circuitry is based on easily available and inexpensive opto-electronic components.

Sl. No:	Method		Lower detection limit	Dynamic range
1	Spectrophotometric method		60ppb	60-1200ppb
2	Laser based EWFS	Using He-Ne Laser emitting at 543.5nm	1ppb	1-1000ppb
		Using White light	1ppb	1-600ppb
3	LED based EWFS		4ppb	4-1000ppb

Table 2.2 Comparison between Spectrophotometric & Fiber optic Evanescent wave methods for measuring nitrite content in water

2.7. Detection of chromium in water

Chromium is one of the toxic metal ions, a trace amount of which dissolved in water is harmful to humans and other organisms. It is usually used in tanning industries for the processing of leather and the ground water supplies are affected by chromium discharges from these industries and can cause liver and kidney damages. According to drinking water standards of World Health Organization, the maximum limit of chromium in water is 50ppb [31]. Detection of these chemicals in water is

usually made by atomic absorption spectrophotometry. However, this method is not sensitive at lower concentrations of the chromium, especially in the parts per billion (ppb) range as in the case of nitrite and ammonia sensing. Hence, a low cost LED based EWFS is designed, fabricated and tested for this propose.

2.7.1. Experimental

Standard water samples having different chromium concentrations are prepared by dissolving potassium dichromate in water. The reagents used for the experiment are 0.25 percent solution of diphenylcarbazide $[\text{CO}(\text{NH}-\text{NH} \text{C}_6\text{H}_5)_2]$ in 50 percent acetone and 3M sulphuric acid. When sufficient quantities of 3M sulphuric acid, diphenylcarbazide solution and water are added to each of the prepared sample solutions of chromium, the color of the test solution becomes violet and the depth of color varies with chromium concentration.

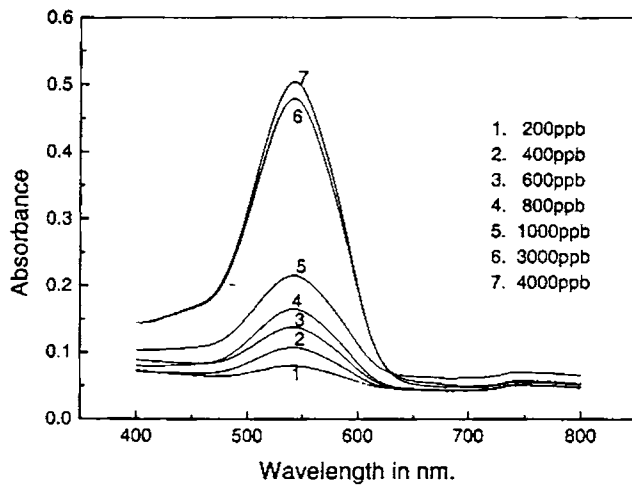


Figure 2.17 Absorption spectra of water samples containing different concentrations of chromium

Preparation of the sensing element and design of the sensor cell are same as that of the evanescent wave fiber optic ammonia and nitrite sensors already explained. Figure 2.17 shows the absorption spectra of water samples containing different chromium concentrations, in the wavelength range 400-700nm, recorded

using a commercial Spectrophotometer (Jasco V –570). It can be seen that the peak of the absorption spectra of the resultant solution of chromium is at 540nm and hence a super bright green LED with a wide emission band of about 80nm (full width at half height) and emitting at a peak wavelength of 558nm is selected to power the sensor.

The experimental set up, electronic circuit for LED modulation and light detecting circuit are the same as shown in figures 2.4, 2.5 and 2.6 respectively except a slight modification in the detecting part. Just like in LED based EW nitrite sensor, the peak detected signals corresponding to the sensing and reference arms are connected to numerator (Z) and denominator (X) inputs of the divider respectively.

2.7.2. Results and Discussions

When the unclad portion of the fiber in the sensing arm is immersed in the prepared sample solution, the evanescent field penetrates into the liquid and interacts with it. Since the wavelength of light passing through the fiber is almost close to the absorption peak of the solution, evanescent wave absorption occurs and it increases with the increase in concentration of chromium. Figure 2.18 shows the variation of

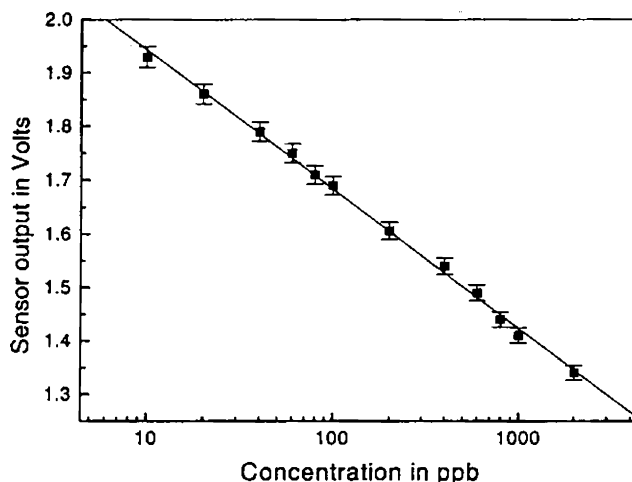


Figure 2.18 Variation of sensor output on various chromium concentrations in water

output voltage for various concentrations of chromium surrounding the unclad portion of the fiber in the sensor arm. The curve clearly shows that the present instrument can measure even a fraction of a ppb, which is comparable with the existing detection limit of chromium. In addition, similar to EWFS for ammonia and nitrite, this sensor also responds in a logarithmic fashion, which enables the instrument to cover a large dynamic range. Nevertheless, this is not the case with conventional spectrophotometric method, which obeys the perfect Beer- Lambert law. It is observed that, in the case of chromium detection using spectrophotometric method, the lower detection limit is around 200ppb, which is well above the permissible level of the chromium in water [35].

The instrument response to various concentrations of chromium are measured using Lab VIEW and is shown in figure 2.19. It is obvious from the figure that the

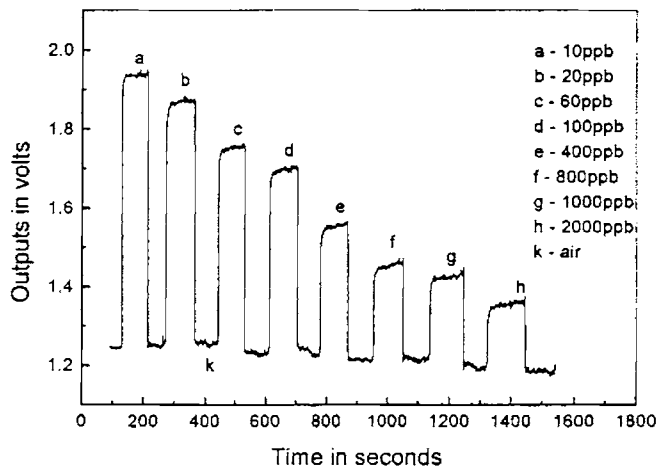


Figure 2.19 Response of the sensor to different concentrations of chromium in water

signal levels are high and is about 1.94V for 10ppb of chromium. The response time, the time required for the readings to get stabilized, is measured by taking the readings continuously in block data collection mode of Lab VIEW and the observed response time is approximately 2 minutes. However, only 3 seconds are required to reach 90%

of the stabilized reading.

It is also observed that after removing each of the standard chromium samples from the sensor arm, the signals come down almost to the initial values. This indicates the reversible nature of the sensing element, which is an added advantage of the system because this eliminates the difficulty of replacing the sensor arm fiber after each measurement. The present EWFS also showed the same behavior after cleaning the unclad portion of the fiber with acetone for repeated measurements. Since evanescent field absorption is the key phenomenon in this setup, any minor changes to surface conditions of the fiber will affect the scale factor of the sensor. In order to avoid this, just like in EW nitrite and ammonia sensors, investigations are performed starting from low concentrations and the sensor cells are carefully cleaned between each sample run.

Table 2.3 shows a comparative study of this sensor with the existing spectrophotometric method and it is clear that LED based EWFS has superior performance in terms of lower detection range, cost, size etc.

Sl.No:	Method	Lower detection limit	Dynamic range
1	Spectrophotometric method	200ppb	200-2500ppb
2	LED based EWFS	10ppb	10-2000ppb

Table 2.3 Comparisons between Spectrophotometric and LED based fiberoptic evanescent wave methods for measuring chromium content in water

2.8. Simultaneous detection of nitrite and chromium content in water

2.8.1. Design

A schematic block diagram of the instrument is shown in the figure 2.20. Separate and identical sensor cells made of glass, each of 15cm length and 3cm diameter, are designed for containing the standard water samples of chromium and nitrite respectively. Identical sensing elements (200/380 μ m multimode, plastic clad silica fibers with 12cm length of the of the cladding at the middle portion of the fibers

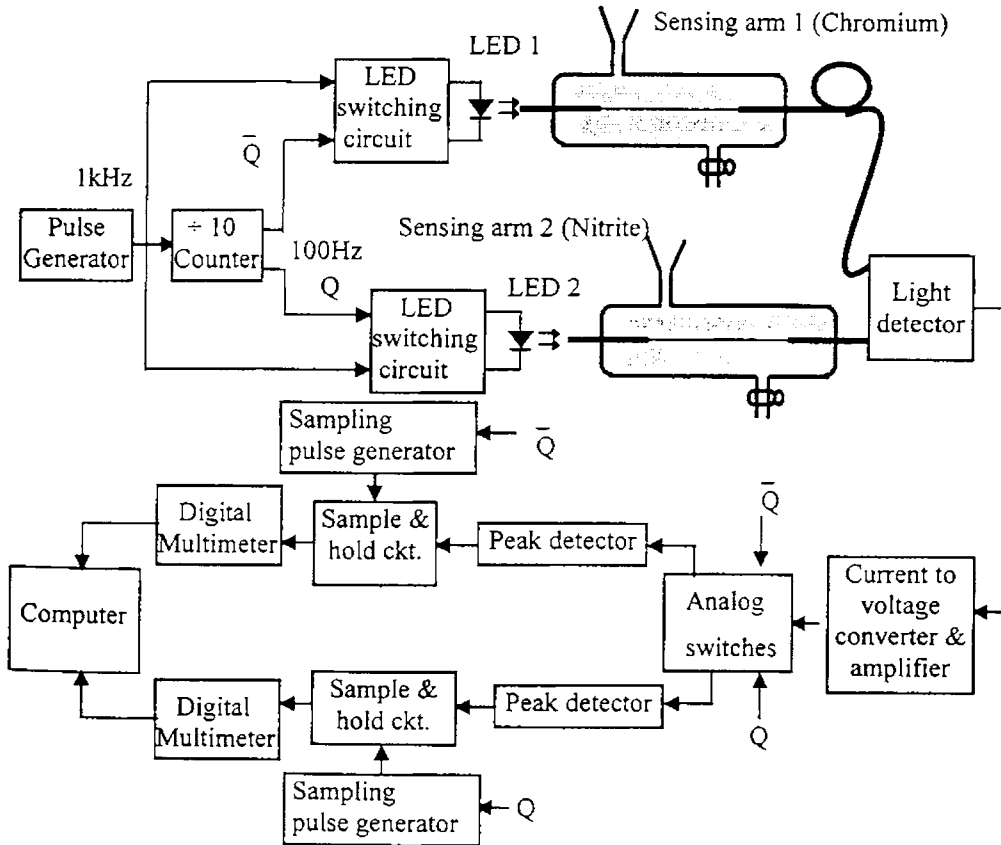


Figure 2.20 Experimental set-up for the simultaneous detection of chromium and nitrite content in water

chemically removed) are fixed in the sensor cells of chromium and nitrite respectively. The square wave modulated light from two identical super-bright green LEDs emitting at a peak wavelength of 558nm are coupled to the sensing arms 1 and 2 through the sensing fibers as shown in figure 2.20.

The electronic circuits used for the modulation of the LEDs and the detection of light from the two arms are shown in figures 2.21 and 2.22 respectively. The square wave modulator for LEDs is based on a standard NE555 timer, which operates at 2kHz. Its output is passed through a D-flip flop (CD4027) in order to achieve a perfect 1kHz signal with 50:50 duty cycle and this signal along with two timing signals are used for generating the modulating signals for the two LEDs. The timing signals Q and \bar{Q} of 100Hz each with opposite phases are derived from the same 1kHz signal by using a divide by 10 counter (CD4017). These timing signals and the 1kHz signal are then fed to the inputs of two AND gates (7408). The two outputs from the AND gates are of the same nature but opposite phase, which enable the LEDs to modulate at 1kHz on a time-sharing basis.

The light signals from the two sensing arms are detected by the PIN photodiode (13 DAH001) and its output is connected to a current to voltage converter followed by an amplifier. After sufficient amplification, the detected signal is fed to two analog switches (CD4016) along with the synchronizing timing signals Q and \bar{Q} from the transmitting side for separating the outputs received from the two sensing fibers. Peak value of the signals are obtained from the peak detectors followed by the sample and hold circuits (LF398). A sampling pulse generator (74121) provides a monoshot sampling pulse of 0.1ms for the sample and hold circuit. The outputs of the sample and hold circuits are connected to digital multimeters (HP34410) which are interfaced to a computer using the GPIB (IEE488) cards. Figure 2.23 shows the output waveforms of the various stages of the electronic circuits shown in figures 2.21 and 2.22.

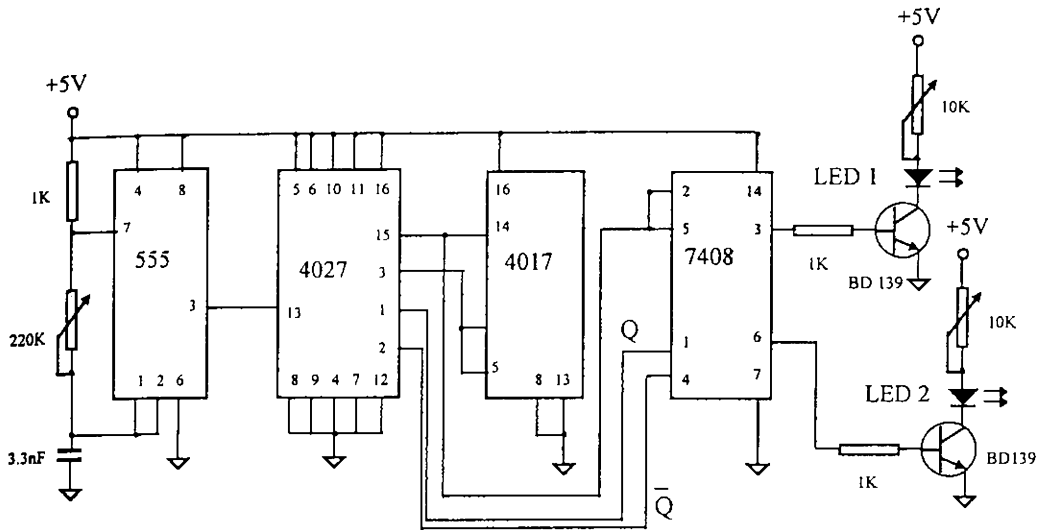


Figure 2.21 Modulating circuit of LEDs

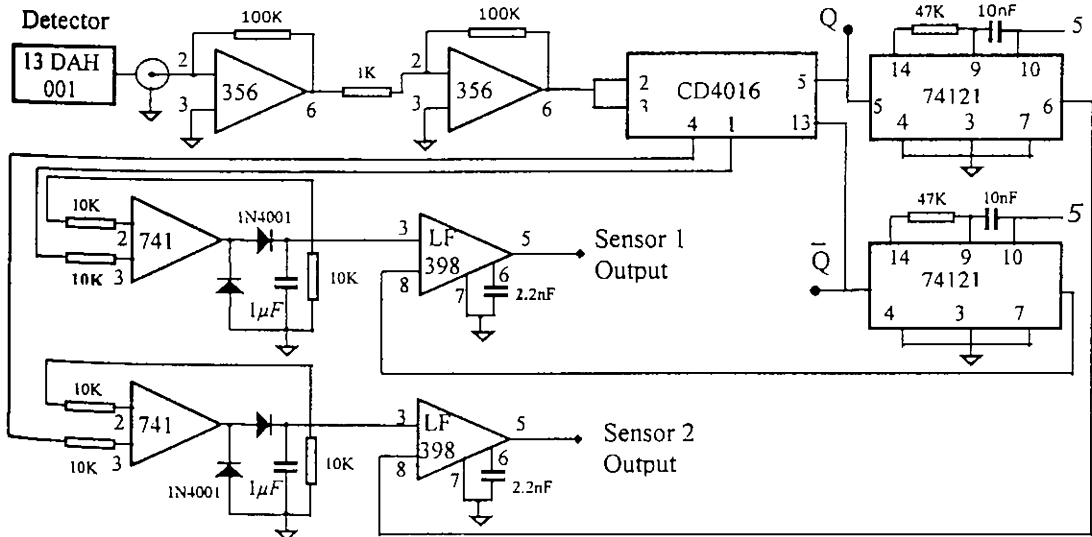


Figure 2.22. Circuit used for processing the light signals from the two sensing arms

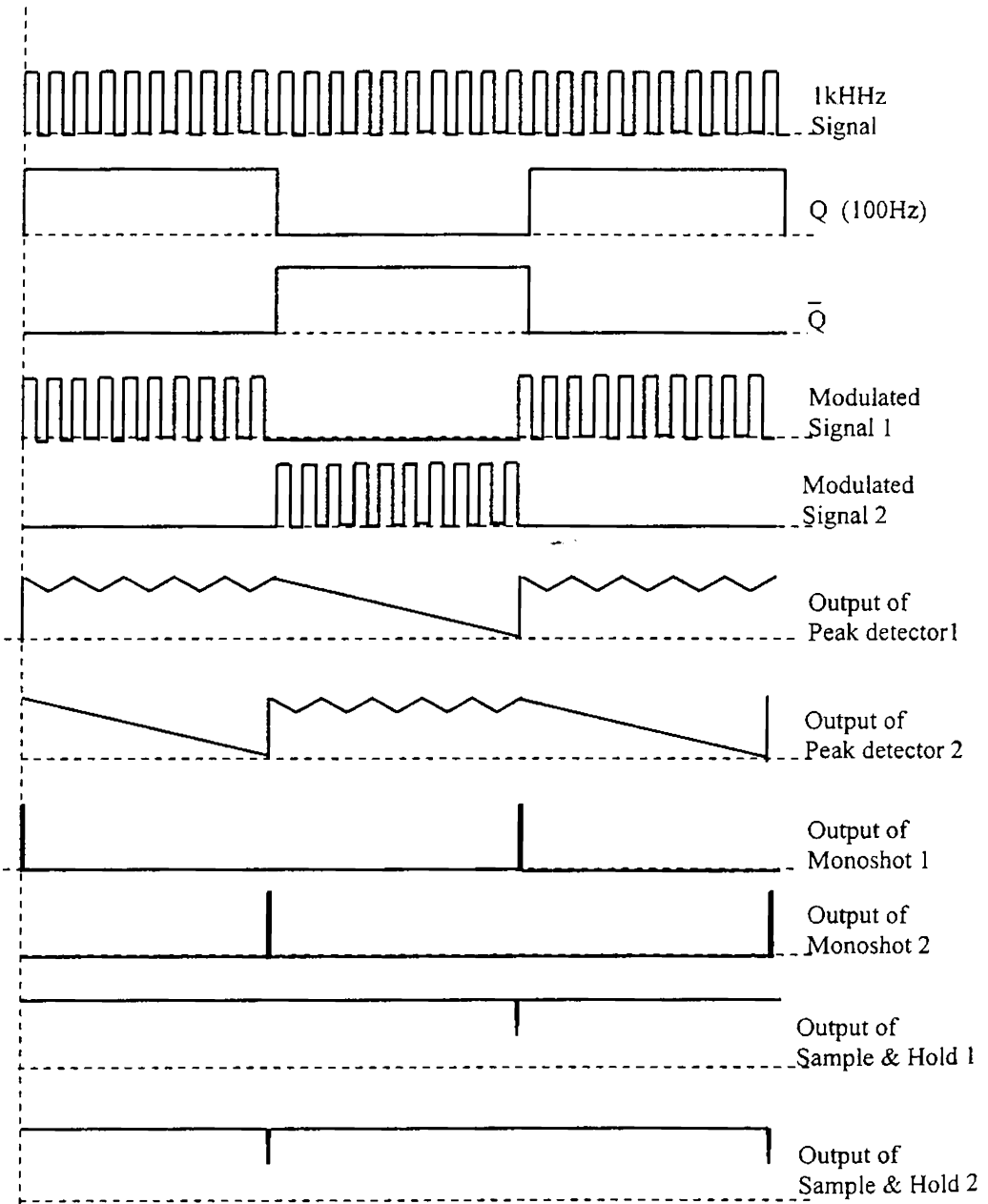


Figure 2.23 Output waveforms of various stages of the electronic circuit

2.8.2. Results and Discussions

Figure 2.24 shows the variation of output voltage for various concentrations of chromium surrounding the unclad portion of the sensing element in the chromium sensor cell and that of nitrite in the nitrite sensor cell of the device respectively. The curves clearly show that the present instrument can measure even a fraction of a ppb, which is comparable with the existing detection limit of chromium and nitrites [36]. It is worth noting here that a linear variation is observed from 10ppb to 2000ppb and 4ppb to 1000 ppb respectively for chromium and nitrite concentrations in water.

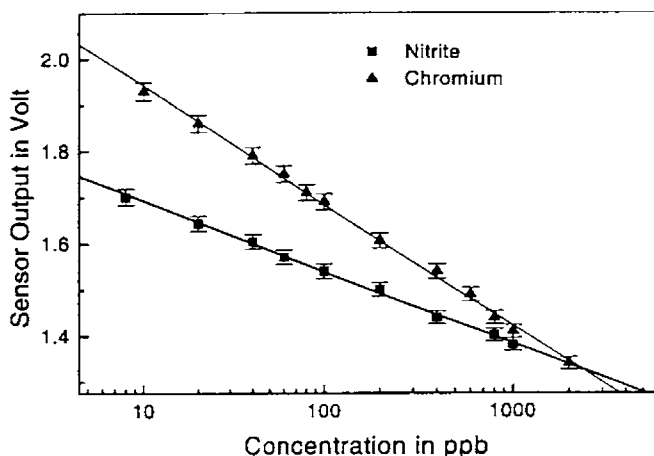


Figure 2.24. Variation of output voltages of sensor arms land 2 with respect to concentrations of chromium and nitrite respectively

In conclusion, this EWFS can be used for sensitive measurements of trace amounts of chromium and nitrite content in water simultaneously with good dynamic range. This sensor is simple, compact and low cost as the circuitry is based on easily available and inexpensive opto-electronic components. The same device can also be used to measure other contaminants in water by simply replacing the LEDs in accordance with the absorption spectra of the selected species. Moreover, with slight modifications in the LEDs switching side and detector part of the electronic circuits,

this device can be used for the simultaneous measurement of many contaminants in water.

2.9. An alternate design of LED based EWFS

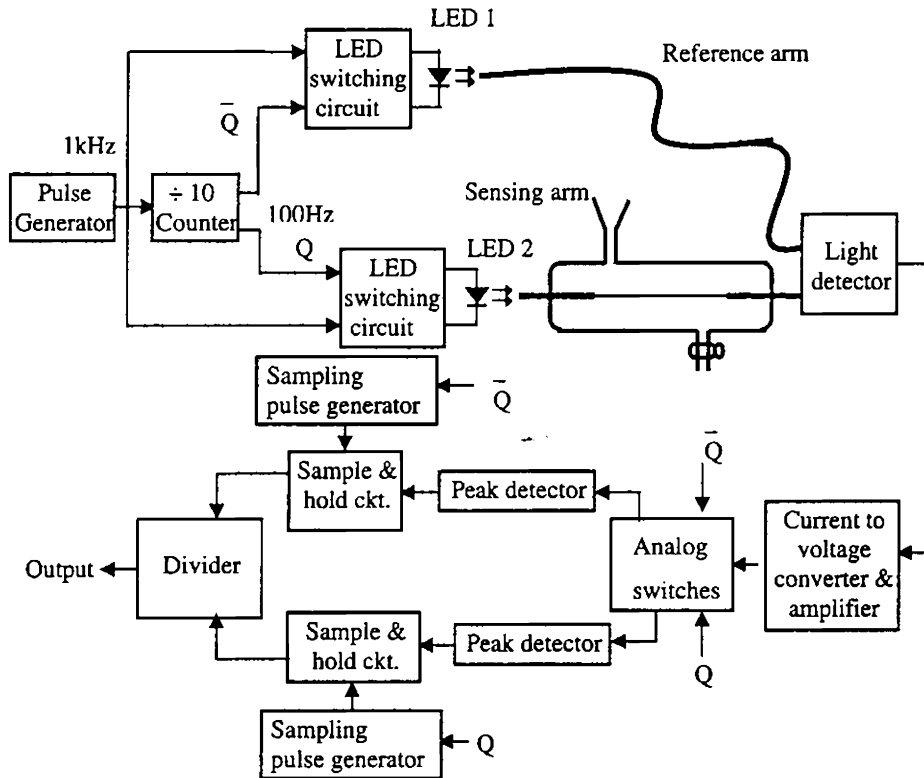


Figure 2.25 An alternate LED based experimental set-up for the detection of pollutants in water

In continuous analogue measurement applications of intensity modulated FOS, there is a requirement that the output from the system should be truly related to the measurand alone. In practice, this condition cannot be easily satisfied due to the variable losses within the optical components such as fiber leads, optical couplers and connectors. In LED based sensors additional measurement unreliability can arise from the instability of the optoelectronic components such as optical sources and

detectors. It is impossible to eliminate these variations in any optical fiber system design but compensation may be applied for the undesirable optical signal losses. The usual approach is to generate a reference signal which may then, in conjunction with the measurand signal, be used to make a relative measurement that is free from these so called common mode variations. The EWFS already explained for the detection of ammonia, nitrite and chromium, the measurand (sensing) and reference arms are fed from a single source and detected separately. The ratio of these detected signals eliminate common mode variations except the detector fluctuations.

In order to eliminate the detector fluctuations, an alternate design can be used where the sensing and reference arms are fed from separate and identical optical sources and detected by using a single detector on a time-sharing basis. A detailed block diagram of this approach is shown in figure 2.25. The electronic circuitry for the modulation of the LEDs and the detection of the signals are same as those shown in figure 2.21 and 2.22 respectively except a slight modification in the detector part. Here, the sample and hold outputs of the sensor and reference arm signals are fed to the two inputs of a divider IC (AD 534) and its output provides the ratio of the two signals. The performance of this setup has been carried out and it shows the same behavior as that of EWFS with single LED and two separate detectors to process the reference and sensing arm signals.

References

1. William F. Pickering, Pollution evaluation – the quantitative aspects, Environmental Science and Technology Series, Volium2, Marcel Dekker, Inc. New York.
2. J. Basset, R.C. Denney, G. H. Jeffery and J. Mendham, Vogel's textbook of Quantitative inorganic analysis, Longman Group Limited, London (1978).
3. W. Rudolf Seitz, Analytical chemistry, 56(1), pp.16A(1984).
4. Kathleen M. Leonard, Sensors and Actuators B (24-25), pp.458-461 (1995).
5. J. Burck, J.P. Conzen, B. Beckhaus and H. J. Ache, Sensors and Actuators B (18-19),295 (1994).
6. Alan Rogers, Meas.Sci.Technol. 10, R75 (1999).
7. Stanley M. Klainer, Johnny R. Thomas and John C. Francis, Sensors and Actuators B ,11, 81(1993).
8. P. Radhakrishnan, V.P.N. Nampoori and C.P.G. Vallabhan, Optical Engineering, 32, 692 (1993).
9. Brain D. McGrath, Optical Fiber Technology, Edited by K.T.V.Grattan and .T. Meggitt, vol.4, (1998), Kulwer Academic Publishers, London.
10. B. D. Guptha and S.K. Khijwania, Fiber and integrated Optics, 17, 63(1998).
11. Shelly John M, Evanescent wave fiber optic sensors: Design, fabrication and characterization, PhD thesis, cochin university of science and technology.
12. Thomas Lee S, Jose Gin, V. P. N. Nampoori and C. P. G. Vallabhan, N V Unnikrishnan and P. Radhakrishnan, J.Opts: Pure Appl. Opt, 3, 355(2001)
13. B. D. Gupta and D.K. Sharma, Elsevier Science Optics Communications, 140, 32 (1997).
14. Philip H Paul and George Kychakoff, Appl. Phys. Lett. 51, 12 (1987).
15. D Gloge, Appl. Opt.10, 2252(1971).
16. Thomas Lee S, Design, fabrication and characterization of fiber optic sensors for physical and chemical applications, PhD thesis, cochin university of science and technology.
17. A. Galdikas, A. Mironas, V. Strazdiene, A. Setkus, I. Ancutiene and V. Janickis, Elsevier Science Sensors and Actuators B 67, 76(2000).
18. R. P. Gupta, Z. Gergintschew , D. Schipanski and P.D. Vyas, "YBCO-FET room temperature ammonia sensor," Elsevier Science Sensors and Actuators B 63, 35(2000).
19. Zhe Jin, Yongxuan Su and Yixiang Duan, Elsevier Science Sensors and Actuators B, 72 , 75 (2001).
20. Otto. S. Wolfbies and Hermann. E. Posch, Analitica Chimica Acta, 185, 321 (1986).
21. M. Mascini and C.Cremisini, Anal. Chim. Acta, 92, 277(1977)
22. W.N. Opdycke, S. J. Parks and M .E. Meyerhoff, Anal. Chim. Acta, 155, 11(1983)
23. Y. Fraticelli and M.E. Meyerhoff, Anal. Chem., 53, 992(1981)

24. J. D. Joseph, *Anal. Chim. Acta.*, 168,249(1985)
25. S. B. Brondman and M. E. Mayerhoff, *Anal. Chim. Acta.*, 162,363(1984)
26. D. C. David, M.C. Willson and D.S. Ruffin, *Anal. Lett.*, 9,389(1976)
27. P. L. Smock, T. A. Orofino, G. M. Wooten and W. S. Spencer, *Anal. Chem.*, 51,505(1979)
28. J. F. Giuliani, H. Woltjen and N. L. Jarvis, *Opt. Lett.*, 8,54(1983)
29. Wolfbeis, H. E. Posch and H. W. Kroneis, *Anal. Chem.*, 57,2556(1985).
30. P. Suresh kumar, C. P. G. Vallabhan, V. P. N. Nampoori and P. Radhakrishnan, *Proc. SPIE*, 4946,166 (2003)
31. Howard S Peavy, Donald. E. Rowe and George Tchobanoglous, *Water quality: Definition, Charecteristics, and Perspecives*, Chapter2 in *Environmental Engineering*, 1985,Mc Graw Hill Book Compony.
32. Brain D. MacCraith, *Optical fiber chemical sensor systems and devices*, chapter 2 in *Optical Fiber Technology*, Edited by K.T.V.Grattan and B.T.Meggitt, vol.4, (1998), Kulwer Academic Publishers, London.
33. B.D. Guptha, Chandra Deep Singh and Anurag Sharma, *Optical Engineering*, 33,1864 (1994).
34. P. Suresh kumar, C. P. G. Vallabhan, V. P. N. Nampoori, V N Sivasankara Pillai and P. Radhakrishnan, *Journal of optics A: Pure and Applied Optic*, Vol 4, 247 (2002)
35. P. Suresh kumar, Thoma Lee S, C. P. G. Vallabhan, V. P. N. Nampoori and P. Radhakrishnan, *Proc. SPIE*, 4903,307(2002)
36. P Suresh Kumar, Thomas Lee S, C P G Vallabhan, V P N Nampoori and P Radhakrishnan, *Optc. Comn.* , 214,25(2002).
37. B. Culshaw and J. P. Dakin, *Optical Fiber Sensors Vol.III*, Artech House, Boston (1996)
38. G. Keiser, *Optical Fiber Communications (II Ed.)* Mc-Graw Hill, Boston (2000).
39. Bishnu P Pal, *Fundamentals of Fiber Optics in Telecommunication and Sensor Systems*, New Age International, Newdelhi (2001).
40. Ajoy Ghatak and K Thyagarajan, *Introduction to Fiber Optics*, Cambridge University Press, UK (2002).
41. J. M. Senior *Optical Fiber Communications (II Ed.)* Prentice Hall India, New Delhi (2001)



Chapter 3

TRACE DETECTION OF CERTAIN WATER POLLUTANTS USING MICROBEND OPTICAL FIBERS

Intensity modulation induced by microbending in multimode fibers is considered as a transduction mechanism for detecting environmental changes such as pressure, temperature, acceleration, magnetic field and electric field. Permanently bent plastic fibers with cladding are found to be a possible substitute for unclad fiber in chemical sensing applications through absorption measurements. This chapter deals with the theory, design, fabrication and characterization of microbend EWFS and its application in water pollution monitoring. Two distinct detection schemes viz., bright-field detection and dark-field detection configurations have been used for the measurements. The performance of this class of sensors is compared with unclad EWFS and standard spectrophotometric method.

3.1. Introduction

Microbend losses have always been a curse to the cable designer, but the same microbend loss effect in optical fiber is effectively exploited by a microbend sensor designer for developing various types of sensors for the measurement of many physical variables [1-26] and in applications such as mode strippers, mode scramblers [27], mode filters, phase shifters [28-29], signal processing [30] etc. Sensors based on microbend loss in optical fiber was first proposed and demonstrated in 1980 and the early interest in these class of sensors was for acoustic and hydrophone applications [31-33]. Since that time, many research works have been conducted in this regard and microbend sensors have been adapted to many different measurement applications.

The significance of microbend sensors are due to their unique set of advantages in addition to the general advantages of fiber optic sensors as explained in chapter 1 and 2. Their unique features include [34]

1. Mechanical and optical efficiency that leads to low parts count and low cost.
2. Easy mechanical assembly that does not require fiber bonding to other components and thus avoids differential thermal expansion problems.
3. Fail-safe fiber sensor, which either produces a calibrated output signal or fails to a state of no light output.

In addition, microbend sensors have been used in hostile environmental applications such as in high temperature zones and explosion hazard areas.

Essentially, microbend sensors are based on coupling and leakage of modes propagating in a deformed fiber. The mechanical perturbation on a multimode fiber waveguide causes a redistribution of light power among many modes in the fiber. The more severe the mechanical perturbation or bending, the more light is coupled to the radiation modes and is lost. Thus, the important characteristics of a microbend fiber optic sensor are that it uses a multimode optical fiber, it is a light intensity sensor and the light intensity decreases with mechanical bending. Usually, the mechanical perturbation on a multimode fiber waveguide is achieved by employing corrugated

plates, which deforms the fiber into a series of sharp bends with small bending radii as shown in fig 3.1. Such periodic bending causes coupling of energy between various guided (core) modes as well as between guided modes and leaky modes (consists of both cladding and radiation modes); the latter causing a loss in transmission as shown in fig 3.2. By tuning the mechanical bend frequency, the microbending loss can be increased by orders of magnitude.

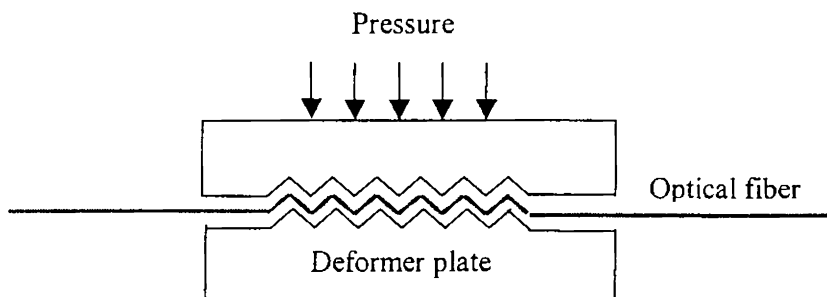


Figure 3.1. A multimode fiber placed in between two corrugated plates for producing microbends

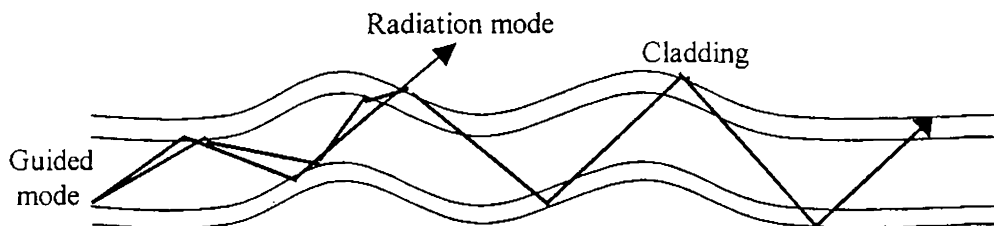


Figure3.2. Mode coupling in a periodic bent fiber

In most of the applications, the bends made on the fiber are temporary since the deformations made on the fiber will vanish if the pressure applied on the corrugated plates is removed, provided the pressure applied is within the elastic range of the fiber. However, a few investigations have been carried out with permanent microbend fibers also [35,36]. Nevertheless, these are essentially an extension of what is done with temporary microbend fibers and are mainly used for measuring physical parameters. Recently, it has been reported that when a permanently

microbend region of a multimode fiber is immersed in an absorbing medium, the optical power propagating through the fiber varies with the concentration of the absorbing species in the surrounding medium [37]. This sensor is sensitive enough to detect concentrations as low as nano moles/litre of a chemical species, with a dynamic range of more than six orders of magnitude. In this context, it would be interesting to examine the feasibility of employing such a permanently bent fiber for the development of different microbend sensors to detect various chemical species. This chapter describes the design and fabrication of a microbend fiber optic sensor for the trace detection of nitrite content in water. Two distinct detection schemes viz., bright-field detection and dark field detection configurations have been used for the measurements.

3.2. Theoretical background

The performance of microbend sensor can be characterized by both ray as well as wave approach of electromagnetic waves [38-45]. It is observed that both approaches agree with the results of the experimental studies. When a fiber is bent into a periodic series of bends having small radii, optical power transmitted through the fiber is coupled between the m^{th} and n^{th} mode so that the spatial frequency of the perturbation satisfies the condition [36]

$$\lambda = \frac{2\pi}{\beta_m - \beta_n} \quad (3.1)$$

where each mode has a propagation constant $\beta_m = n_1 k \cos(\theta_m)$ with θ_m representing the angle which the mode's equivalent ray makes with the axis of the fiber. If the core index is n_1 and the cladding index is n_2 , each guided mode has discrete propagation constant between $n_1 k$ and $n_2 k$. Energy coupled into a radiation mode, $\beta < n_2 k$, is lost. There are no modes with $\beta > n_1 k$, and there is a continuum of radiation modes with $\beta < n_2 k$. Furthermore, many degenerate modes exist; each m represents a group of modes with nearly identical propagation constant. The total

number M of such modal groups is not the same as the total number of guided modes. A general fiber will have power law refractive index profile as [38],

$$n^2(r) = n^2(0) \times \left[1 - 2\Delta \left(\frac{r}{a} \right)^\alpha \right] \quad (3.2)$$

where $\Delta = \frac{[n^2(0) - n^2(a)]}{2n^2(0)}$ (3.3)

Here $n(0)$, $n(r)$ and $n(a)$ are the refractive indices at distances 0 , r and a from the fiber axis, respectively, a is the core radius and α is a constant. Applying the WKB approximation to the solution of the dielectric waveguide problem, it can be shown that the distance in β space between adjacent guided modes is given by [34]

$$\beta_{m+1} - \beta_m = \frac{2}{a} \left(\frac{\alpha\Delta}{\alpha+2} \right)^{1/2} \left(\frac{m}{M} \right)^{(\alpha-2)/(\alpha+2)} \quad (3.4)$$

In the case of step index fiber where $\alpha = \infty$, the spacing is given by [36]

$$\beta_{m+1} - \beta_m = \frac{2\sqrt{\Delta}}{a} \frac{m}{M} \quad (3.5)$$

This means that the separation of modes in β space depends on the order of the modal groups m . In the case of graded-index fiber (parabolic) with $\alpha = 2$, the spacing is given by [36]

$$\beta_{m+1} - \beta_m = \frac{\sqrt{2\Delta}}{a} \quad (3.6)$$

Therefore, the distance between modal groups in β space is a constant. In other words, the modes are spaced evenly in β space. This means that one fixed spatial frequency of the microbends will transfer power back and forth between all pairs of adjacent modes. For the step index case, however, the spacing between the modes is independent of the mode index. A particular λ will couple light between one specific pair of modes. The total number of modal groups M can be determined by ascertaining how many modes will fit into the allowed β space ($n_2 k < \beta < n_1 k$),

and the number of modal group is related to the total number of modes by

$$N = M^2 \text{ (step index or graded index fiber)} \quad (3.7)$$

For the step index case, in theory, energy will be transferred back and forth in one specific mode pair. In practice, therefore, mode coupling is induced in the neighborhood of β space, and this region will be somewhat wider in the higher mode regime than among the lower order modes, whose spacing varies rapidly. As the number of modes in a step index fiber becomes larger, the mode spacing for the higher order modes varies much more slowly from mode to mode than for a step index fiber supporting small number of modes. For many mode step index fiber, the highest order modes are spaced at virtually identical intervals. In the case of a step index fiber, higher order modes having large m can be coupled with a small periodicity λ . The critical value of λ (λ_c) which is required for coupling of guided power to leakage power occurs when $m = M$ and can be found by equating (3.1) and (3.5) to obtain [38]

$$\lambda_c = \frac{\pi a}{\sqrt{\Delta}} = \frac{\sqrt{2\pi a n_0}}{NA} \quad (3.8)$$

However, for a parabolic index fiber the critical value of the periodicity λ is [38]

$$\lambda_c = \frac{\sqrt{2\pi a}}{\sqrt{\Delta}} = \frac{2\pi a n_0}{NA} \quad (3.9)$$

This implies that for a reasonable multimode fiber (N in thousands), the difference in microbend sensor sensitivity between step index and graded fibers will be small. The graded index fiber exhibits a resonant response whereas the step index fiber exhibits a threshold response for the detection of various physical variables. However, a graded index fiber will ultimately have a greater dynamic range, due to accessibility of the power from the lower-order modes, which can be coupled into higher modes by the same spatial bend frequency that causes the loss.

This approach of mode coupling between neighbouring modes is valid for small bending amplitudes only. However, for larger bending amplitudes, the guided power from even lower order modes can be coupled to leaky modes and back. Since the bending is periodic, this coupling from the core to the cladding modes is of oscillatory nature. The leaky modes thus generated consists of both cladding and radiation modes. The radiation modes escape out of the core and the cladding, whereas the cladding modes continue to propagate along the fiber. After the bent portion of the fiber, there is little power coupling between guided and unguided modes and they continue to propagate without much interaction. This power in the cladding modes can be measured by placing an index matching liquid over the cladding of the fiber just beyond the bent portion. Such a measurement scheme is termed as the dark field detection configuration. Likewise, the power carried by the core modes is determined in the bright field detection configuration.

3.3. Experimental

3.3.1. Preparation of Permanent Microbent Fiber

The deformer plates for making permanent microbends in fiber are made with highly tensile plastic material. The pitch of the corrugation is 1 mm and the total length of the plates used is 40 mm. A series of permanent microbends is introduced onto a 30 cm bare step index plastic fiber of core diameter 380 μm and numerical aperture 0.3, by placing the fiber in between a pair of deformer plates and applying moderately high pressures of a few atmospheres as shown in figure 3.1.

3.3.2. Experimental set-up

A schematic diagram of the experimental set-up for the detection of traces of nitrites in water using permanent microbend optical fiber as sensing element is shown in fig.3.3. The sensor cell design and the experimental set-up are the same as that explained in chapter 2 (figure2.3) for the detection of various pollutants in water, but the sensing element and the detection schemes are different. The experiments are carried out using a He-Ne laser emitting at 543.5nm as source because the absorption

peak of the resultant solution of the chemical reaction is around 545nm (figure 2.11).

Preparation of the test nitrite solution, reagents used and the chemistry involved are explained in detail in section 2.6.3 of chapter 2. When the microbend portion of the fiber is immersed in test water containing nitrite, the evanescent field penetrates into the liquid through the microbend region and interacts with it. Since the wavelength of light passing through the fiber is within the absorption band of the solution, evanescent wave absorption occurs and it increases with the increase in concentration of nitrite in water.

The optical fiber is introduced into the sensor cell through the holes provided at the sides so that most of the microbend region of the fiber is within the cell and remains straight as shown in figure 3.3. The light from the laser source is launched into one end of the fiber using a short focal length lens. The light emerging from the farther end of the fiber is fed to a light detector unit D_2 (Digital Power Meter 45-545, Metrologic make) that digitally displays the detected optical power (core mode intensity). To detect the power carried by the cladding modes, an index matching liquid is placed surrounding the bare optical fiber just beyond the sensing region. A part of the power leaked out through the index matching liquid is detected using the detector D_1 (Digital Power Meter 45-545, Metrologic make).

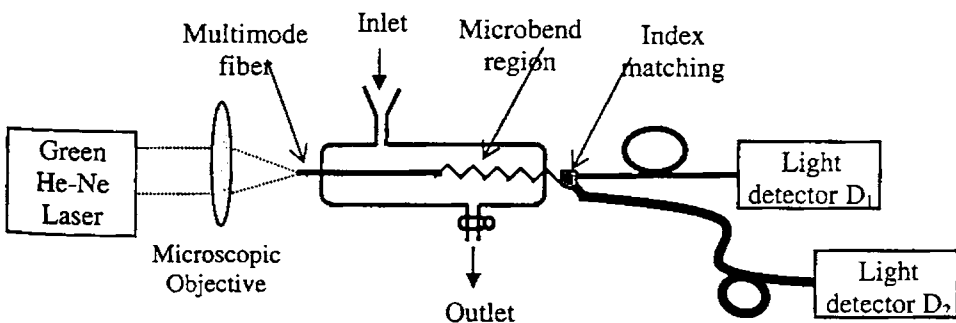


Figure3.3. Schematic diagram of the experimental setup

3.4. Results and Discussion

As explained, the measurements are carried out in two detection configurations. The first one is the bright field detection scheme in which the core mode intensity is measured by using the detector D_2 . Figure 3.4 shows the variation of core mode intensity from the microbend fiber as a function of logarithm of concentration of the nitrite content in water surrounding the bent portion of the optical fiber. From the plot, it is clear that the dynamic range of the present sensor is from 1ppb to 800ppb.

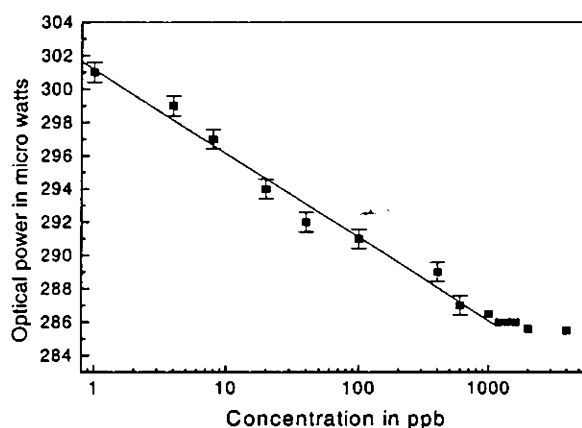


Figure 3.4. Variation of core mode power with different concentration of nitrite in water

The observed effect can be explained as follows [37,46,47]. It has been proven theoretically as well as experimentally that when periodic microbending is induced along the fiber axis, light power is coupled between modes. Conventional microbend sensors work on the principle that when a fiber is subjected to squeezing in between a pair of corrugated plates, a loss of transmitted intensity takes place by virtue of mode coupling between guided modes (core modes) and the leaky modes which consists of both cladding modes and radiation modes. Of these two, the radiation modes will leak out of the fiber into the surrounding medium whereas the

cladding modes will travel through the fiber. The performance of the present sensor is due to the absorption of evanescent waves, which penetrates out from the cladding to the surrounding medium. Therefore, the behavior of the present sensor is expected to be similar to that of an evanescent wave fiber optic sensor, which is usually fabricated by removing the cladding from a portion of the optical fiber.

The experimental observations confirm the fact that the bent portion of the fiber essentially behaves as an unclad region of a multimode fiber, which is conventionally used for evanescent wave spectroscopy. The conventionally used expression for evanescent wave spectroscopy is

$$P(l) = P_0 \exp(-\gamma Cl) \quad (3.10)$$

where $P(l)$ and P_0 are the power transmitted through the fiber with and without an absorbing liquid over the unclad portion respectively; C is the concentration of the absorbing species; l is the length of the sensing region and γ is the molar evanescent wave absorption coefficient which is given by, $\gamma = r_f \alpha_m$ (3.11)

where r_f is the effective fraction of the total guided power in the sensing region and α_m is the molar absorption coefficient of the absorbing species. However, the fraction r_f is different for different modal groups and the expression can be modified to better fit in with the experimental results as

$$P(l) = P_0 \left[\sum_i \exp(-\gamma_i Cl) \right] \quad (3.12)$$

where γ_i are the molar evanescent wave absorption coefficients of different modal groups in a multimode fiber having different penetration depths. However, the mode coupling process is a reversible phenomenon so that the power transferred to the cladding modes will again be coupled back to the core modes [48]. The radiation intensity thus coupled back will depend on the absorption of the medium surrounding the cladding. This recoupling of the cladding mode power is considered to be the

major contributing factor to the observed effect of variation of guided mode intensity with change in absorbance of the surrounding medium.

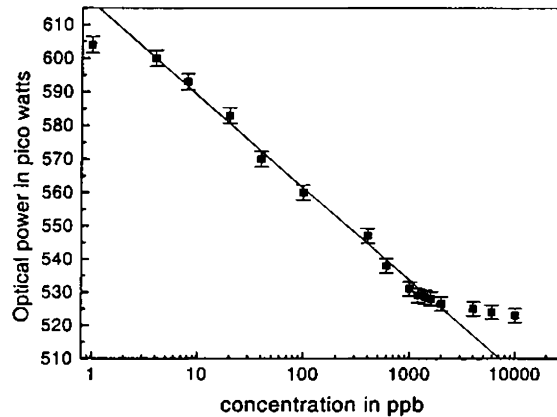


Figure 3.5. Variation of cladding mode power with different concentration of nitrite in water

It is noted that the amount of power recoupled from cladding modes to core modes need not be cent percent. Hence, beyond the sensing region some power will be transmitted through the fiber as cladding modes as well. The optical power present in such cladding modes will be inversely proportional to the amount of absorption in the microbent region. This variation of the cladding mode power with respect to the change in concentration of the absorbing medium surrounding the sensing (microbent) region is utilized in the second detection configuration called dark field detection scheme [37]. The variation of cladding mode power with different concentrations of nitrite obtained from detector D_1 is shown in figure 3.5. Here the dynamic range is from 1ppb to 3000ppb. A comparison of figures 3.4 and 3.5 shows that the dynamic range of the dark field detection scheme is higher than that of the bright field detection scheme.

A comparative study of different methods used for the detection of nitrite content in water is summarized in table 3.1. From the table it is clear that microbent fiber optic method is superior compared to conventional spectrophotometric method

and unclad EWFS in terms of the dynamic range and the length of the sensing region. The data corresponding to EWFS and spectrophotometric method are taken from chapter 2.

Sl no	Method		Lower detection limit	Dynamic range	Sensing Length
1	Spectrophotometric method		60ppb	60-1200ppb	
2	Laser based Microbend Fiber Optic Sensor	Core mode	1ppb	1-800ppb	4cm.
		Cladding mode	1ppb	1-3000ppb	
3	Laser based EWFS		1ppb	1-1000ppb	12cm.

Table 3.1 Comparison of different optical based sensing methods for measuring nitrites content in water.

References

1. Murtaza G, Jones S L and Senior J M, *Fiber and integrated optics* 20, 53 (2001)
2. Pierce SG, MacLean A and Culshaw B, *App. Opt.* 39, 4569 (2000)
3. Xie G P, Keey S L and Asundi A, *Optics And Lasers In Engineering*, 32, 437 (1999)
4. Donlagic D and Culshaw B, *Phys. Lett.* 76, 2331 (2000)
5. Donlagic D and Culshaw B, *J. Lightwave Tech* 17, 1856 (1999)
6. W C Michie, B Culshaw, I McKenzie, M Konstantakis, N B Graham, G Moran, F Santos, E Bergqvist and B Carlstrom, *Opt. Lett.* 20, 103 (1995)
7. A. MacLean, C. Moran, W. Johnstone, B. Culshaw, D. Marsh, V. Watson and G. Andrews, OFS 2000, 14th International Conference on Optical Fiber Sensors, 11-13 October 2000, Venice, Italy
8. Luo F, Liu J Y, Ma N B and Morse T F, *Sens. Act. A* , 75, 41 (1999)
9. Stolken J S and Evans A G, *Acta Materialia*, 46, 5109 (1998)
10. Yoshino T, Inoue K and Kobayashi, *IEE Proc.-Optoelectronics*, 144, 145 (1997)
11. Donlagic D and Zavrnsnik M, *Opt. Lett.* 22, 837 (1997)
12. Hastings M C, Chiu B and Nippa D W, *Nuclear Engineering And Design*, 167, 239 (1997)
13. Jones S L, Murtaza G, Senior J M and Haigh N, *Opt. Fib. Tech.* 4, 471 (1998)
14. Arya V, Murphy K A, Wang A B and Claus R O, *J. Lightwave Tech.* 13, 1998 (1995)
15. Suopajarvi P, Lyori V, Nissila S, Kopola H and Johansson R, *Indicating Opt. Engg.* 34, 2587 (1995)
16. Mccollum T, Spector G B, *Rev. Sci. Instru.* 65, 724 (1994)
17. Emge S R and Chen C L, *Array Sens. Act. B*, 3, 31 (1991)
18. Vengsarkar A M, Murphy K A, Tran T A and Claus R O J. *Acou. Soc. Am.* 88, 419 (1990)
19. Mavadat R, *Sens. Act.* 6, 289 (1984)
20. Diemeer M B J and Trommel E S, *Opt. Lett.* 9, 260 (1984)
21. Asawa C K, Yao S K, Stearns R C, Mota N L and Downs J W, *Elec. Lett.* 18, 362 (1982)
22. Lagakos N, Trott W J, Hickman T R, Cole J H and Bucaro J A *IEEE J. Quan. Elec.* 18, 1633 (1982)
23. N Chandrasekaran and Pradeep Kumar, *J. Instrum. Soc. India*, 30, 151 (2002)
24. W B Spillman Jr. and D H McMahon, *Appl. Phys. Lett.* 37, 145 (1980)
25. S T Shiue and T Y Shen, *Modelling and Simulation in Materials Science and Engineering*, 9, 207 (2001)
26. T G Giallorenzi, J A Bucaro, A Dandridge, G H Sigel, J H Cole, S C Rashleigh and R G Priest, *IEEE Trans. On Microwave Theory and Tech.* 30, 472 (1982)

27. Anderson B L and Qi Z, O Appl. Opt. 34, 8082 (1995)
28. Czaplak D S, Rashleigh S C, Taylor H F and Weller J F, J. Lightwave Tech., 4, 50 (1986)
29. A J Romano, J A Bucaro and J J Shirron, J. Lightwave. Tech. 14, 1992 (1996)
30. D Marcuse, Bell Syst. Tech. J. 51, 229(1972)
31. J N Fields and J H Cole, Appl. Opt. 19, 3265 (1980)
32. J N Fields et al., Acoust. Soc. Am. 67,816(1980)
33. N. Lagakos et al., Proc.CLEO'81. Vol.100, (1981)
34. J W Berthold III, IEEE J. Lightwave Tech. 13, 1193 (1995)
35. Jonathan D Weiss, J. Lightwave Tech. 7, 1308 (1989)
36. Betty Lise Anderson, Jill A Brosig, Opt. Engg, 34, 108 (1995)
37. Thomas Lee S, Nibu A George, P Sureshkumar, P Radhakrishnan, C P G Vallabhan and V P N Nampoorei Opt. Lett, 26, 1541 (2001)
38. Nicholas Lagakos, J H Cole and J A Bucaro, App. Opt. 26, 2171 (1987)
39. D Marcuse, Bell Syst. Tech. J. 51, 229(1972)
40. D Marcuse, Bell Syst. Tech. J. 51, 1199 (1972)
41. D Marcuse, Bell Syst. Tech. J. 52, 817 (1973)
42. D Marcuse, Bell Syst. Tech. J.52, 1423 (1973)
43. D Marcuse, Theory of dielectric optical waveguides, Academic Press, New York (1974)
44. D Marcuse, J. Opt. Soc. Am. 66, 216 (1976)
45. D Marcuse, J. Opt. Soc. Am. 66, 311 (1976)
46. Thomas Lee S, K Geetha, P Radhakrishnan, C P G Vallabhan and V P N Nampoorei Opt. Eng, 41, 3260 (2002).
47. Thomas Lee S, B Aneeshkumar, P Radhakrishnan, C P G Vallabhan and V P N Nampoorei Opt. Commun, 205, 253 (2002).
48. K Nakamura and T Yoshino, Light wave Technology, 15, 304 (1997)



Chapter 4

APPLICATION OF LONG PERIOD GRATING IN WATER POLLUTION MONITORING

Long period gratings (LPGs) are a relatively new class of fiber optic devices that act to couple light from the propagating fiber mode to cladding modes, producing a series of attenuation bands in the fiber transmission spectrum. The resonance wavelengths of the attenuation are sensitive to local environment experienced by the fiber. LPGs are normally fabricated in single mode fibers, but LPGs on multimode fibers also have some applications. This chapter presents the theory, design, fabrication and characterization of an optical fiber sensor based on evanescent wave absorption in LPG on multimode optical fiber for trace detection of chromium content in water. Moreover, a sensitive, reliable and compact fuel level indicator using LPG in multimode fiber, for detecting fuel levels in motor vehicles, is also included in this chapter

4.1. Introduction

The continuing growth of fiber optics can be attributed largely to the successful replacement of bulk optical components with equivalent fully integrated in-line fiber devices. The latest example is fiber gratings, which represent a dynamic new technology that has exploded out of the research environment vigorously into the commercial market. They present new and interesting solutions to some of the sticky problems inherent in fiber lasers, erbium doped fiber amplifiers (EDFA) and other components. In addition, fiber gratings represent innovative solutions to some filter and sensor issues, as well as providing interesting applications in WDM Add / Drop multiplexers (WADM).

Gratings, both amplitude and phase, are optical components which diffract a beam of light. Grating structures in optical fibers, resulting from self-organised refractive index was first fabricated by Hill and co-workers at the Communication Research Center in Canada in 1978 [1]. During the course of experiments on stimulated Brillouin scattering, they launched light from a single-frequency Argon laser at 488 nm into germania-doped core of a silica fiber. After several minutes, a substantial fraction of the input power was reflected as a result of the unexpected growth of a persistent refractive index grating in the fiber core, seeded by Fresnel reflection at the fiber end-face. Spectral measurements, done indirectly by strain and temperature tuning of the fiber grating, confirmed that a very narrow band Bragg grating filter had been formed over the entire 1m length of the fiber. This phenomenon subsequently called 'Hill grating' was an outgrowth of research on the nonlinear properties of germanium doped silica fiber. The problems encountered by Hill gratings such as fixed and narrow operating range was removed by the discovery of external writing or side writing technique by Meltz et.al. in 1989 [2].

Fiber gratings in general are classified into fiber bragg grating (FBG) or short period grating and long period grating (LPG) having typical grating period of $1 \mu\text{m}$ and $100 \mu\text{m}$ respectively. In an FBG, the diffracted light travels contra-directionally

to the light launched and in an LPG, the diffracted light is co-directional with the launched light.

The phenomenon that enables the fabrication of gratings is ultraviolet (UV) photosensitivity, in which the index of refraction of the germanium-silica core of an optical fiber is increased permanently through exposure to UV light, typically at around 248 nm. Changes in the index of refraction as high as 0.01 have been observed, although for most devices the changes used are 0.001 or less. The optical intensities needed for creating these effects are quite high. Typical sources are excimer lasers, frequency-doubled argon-ion lasers, or frequency-quadrupled Nd:YAG lasers.

4.2. Short Period Gratings

A fiber Bragg grating is a periodic variation of the refractive index of the fiber core along the length of the fiber. The principal property of FBG is that they reflect light in a narrow band width that is centered about the Bragg wavelength, λ_B , which is given by $\lambda_B = 2N_{eff} \Lambda$, where Λ is the spatial period (or pitch) of the periodic variation and N_{eff} is the effective refractive index for light propagating in a single mode, usually the fundamental mode of a monomode optical fiber. The transmitted and reflected signals in a fiber Bragg grating are schematically represented in figure 4.1. The refractive index variations are formed by exposure of the fiber core to an intense optical interference pattern of UV light. The capability of light to induce permanent refractive index changes in the core of an optical fiber has been named as photosensitivity.

When a single mode fiber is exposed to a pair of interfering UV beams as shown in figure 4.2, at the regions of constructive interference, the local refractive index increases whereas at the regions of destructive interference, there is no index change due to the negligible UV light intensity. Therefore, an exposure to an interference pattern will result in a periodic refractive index modulation along the

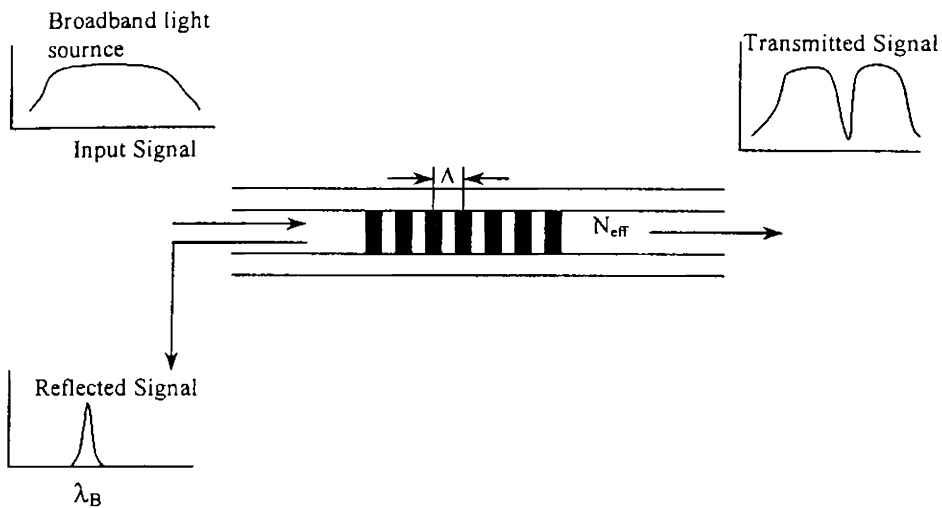


Figure 4.1. The transmitted and reflected signals in a fiber Bragg grating

between the interference fringes. When light is made to propagate through such a fiber with a periodically modulated refractive index, this periodic perturbation couples power mainly between two modes that satisfy the quasi phase matching condition. According to this if β_1 and β_2 are the propagation constants of two modes,

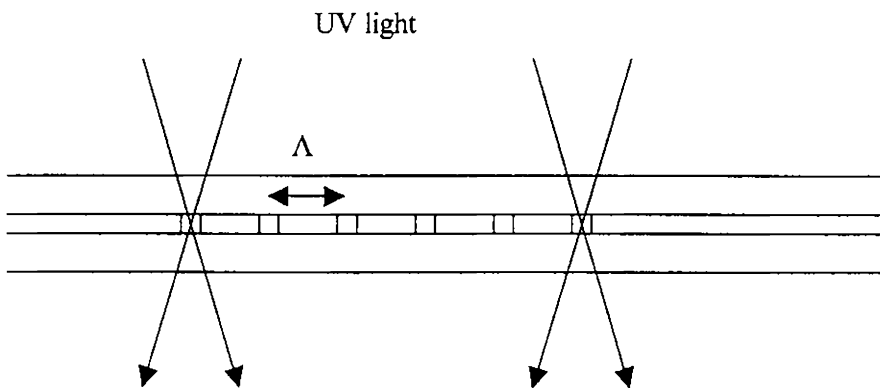


Figure 4.2. Interfering UV beams on a single mode fiber creates constructive and destructive interference

then a periodic perturbation with a period Λ will induce coupling between these modes [3] if,

$$\beta_1 - \beta_2 = K = \pm 2\pi/\Lambda \quad (4.1)$$

The propagating light beam is strongly coupled to the mode propagating in the backward direction at a certain wavelength satisfying the condition,

$$\beta_g - (-\beta_g) = K = 2\pi/\Lambda \quad (4.2)$$

where β_g and $-\beta_g$ are the propagation constants of the forward and backward propagating guided modes respectively. This condition is called Bragg condition.

If N_{eff} is the effective index of the mode, then

$$\beta_g = (2\pi/\lambda_B)N_{eff} \quad (4.3)$$

Substituting equation (4.3) to equation (4.2) yields

$$\lambda_B = 2\Lambda N_{eff} \quad (4.4)$$

which is the Bragg wavelength. In these types of gratings contra directional coupling takes place and have gratings periods of the order micrometer or less.

Physically, at each change in refractive index some light is reflected. If the reflections from points that are a spatial period apart are in phase, then at the Bragg wavelength, the various multiple reflections add in phase leading to a strong reflection. Thus, an FBG has the property that it can strongly reflect light at a design wavelength corresponding to a specific period of the grating and is transparent to other wavelengths. It is this interesting wavelength dependant characteristic of FBGs which is the basis for a number of technological applications in the area of optical fiber communications and sensor systems. FBGs are now commercially available and find applications as laser diode stabilizers [4], mode converters [5], fiber amplifiers, fiber lasers [6], band pass filters [7], add drop filters [8,9], dispersion compensators [10], optical sensors [11-20], etc.

4.3. Long Period Gratings

As discussed in the previous section, contradirectional coupling occur in short period grating and such gratings have periods of a micrometer or less. However, fiber gratings can also be used to couple light from one mode to another propagating mode along the same direction (co-directional coupling). In 1995, Vengsarkar *et al* [21] introduced this new type of fiber grating device, long period grating (LPG) to the optics community. LPG consists of a refractive index modulation in the core of optical fibers and this couples the guided core mode to the co-directional propagating cladding mode. The light in the cladding quickly decays due to losses at the cladding /air interface, leaving a series of attenuation bands or resonances in the guided mode as shown in figure 4.3 of the transmission spectrum of a typical LPG. A typical LPG has a period of hundreds of microns, a length of about 1-3cm and an index modulation depth of 10^{-4} or greater. It employs similar technology to that needed to produce the more widely used short period gratings.

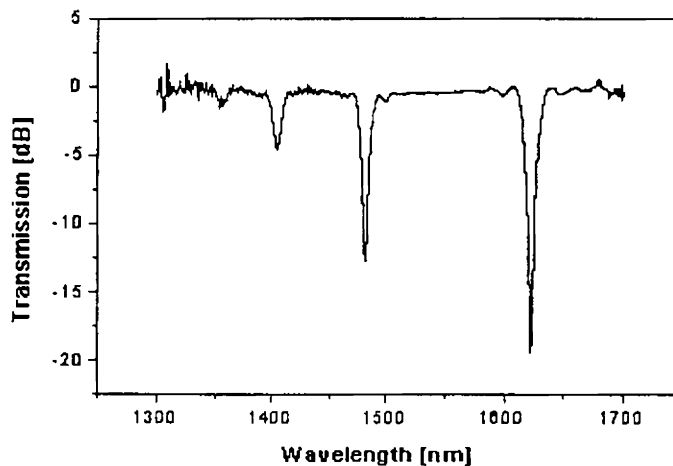


Figure 4.3. Transmission Spectrum of a typical LPG

If β_1 and β_2 are the propagation constants of the two forward propagating guided modes in a fiber that needs to couple, then the required grating period is obtained from the Bragg condition [3]

$$\beta_1 - \beta_2 = K = 2\pi/\Lambda \quad (4.5)$$

where Λ is the period spacing of the grating. If n_{e1} and n_{e2} are the effective indices of the modes, then

$$\Lambda = \lambda_0 / (n_{e1} - n_{e2}) \quad (4.6)$$

where $\beta_1 = 2\pi n_{e1} / \lambda_0$ and $\beta_2 = 2\pi n_{e2} / \lambda_0$. If we consider LP₀₁ and LP₁₁ modes or two orthogonally polarized modes of a birefringent fiber then, $(n_{e1} - n_{e2})_{\max} = \Delta n$, where Δn is the index difference between core and the cladding. Since Δn lies between 0.005- 0.01, the required period lies between 100 and 200 times the optical wavelength -ie, periodicities greater than 100 μm . Such gratings are referred to as long period gratings.

One of the interesting classes of long period gratings involves coupling from the guided LP₀₁ modes to the forward propagating cladding modes- ie, those modes that are guided by total internal reflection at the cladding-air interface. Such cladding modes are lossy due to the large scattering losses at the cladding-air interface as well as bends and other perturbations. Since the periodic coupling process is wavelength selective, this coupling acts as a wavelength selective loss element that is finding applications in many areas such as gain flatteners in erbium doped fiber amplifiers (EDFA), band rejection filters [21,22] optical sensors [23-30] etc.

4.4. Grating fabrication Techniques

Generally, fiber grating techniques can be classified into two categories, internal writing techniques and external or side writing techniques. In the first case, the exposing radiation is launched into one end of the fiber and guided by the core

internal writing technique, which includes the Hill gratings, Rocking filters and gain saturation gratings, the gratings are formed by two photon absorption resulting from the interference of two counter propagating beams in an optical fiber known as the self organized refractive index. The more versatile and widely used external writing techniques such as interferometric (Holographic), phase masks, amplitude masks and point-by-point technique employ external UV writing procedure by single-photon absorption.

4.4.1. Holographic Technique

Holographic technique, shown schematically in Figure 4.4, makes use of an external interferometric scheme similar to that used for holography. In this method, UV light from a laser is split into two making an angle 2θ and allowed to interfere to form a standing wave pattern of periodic spatial light intensity that writes a corresponding periodic index grating in the core of the fiber [31,32]. A cylindrical lens is used to expand the beam along the fiber length.

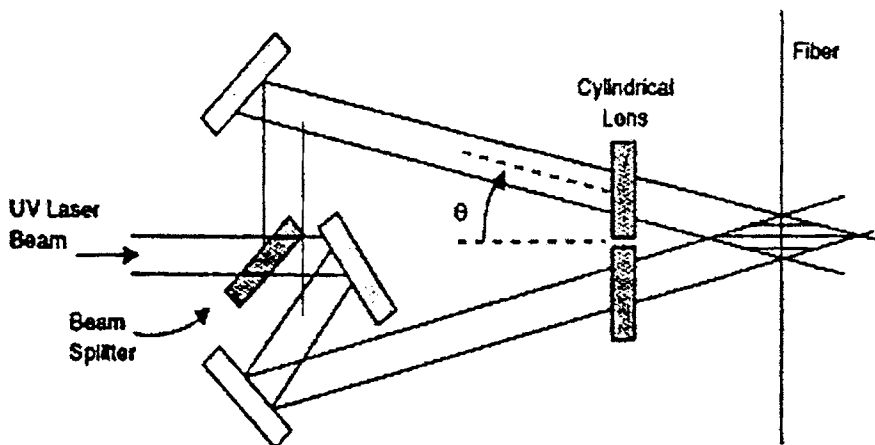


Figure 4.4. Schematic illustration of the dual-beam holographic technique.

The grating period Λ is related to the ultraviolet laser wavelength λ_{UV} and the angle 2θ made by the two interfering beams through the simple relation,

$$\Lambda = \frac{\lambda_{UV}}{2 \sin(\theta)} \quad (4.7)$$

The most important feature of the holographic technique is that the grating period Λ can be varied over a wide range by simply adjusting the angle θ . Moreover, the gratings formed are stable and remain unchanged even when the fiber is heated to 500°C. An inherent problem of this technique is that it requires an ultraviolet laser with excellent temporal and spatial coherence. Excimer lasers commonly used for the purpose have relatively poor beam quality and require special care to maintain the interference pattern over the fiber core over duration of several minutes.

4.4.2. Phase Mask Technique

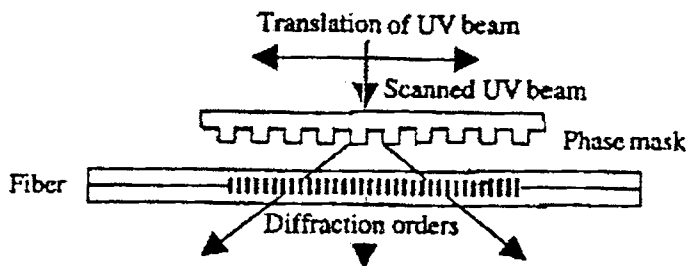


Figure 4.5. Schematic illustration of a phase mask interferometer used for making fiber gratings

This non-holographic technique uses a photolithographic process that is commonly employed for the fabrication of integrated electronic circuits. In this technique ultraviolet light, which is incident normal to a phase mask, is diffracted by its periodic corrugations [33,34]. The phase mask is made on a quartz substrate on which a patterned layer of chromium is deposited using electron-beam lithography in combination with reactive-ion etching. The shape of the periodic pattern approximates a square wave profile. The optical fiber is placed almost in contact with the corrugations of the phase mask as shown in the figure 4.5. When the ultraviolet laser beam falls normally on the phase mask, it is diffracted into several beams in the Raman-Nath scattering regime. The zeroth-order beam (direct transmission) is blocked or cancelled by an appropriate technique. The two first-order diffracted

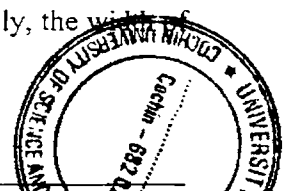
beams interfere on the fiber surface and form a periodic intensity pattern. The grating period is exactly one-half of the phase mask period.

The main advantage of the phase mask method is that it greatly simplifies the manufacturing process for Bragg gratings having high performance. Furthermore, the phase mask technique allows fabrication of fiber gratings with a variable period (chirped gratings) and can also be used to tailor the periodic index profile along the grating length. It is also possible to vary the Bragg wavelength over some range for a fixed mask periodicity by using a converging or diverging wavefront during the photolithographic process. On the other hand, the quality of fiber grating (length, uniformity, etc.) depends completely on the master phase mask, and all imperfections are reproduced precisely.

Long gratings can be formed by scanning the phase mask or by translating the optical fiber itself such that different parts of the optical fiber are exposed to the two interfering beams. In this way, multiple short gratings are formed in succession in the same fiber. Any discontinuity or overlap between the two neighbouring gratings, resulting from positional inaccuracies, leads to the so-called stitching errors (also called phase errors) that can affect the quality of the whole grating substantially if left uncontrolled.

4.4.3. Point-by-Point Fabrication Technique

This technique bypasses the need of a master phase mask and fabricates the grating directly on the fiber, period by period, by exposing short sections of the fiber to a single high-energy pulse. The fiber is translated by a distance before the next pulse arrives, resulting in a periodic index pattern such that only a fraction in each period has a higher refractive index [35,36]. The method is referred to as point-by-point fabrication since a grating is fabricated period by period even though the period Λ is typically below $1 \mu\text{m}$. The technique works by focusing the spot size of the ultraviolet laser beam so tightly that only a short section is exposed to it. Typically, the width of



the beam is chosen to be half of the period, although it could be a different fraction if so desired.

There are a few practical limitations of this technique. First, only short fiber gratings (< 1 cm) are typically produced because of the time-consuming nature of the point-to-point fabrication method. Second, it is hard to control the movement of a translation stage accurately enough to make this scheme practical for long gratings. Third, it is not easy to focus the laser beam to a small spot size that is only a fraction of the grating period. However, the main advantage of this technique is that the writing beam need not have a very high degree of coherence. Moreover, the point-by-point fabrication method is quite simple and suitable for long-period gratings in which the grating period exceeds tens of micrometers. Hence, in the present investigation this technique is employed for making LPGs on multimode fibers which are used for various sensor applications.

4.4.4. Amplitude mask technique

A simple and efficient way of fabricating LPGs is the amplitude mask technique where an amplitude mask with variable transmittance is used to modulate the UV light falling on the optical fiber. The variations in the mask include using photolithographic chromium-silica mask [21,22], etched dielectric mirrors [37], or microcontact [38] printing of the masks onto the fiber surface.

4.5. Fiber Grating Sensors

Fiber gratings, both short period and long period, provide innovative solutions to optical filters and to the development of various sensors. A number of chemical and physical parameters such as load, strain, temperature, pressure, acceleration, vibration etc. can be measured by using fiber grating sensors. In strain sensors the strain responses arises due to the physical elongation of the grating region (and corresponding fractional change in grating pitch) or change in fiber refractive index due to photo elastic effects. The thermal response arises due to the inherent thermal expansion of the fiber material and the temperature dependence of the refractive index.

4.6. LPG Sensor for Detecting Chemical Species

In recent years, there has been significant progress in the field of fiber optic sensors for the detection of various chemical species. Now they are extensively used for the measurement of the concentration of various chemicals in industrial and biomedical applications. Fiber optic chemical sensors have a number of advantages, which are explained in detail in chapters 1 and 2. Long period gratings (LPGs) are a relatively new class of fiber optic devices that act to couple light from the propagating fiber mode to cladding modes, producing a series of attenuation bands in the fiber transmission spectrum. The resonance wavelengths of the attenuation are sensitive to local environment experienced by the fiber.

LPGs are normally fabricated in single mode fibers but LPGs in multimode fibers also have some applications [39]. In this section the details of the design and fabrication of an optical fiber chemical sensor, based on evanescent wave absorption in long period grating (LPG) in multimode optical fibers, for the trace detection of chromium as well as nitrite content in water are described. In this technique, the long period grating fabricated on multimode plastic clad silica (PCS) fiber exhibits the same behavior as the microbend region of a microbend sensor described in chapter 3 (The theory of mode coupling [3], which is the basis of grating based sensors, is not discussed here). The detection limit of the sensor is a few parts per billion (ppb) and the operating range is more than 3 orders of magnitude. The sensing length of the sensing element is only 10mm, but the dynamic range is as good as that of the conventional unclad evanescent wave sensors or microbend sensors.

4.6.1. Experimental details

The reagents and chemistry used for the detection of nitrites and chromium content in water using EWFS as explained in chapter 2 are employed in the present case also and hence they are not mentioned here. Long periodic gratings are written on an unjacketed multimode, PCS fiber (200/380 μ m) by point by point method with UV irradiation (single shot 355nm) from a pulsed Nd – YAG laser (Spectra Physics

GCR-170) operated in the Q – switched mode. This LPG region, which has a length of 10mm and periodicity of 100 μ m, acts as the sensing region. Different types of experimental setups are used for the detection of nitrite and chromium. A laser based experimental set-up used for the detection of nitrites is shown in Figure 4.6, which is similar to that used in microbent chemical sensing [42]. The sensing element is introduced into a sensor cell made of cylindrical glass tube of 15cm length and 3cm diameter, through the holes provided at the sides so that grating region of the fiber is within the glass tube and remains straight. An intensity stabilized green Helium-Neon laser (JDS Uniphase) emitting at 543.5nm is coupled to one end of the fiber using a microscopic objective having the same numerical aperture. The light emerging from the farther end of the fiber is detected by two detectors D_1 (Newport 1815-C) and D_2 (Infos M-100), which independently measure core-mode and cladding-mode power. An index matching liquid placed in the sensing fiber just after the grating region taps the cladding mode power variation in the sensing region.

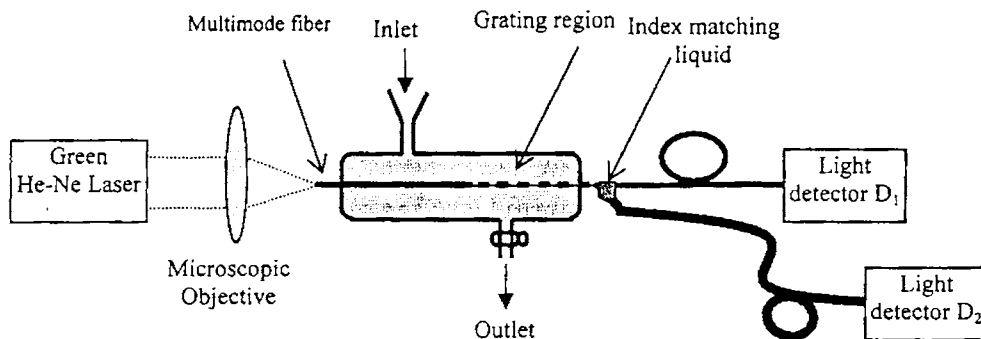


Figure 4.6. Experimental set-up for LPG based nitrite sensing

Figure 4.7 shows the schematic diagram of an LED based fiber optic sensor employed for the detection of chromium in water using LPG as the sensing element. The electronic part of the set up is almost the same as that used in LED based EWFS explained in chapter 2 for the detection of various pollutants like ammonia, nitrite, chromium, etc. in water. The multimode fiber with the LPG is placed in the sensing arm and an identical piece of fiber without LPG is placed in the reference arm. The square wave modulated light from a super bright green LED with a wide emission

band of about 80nm (full width at half height) and emitting at a peak wavelength of 558nm is simultaneously guided through the sensing and reference arm fibers. Outputs from the two arms are detected separately by identical PIN photo detectors (Light detector 1 and 2) and the detected signals are processed separately. Finally, the ratio detector gives the ratio of the two processed signals. Since the two arms are driven from a single source, any power supply fluctuations or ambient variations of the LED cause equal effects on the sensing and reference arm signals and hence these effects will be nullified at the divider output. Moreover, the light detectors 2 and 3 give the cladding mode and core mode power variations respectively. This double detection facility improves the reliability of the system. Normally the dynamic range obtained using the cladding mode power detector is large compared to core mode power detector [40] and hence the output of detector 2 is taken as the sensor arm output.

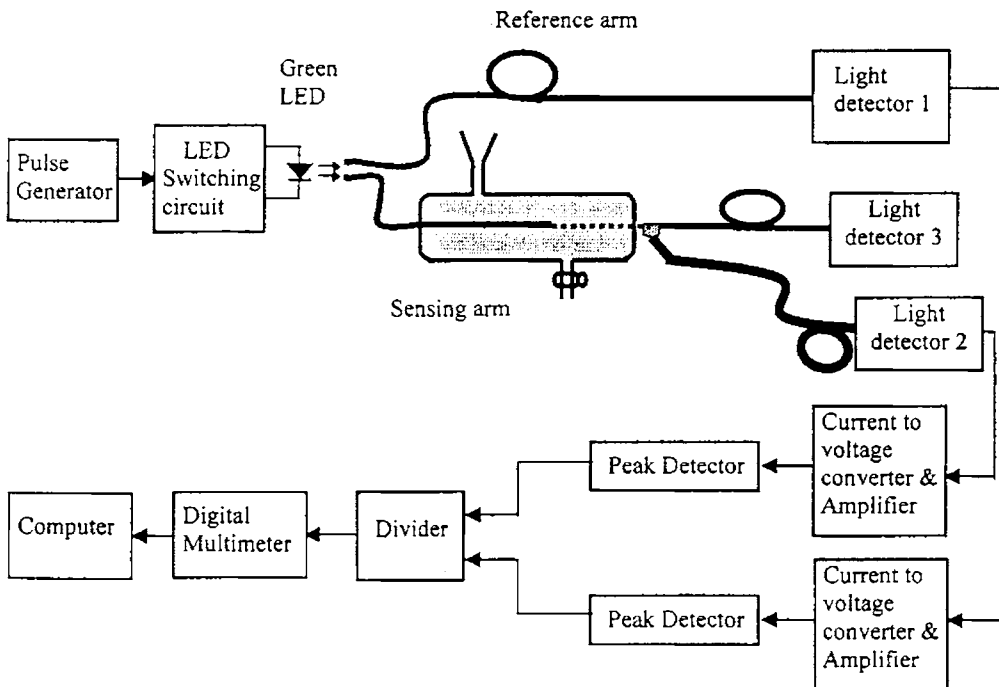


Figure 4.7. Experimental set-up for LPG based chromium sensing

4.6.2. Results and Discussion

The optical power transmitted through a fiber as core modes at a wavelength λ , gets coupled between core modes and cladding modes at the grating region and can be expressed as [26]

$$\lambda = (n_{\text{core}} - n_{\text{clad}})\Lambda \quad (4.8)$$

where Λ is the period of grating, n_{core} is the effective refractive index of the core modes and n_{clad} is the effective refractive index of the cladding modes. In single mode fibers, there exists only one core mode and many cladding modes, the core-cladding coupling occurs at certain specific wavelengths. However, in multimode fibers with large number of core modes, the core-cladding coupling occurs at all wavelengths. A schematic representation of the coupling between the core modes and cladding modes at a wavelength is shown in Figure 4.8. Hence, in chemical sensing applications of LPGs on multimode fibers, a part of the cladding mode power extends out of the cladding, as evanescent wave tail, and will be absorbed by an absorbing species that surrounds the cladding just like power coupling in the microbent region of a fiber optic microbent chemical sensor [40].

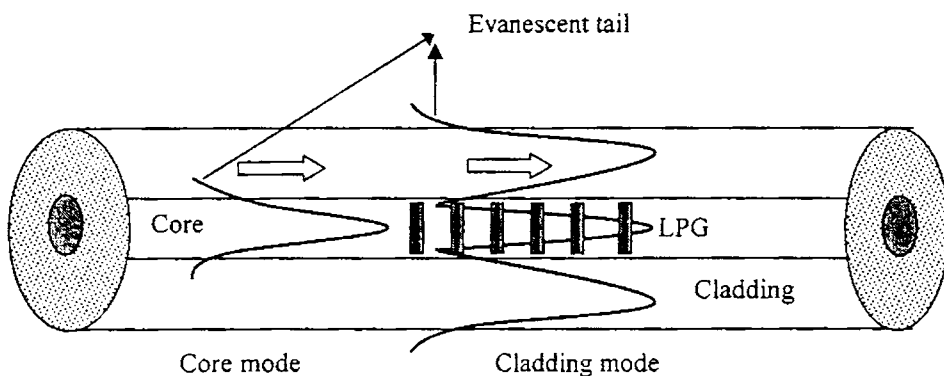


Figure 4.8. The core mode-cladding mode power coupling at the LPG region and the corresponding evanescent tail

The fundamental equation that deals with evanescent wave sensing by conventional unclad fiber when power is assumed to be distributed equally among all the modes is given by [41]

$$\frac{P_{out}}{P_{in}} = \frac{1}{N} \sum_{v=1}^N \exp(-\alpha \eta_v Cl) \quad (4.9)$$

where P_{out} is the output power, P_{in} is the input power of the fiber, N is the total number of modal groups where each value of N represents a group of modes having the same penetration depth, α is the molar absorption coefficient, η_v is the modal fractional power in the cladding for v^{th} core mode and l is the interaction length between the evanescent field and the absorbing species of concentration C . However, in the present case, for a particular operating wavelength, say 543 nm, all the core modes is not coupled to cladding modes, but coupling takes place only for those modes which satisfy equation 4.8. A part of this cladding power extends out of the cladding as evanescent tail, similar to the evanescent tail of core modes allowing the optical power to be absorbed by the absorbing chemical species that surrounds the cladding region. Such absorption reduces the cladding mode power which is similar to the phenomenon occur in microbend chemical sensing.

When the grating region of the fiber is immersed in the test solution of **nitrite**, the evanescent field penetrates into the liquid and interacts with it. Since the wavelength of light passing through the fiber is almost close to the absorption wavelength of the solution (540nm), evanescent wave absorption occurs and it increases with the increase in concentration of nitrite ion. Figure 4.9 shows the variation of cladding mode power obtained from detector 2 with concentration of nitrite surrounding the grating region of the fiber in the sensor cell. The curve clearly shows that the present instrument can measure even a fraction of a ppb, which is comparable with the existing detection limit of nitrites in water. In addition, the sensor responds in a logarithmic fashion, which enables the instrument to cover a large dynamic range varying from 1ppb to 1000ppb.

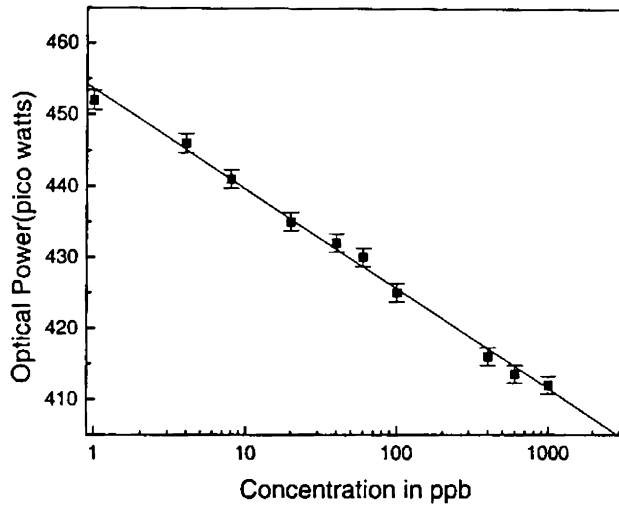


Figure 4.9. Variation of cladding mode optical power with respect to nitrite concentrations

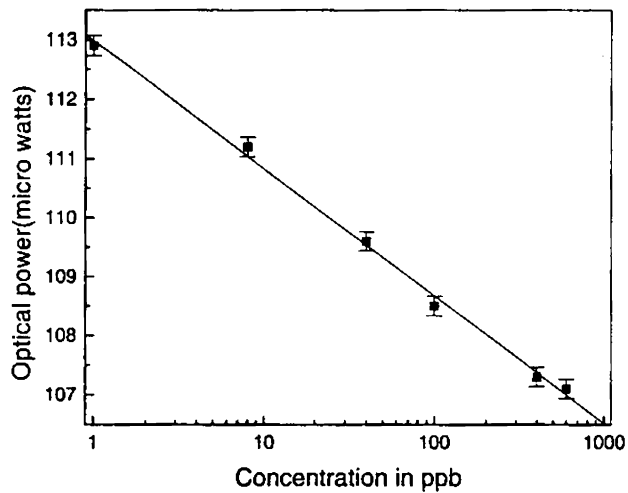


Figure 4.10. Variation of core mode power with respect to nitrite concentration

It may be noted that the index matching liquid has to be placed as close as possible to the grating region in order to have maximum cladding power. It is also observed that the core mode optical power variation obtained from detector 1 shows the similar behaviour as that of cladding mode power variation obtained from detector 2, but the dynamic range is less (figure 4.10). However, this double detection scheme proves the reliability and accuracy of the results.

In the case chromium detection, the peak detected signals corresponding to the sensing and reference arms are connected to the numerator and denominator inputs of the divider circuit respectively as shown in figure 4.7. Under idle condition (no samples in the sensing arm), the coupling between the LED and fibers are adjusted in such a way that almost equal amount of light passes through the sensing and reference arm fibers and the output is set to zero volts. During sample runs the output from the sensing arm decrease with increase in concentration of chromium due

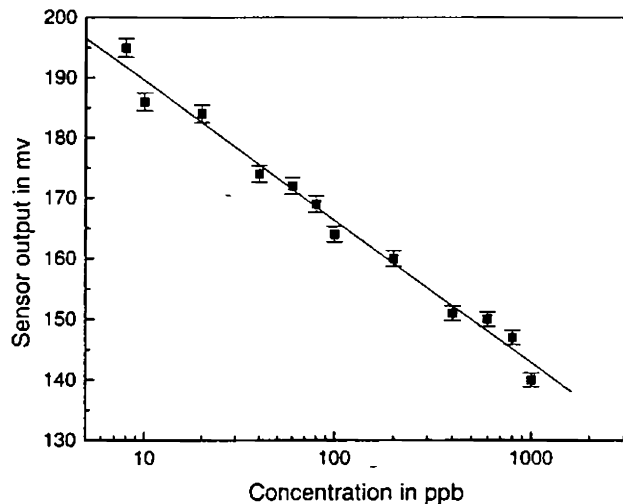


Figure 4.11. Variation of sensor output (cladding mode) with respect to chromium concentrations

to evanescent absorption in the grating region and hence the output of the divider decreases. Figure 4.11 shows the variation of output voltage(cladding mode) with various concentrations of chromium surrounding the grating region of the fiber in the sensor cell. The curve clearly shows that the present instrument can measure even a fraction of a ppb, which is comparable with the existing detection limit of chromium in water [42].

It is also observed that both nitrite and chromium sensors using LPG on a multimode fiber as sensing elements exhibits the same reversible nature as that of the corresponding conventional unclad EWFS discussed in chapter 2. That is, after removing each of the standard nitrite or chromium samples from the sensor cell, the signals came back almost to the initial values. This eliminates the difficulty of replacing the sensor arm fiber after each measurement

A comparative study of dynamic range, length of the sensing element, etc. of different fiber optic sensors for the trace detection of nitrite and chromium

Sl. No:	Sensing method		Dynamic range		Sensing length
			Nitrite sensor	Chromium sensor	
1	EWFS using unclad fiber		1-1000ppb (Laser Source)	10-2000ppb (LED source)	12cm
			4-1000ppb (LED Source)		
2	Microbend Sensor	Core mode	1-800ppb (Laser Source)		6cm
		Cladding mode	1-3000ppb (Laser Source)		
3	LPG Sensor	Core mode	1-600ppb (Laser Source)		1cm
		Cladding mode	1-1000ppb (Laser Source)	10-2000ppb (LED source)	

Table 4.1. Comparative study of different fiber optic sensors for the trace detection of nitrite and chromium contaminant in water

contaminant in water is shown in table 4.1. The data corresponding to EWFS and microbend sensors are taken from chapter 2 and 3 respectively. From the table it is clear that the length of the sensing region of the LPG sensors is only 10mm, but the dynamic range are as good as that of the conventional unclad evanescent wave sensors or microbend sensors.

4.7. Fuel level indicator using LPG in multimode optical fibers

Fuel level indicator is an essential requirement in all motor vehicles for knowing the volume of fuel in the fuel tank. Presently, wide range of techniques involving mechanical and electrical methods are being used for this proposes. Here, a fuel level sensor based on refractive index sensitivity of long period grating in multimode optical fiber is discussed. In the present sensor, the refractive index sensitivity of the LPGs is exploited to measure the length of the fiber immersed in petrol or diesel. A block schematic of the experimental set-up is shown in figure 4.12.

Long periodic gratings are written on an unjacketed multimode, PCS fiber (200/380 μm) at regular intervals (every one inch) by point-by-point method with UV irradiation (single shot 355nm) from a pulsed Nd – YAG laser (Spectra Physics GCR-170) operated in the Q – switched mode. Each LPG region has a length of 5mm and periodicity of 100 μm . The multimode fiber with the LPG acts as the sensing arm fiber. This is passed through the fuel container in such a way that the LPG written regions are within the container and an identical piece of fiber without LPGs is placed in the reference arm as shown in the figure. The square wave modulated light from a super bright green LED with a wide emission band of about 80nm (full width at half height) and emitting at a peak wavelength of 558nm is launched to the reference and sensing arm fibers. Outputs from the two arms are detected separately by identical PIN photo detectors (Light detector 1 and 2) and the detected signals are processed separately. Finally, the divider gives the ratio of the two processed signals. Since the two arms are driven from a single source, any power supply fluctuations or ambient

variations of the LED cause equal effects on the sensing and reference arm signals and hence these effects will be nullified at the divider output.

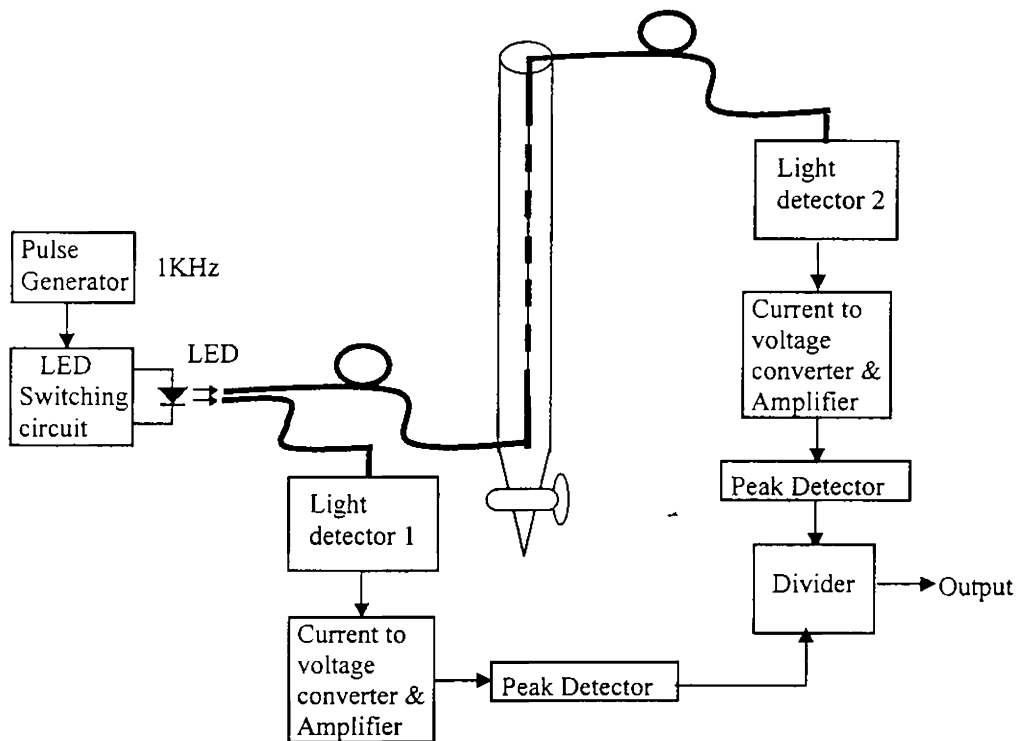


Figure 4.12. Block schematic of the Fuel level indicator using LPG in multimode optical fibers

The experiment is carried out by using petrol as the fuel. Figure 4.13 shows the variation of divider output voltage with fuel level variation for eight grating regions, each separated by one inch. In multimode fiber, the long period grating behaves like a microbend and coupling takes place between various guided modes as well as between guided modes and cladding modes. Hence, when a grating region is immersed in the fuel, its surrounding refractive index changes and hence light intensity at the output end of the sensing arm fiber changes just like immersing an unclad or micro bend region of a fiber in a liquid. When the fuel level increases, more and more grating regions are immersed and the output varies accordingly. It is observed that an LPG of length 10mm fully immersed in the fuel gives

approximately 8mV change in the output reading.

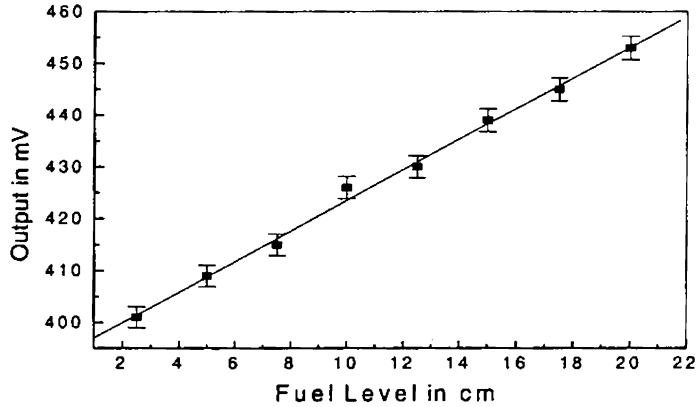


Figure 4.13. Variation of the output of the fuel level indicator with different fuel levels

Here, it is concluded that the present system is sensitive, reliable and compact. Moreover, due to the use of inexpensive opto-electronic components the cost of the system is very much reduced. The same system can also be modified for measuring refractive index and level sensing of various liquids.

References

1. K. O. Hill, Y. Fujii, D. C. Johnson and B. S. Kawasaki, *Appl. Phys. Lett.*, 32, 647 (1978)
2. G. Meltz, W. W. Morey and W. H. Glenn, *Opt. Lett.* 14, 823 (1989)
3. Ajoy Ghatak and K. Thyagarajan, *Introduction to fiber optics*, Cambridge University press, first south Asian edition (1999)
4. D. M. Bird, J. R. Armitage, R. Kashyap, R. M. A. Fatah and K. H. Kameron, *Electron. Lett.* 27, 1115 (1991)
5. F. Bilodeau, K. O. Hill, B. Malo, D. C. Johnson and I. M. Skinner, *Electron. Lett.* 27, 682 (1991)
6. G. A. Ball and W. W. Morey, *IEEE Photon. Technol. Lett.*, 3, 1077 (1991)
7. F. Bilodeau, K. O. Hill, B. Malo, D. C. Johnson and J. Albert, *IEEE. Photon. Technol. Lett.* 7, 388 (1995)
8. L. Dong, P. Hua, T. A. Birks, L. Reekie and Pt. S. J. Russell, *IEEE. Photon. Technol. Lett.* 8, 1656 (1996)
9. D. K. W. Lam and Garside, *Appl. Opt.* 20, 440 (1981)
10. K. O. Hill, B. Malo, F. Bilodeau, S. Theriault, D. C. Johnson and J. Albert, *Opt. Lett.*, 20, 1438 (1995)
11. X. M. Tao, L. Q. Tang, W. C. Du and L. C. Choy, *Composites Sci. Technol.*, 60, 657 (2000)
12. G. Duck and M. M. Ohn, *Opt. Lett.*, 25, 90 (2000)
13. N. Takashi, K. Yoshimura, S. Takashi and K. Imamura, *Ultrasonics*, 38, 581 (2000)
14. N. Takashi, K. Yoshimura, S. Takashi and K. Imamura, *IEICE Trans. Elect.* 82, 275 (2000)
15. X. W. Shu and D. X. Huang, *Opt. Comm.*, 171, 65 (1999)
16. A. I. Gusarov, F. Beghmans, O. Deparis, A. F. Fernandez, Y. Defosse, P. Megret, M. Decretton and M. Blondel, *IEEE Photon. Technol. Lett.*, 11, 1159 (1999)
17. L. Yu-Lung and C. Han-Sheng, *Meas. Sci. Technol.* 9, 1543 (1998)
18. N. Takashi, A. Hirose and S. Takashi, *Opt. Rev.*, 4, 691 (1997)
19. G. P. Brandy, K. Kalli, D. J. Webb, D. A. Jackson, L. Reekie and J. L. Archambault, *IEE, Proc.-Optoelectronics*, 144, 156 (1997)
20. A. M. Vengsarkar, J. A. Greene and K. A. Murphy, *Opt. Lett.*, 16, 1541 (1991)
21. A. M. Vengsarkar, P. J. Lemaire, J. B. Judkins, V. Bhatia, T. Erdogan and J. E. Sipe, *IEEE J. Lightwave Technol.*, 14, 58 (1996)
22. A. M. Vengsarkar, J. R. Pedrassani, J. B. Judkins, P. J. Lemaire, N. S. Bergano and C. R. Davidson, *Opt. Lett.*, 21, 336 (1996)
23. K. T. V. Grattan and T. Sun, *Sens. Act. A.* 82, 40 (2000)

24. A. D. Kersey, M. A. Davis, H. J. Patrick, M. LeBlanc, K. P. Koo, C. G. Askins, M. A. Putnam and E. J. Friebele, *IEEE J. Lightwave Technol.* 15, 1442 (1997)
25. K. O. Hill and G. Meltz, *IEEE J. Lightwave Technol.*, 15, 1263 (1997)
26. T. Erdogan, *IEEE J. Lightwave Technol.* 15, 1277 (1997)
27. V. Bhatia and A. M. Vengsarkar, *Opt. Lett.*, 21, 692 (1996)
28. V. Grubsky and J. Feiberg, *Opt. Lett.* 4, 203 (2000)
29. J. L. Archambault and S. G. Grubb, *IEEE J. Lightwave Technol.* 15, 1578 (1997)
30. H. J. Patrick, A. D. Kersey and F. Bucholtz, *IEEE J. Lightwave Technol.* 16, 1606 (1998)
31. M.M. Broer, R.L. Cone and J. R. Simson, *Opt. Lett.* 16, 1391(1991)
32. V. Mizrahi and J. E Spie, *IEEE J. Lightwave Technol.* 11, 1513 (1993)
33. H. J. Patric, C G Akins, R. W. McElhlon and E. J. Friebele, *Electrn. Lett.*, 33, 1167(1997)
34. J. A. Rogers, R. J. Jackman, C. G. Whitesides, J. L. Wagener and A. M. Vengsarkar, *Appl.Phys.Lett.*, 70, 7(1997)
35. V. Grubsky, A. Skorucak, D. S. Starodubov and J Feinberg, *IEEE Photonics Technol. Lett.* 11, 87(1999)
36. E. M. Dianov, D. S. Stardubov, S. A. Vasiliev, A. A. Frolov and O.I. Medvedkov, *Opt. Lett.* 22, 221(1997)
37. B. Malo, S Theriault, D. C. Johnson, F. Bilodeau, J. A Albet and K. O. Hill, *Electron.Lett.*, 31,223(1995)
38. J. Albert, K. O. Hill, B. Malo, S. Theriault, F. Bilodeau, D. C. Johnson and L. E Erickson, *Electron.Lett.*, 31,222(1995)
39. T Mizunami, T V Djambova, T Niiho and S. Guptha, *IEEE J. Ligtwave Technol*, 18 (2000) 230
40. Thomas Lee S, Nibu A George, P. Suresh Kumar, P. Radhakrishnan, V. P. N. Nampoori and C. P. G. Vallabhan, *Optics Letters*, 26, 1541 (2001)
41. O G Saracoglu and S Ozsoy, *Opt. Engg*, 41 (2002) 598
42. P. Suresh Kumar, P. Radhakrishnan, V. P. N. Nampoori and C. P. G. Vallabhan, *Proceedings of SPIE*, 5116, 348 (2003)



Chapter 5

FIBER OPTIC EVANESCENT WAVE SENSORS FOR AMMONIA GAS SENSING

This chapter describes the design, development and characterization of two different types of fiber optic sensors viz. unclad evanescent wave fiber optic sensor (EWFS) and long period grating (LPG) EWFS for the detection of toxic ammonia gas. Sol-gel technology is used in both the cases for immobilizing a reversible ammonia sensitive dye on the unclad or LPG region of the fiber. Ammonia gas permeating into the immobilized dye converts the color of the dye reversibly from yellow to blue with increasing concentration of ammonia gas. The concentration of ammonia gas can be determined by measuring the absorption at a given wavelength. The response time, recovery time, reusability etc of the developed sensors are also illustrated. The techniques described here are also relevant to the detection of a wide range of other gases.

5.1. Introduction

Ammonia plays an important role in atmospheric chemistry and gives rise to serious environmental problems. The excess presence of ammonia in the atmosphere causes direct and indirect damage to human being and to the ecosystems, the indirect effect being more serious and widespread than the direct effect [1]. Due to an increasing environmental awareness and stricter regulations for pollution control, on-line monitoring of ammonia gas has got wide-spread interest. Moreover, in industry, continuous ammonia measurement is desired in food and clinical analysis.

On-line determination of ammonia in gaseous or liquid state is often accomplished by potentiometric electrodes [2-4]. But this type of sensors have the disadvantages like (a) they do not lend themselves to miniaturization: (b) they are not easy to sterilize: (c) short life time: (d) their performance can be affected by surface potentials and results in signal drift: and (e) they require reference electrodes. Other class of ammonia sensing device is commercial infrared gas analyzers. The infrared devices, although quite sensitive, are nevertheless expensive and bulky.

Spectrophotometric methods of sensing chemical species are not a new technique. Spectrophotometers are used for the recognition of a wide range of chemical species from their characteristic absorption, fluorescence or Raman spectra. Optical gas sensing methods are essentially similar, but usually are more dedicated versions of such spectrophotometers. All are based on the irreversible change in color occurring as a result of a chemical reaction. These methods are suitable for the determination of total ammonia concentration, but frequently require separation of the analyte from the sample or masking of possible interferents. This makes the procedures time-consuming and complicated. Typical examples are the well known indophenol method, Nessler's method or the Berthelot reaction [5,6].

Most of these problems can be solved by using optical methods, ideally in combination with fiber optics. Most of the fiber optic gas sensors are based on simple absorption; although sensors based on Raman scattering mechanism or fluorescence

effect have been reported. The first description of an organic film-coated optical waveguide sensor for vapor detection was published by Hardy et al [7] in 1975. A picrate dye was used as the selective chemical indicator for cyanide vapors. Subsequently, David et al. [8] and Orofino et al. [9] described a similar device incorporating a ninhydrine-coated quartz rod that could detect ammonia vapor concentrations below 100 ppb. For both of these devices, however, the dye reactions are chemically irreversible and hence are of limited practical use. In 1983, Guiliani et al. [10] reported a reversible sensor for ammonia gas consisting of a 90mm long commercial soda-glass capillary tube coated with an oxazine perchlorate dye. However, the lowest detectable ammonia concentration reported was about 10ppm. After that, Beyler et al. reported a fiber optic sensor employing immobilization of ammonia sensitive dye on the fiber surface [11]. Nevertheless, this method appeared to have problems in achieving the necessary reversibility.

Porous glass optical fiber with an associated dye has also been used as a sensor for the detection of ammonia vapors at low concentrations [12]. The porous structure that remains after selective heat treatment, phase separation and chemical leaching of a borosilicate glass imparts a high surface area to the fiber core. Ammonia vapors permeating into the porous zone, which is pretreated with a reversible pH dye indicator, produce a spectral change in transmission. The resulting pH change is measured by in-line optical absorbance and is proportional to the ambient-ammonia concentration. Possible problems that could occur with this method include surface absorption, contamination etc.

A porous cellulose tape impregnated with a processing solution which changes color with ammonia gas has been used for ammonia gas sensing [13-15]. Nobuo Nakano et al. reported tape monitor based on the change in fluorescence intensity of a pH indicator (Eosine) put on the tape for the detection of ammonia gas in air [16]. Exposure of ammonia gas to the tape increases the pH of a solution existing in the tape. The resultant compound produced with ammonia gas shows an excitation maximum at 460nm and fluorescence maximum at 550nm. The degree of

the change in fluorescence intensity is proportional to the concentration of ammonia gas at a constant sampling time and flow rate. However, the sensitivity and precision of these methods should be significantly improved when measurements are made without removing the tape from the sampling chamber.

Another method for ammonia gas sensing is by using conducting polymers. They are a new class of sensing materials, which can be prepared by a simple oxidative polymerization method. They exhibit reversible pH-induced spectroscopic and gas induced conductivity changes. Conducting polymer gas sensors commonly rely on conductivity changes that occur when they are exposed to certain gases. The dc conductivity of a polypyrrole film decreases with increasing ammonia gas concentration and an ammonia gas sensor based on this property has been reported [17]. Similarly, the dc conductivity of polyaniline also depends on ammonia gas concentration. A polyaniline film containing nickel prepared by electrochemical oxidation could detect ammonia gas in the range 1-10000ppm at room temperature [18,19,20]. However, the response time of these sensors depends on temperature and heating is required to regenerate the sensor.

Within the last decade, sol-gel route opened up new possibilities for the fabrication of fiber optic sensors for different gases [21-30] and a wide variety of metal ions in solutions [31,32]. The sol-gel process is a liquid-phase method of preparing glasses and ceramics at ambient temperatures, by the hydrolysis and polymerisation of organic precursors followed by room temperature curing. Klein et al. reported a fibre optic evanescent wave integrated ammonia sensor using this technology [33]. The sensitive element of that sensor is a strip waveguide, fabricated by field-assisted ion exchange, coated with an immobilised indicator dye. However, the sensitivity of the sensor can be further improved by using optical fiber itself as the sensing element instead of glass slide and when multiple sol-gel coating are used at the sensing region instead of single coating [34] for immobilisation of the dye.

In the coming sections, we discuss two novel fiber optic sensors, viz. unclad fiber optic evanescent wave sensor (EWFS) and long period grating (LPG) EWFS, for ammonia gas detection that eliminate most of the difficulties and disadvantages of the above mentioned methods. In both these sensors, a part of the optical fibre itself is employed for making the sensing region and multilayer sol-gel coating is provided at the sensing region for immobilizing the ammonia sensitive dye, bromocresole purple, by dip coating method.

5.2. Sol-gel technology

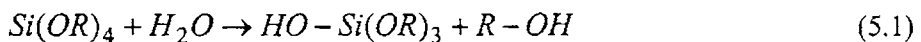
The sol-gel process is a well-known method for chemical synthesis and for the preparation of numerous ceramic and glassy materials. This method typically involves the hydrolysis and condensation of metal alkoxide precursors to form gels which are later densified at much lower temperatures than are required by conventional ceramic processing techniques [35]. The versatility of this process is evidenced from the silicate based systems, which have been developed into a wide variety of final products ranging from catalytic supports [36] and photochromic glasses [37] to planar waveguides[38] and fiber optic preforms[39]. The process can be tailored to yield materials of the desired composition and physical properties in the form of powders, fibers, thin films and monoliths [40]. One of the advantages of using sol-gel process is a high degree of purity and homogeneity due to mixing at near molecular levels. Moreover, due to the low processing temperatures, amorphous compositions, which are unstable if produced by melting, can be made by the sol-gel route.

By extending this concept to include organic compounds, which decompose at high temperatures, a completely new class of materials has emerged since the early 1980s [41-46]. These compounds can be dyes, biomolecules such as enzymes or monomers, which subsequently polymerize. The sol-gel derived xerogels doped with organic dyes have been extensively used in dye-based lasers [43], as structural probes [44] and as chemical sensors [45-46]. This type of glass can be porous, where the porosity and hence the refractive index can be controlled over a wide range by

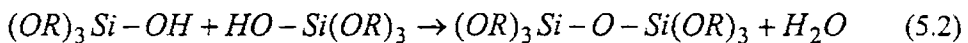
adjusting the fabrication conditions such as temperature or pressure. The inorganic gel is chemically and photochemically stable as compared with polymers and solvents. Since the gel can be easily formed into fibers and coatings, they can be coupled with optical fibers to form miniaturized sensors for on-line monitoring.

5.2.1. Sol-gel chemistry

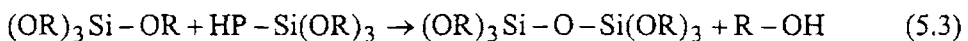
The main processes that involve in the sol-gel glass or ceramic production are hydrolysis and condensation of a metal alkoxide precursor (starting material). The precursor used in the present investigation is tetraethyl orthosilicate ($\text{Si}(\text{OR})_4$). The hydrolysis reaction proceeds through three steps, which are described by nucleophilic substitution [47,48]. In the first stage of hydrolysis, the nucleophilic attack of the positively charged metal atom results from its interaction with negatively charged oxygen atom that is associated with a water molecule and as a result, the coordination number of the metal atom increases. Subsequently, the transfer of a positively charged proton to a negatively charged OR group of the metallo-organic precursor occur and finally, the R-OH molecule is released as the product, completing the sequence of hydrolysis reaction. Equation 5.1 represents the hydrolysis reaction of the tetraethyl orthosilicate precursor.



The hydrolysis of a silicon alkoxide yields silanol groups (Si-OH) and ethanol. These silanols eventually undergo the condensation reaction, where, two partially hydrolysed molecules are linked together as shown in equations 5.2 and 5.3.



or



According to equation 5.2 and 5.3, an alcohol condensation may be responsible for the polymerization of hydroxylated groups, so that condensation by this mechanism results in the bridging of an oxygen atom between two silicon atoms. Once a hydrated metal group is formed, each of the above chemical equations are possible, and

therefore a competition between the hydrolysis and polycondensation reactions continues throughout the remainder of the sol-gel process [49].

5.2.2. Sol-gel coating methods

The most important application of sol-gel processing is for coating and thin films production such as electronic films, porous coatings, protective coatings and optical coatings [40,50]. The two widely practiced methods of sol-gel deposition are dip-coating and spin coating.

5.2.2.1. Dip-coating:

Dip coating is a simple way of depositing films onto a substrate such as small

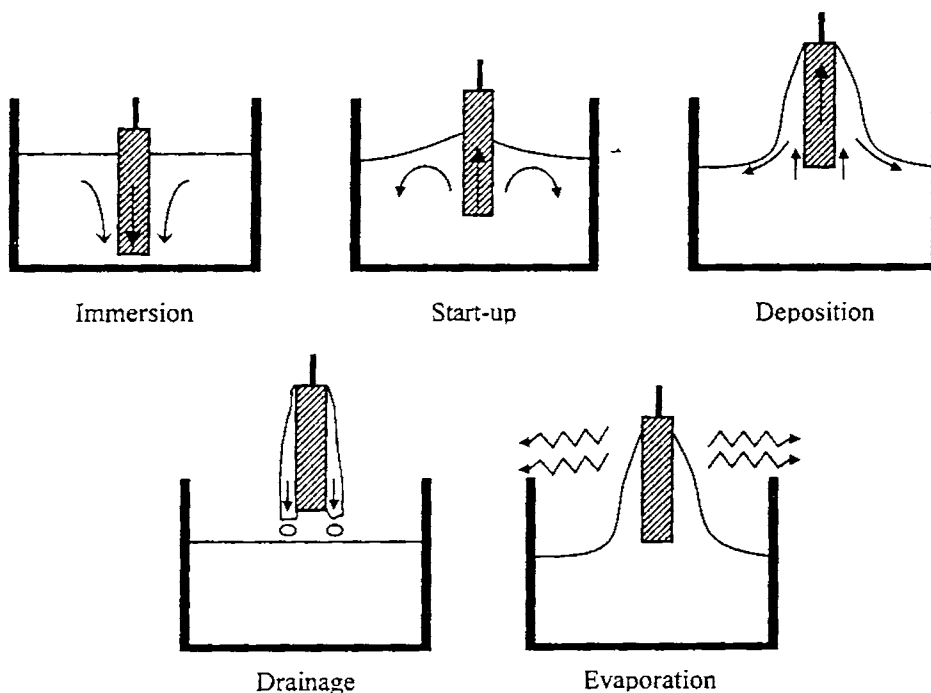


Figure 5.1: Stages of the dip coating process
slabs, cylinders etc. The processes involved in dip-coating method are immersion, start-up, deposition, drainage and evaporation, which are pictorially illustrated in figure 5.1. The thin film thickness, h is given by the relation [51]

$$h = \left[0.94 (\eta U_0)^{2/3} \right] / \left[\gamma_{LV}^{1/6} (\rho g)^{1/2} \right] \quad (5.4)$$

where η , U_0 , γ_{LV} , ρ and g are respectively the viscosity of the sol, substrate speed, sol-vapor surface tension, density of the sol and acceleration due to gravity.

5.2.2.2. Spin coating

Spin coating process is a more dynamic process than dip coating and is divided into four stages: deposition, spin-up, spin-off and evaporation as shown in figure 5.2. Deposition is the direct addition of the sol to the substrate surface, usually in excess of the actual coating amount. In the next stage, spin-up causes the excess liquid to flow radially outward, driven by centrifugal force. During spin-off stage, liquid flows to the perimeter of the substrate, eventually leaving as droplets. The uniform thin film thickness h is given by the formula [52]

$$h = h_0 / \left(1 + 4\rho\omega^2 h^2_{ot} / 3\eta\right)^{1/2} \quad (5.5)$$

where h_0 is the initial thickness, t is the time, and ω is the angular velocity. The main advantage of spin coating is the film uniformity due to balancing the induced centrifugal force (pushing outward) with the resistive viscosity force (pushing inward).

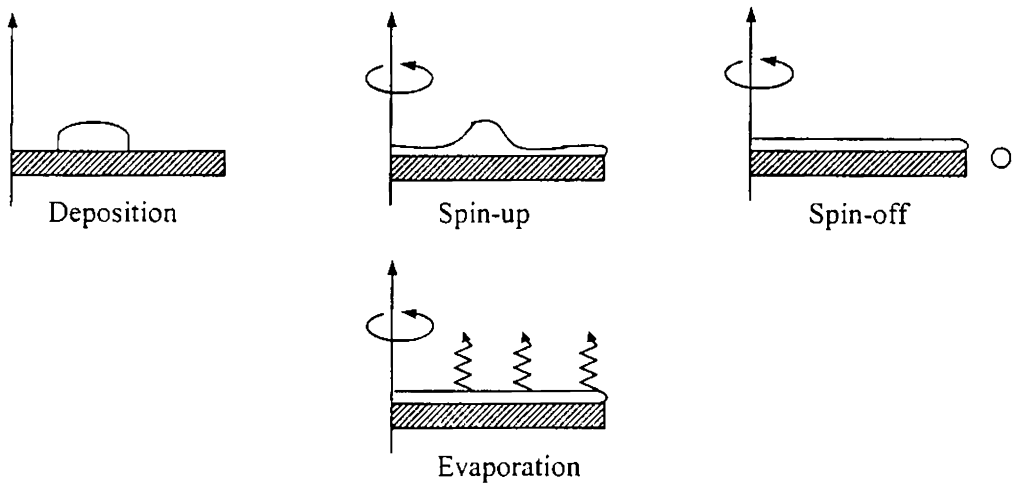


Figure: 5.2: Stages of spin coating process

5.2.3. Dye encapsulation in sol-gel matrix

As mentioned earlier, sol-gel process is a method that is used for the room temperature production of ceramics especially glass. This type of glass, viz. sol-gel glass can be porous, where the porosity and hence the refractive index can be controlled over a wide range by adjusting the fabrication conditions such as temperature or pressure. The sol-gel method is a convenient way to synthesise a host matrix for organic and organometallic dopants [53]. The organic dye to be encapsulated is added to the sol after partial hydrolysis of the precursor. As the degree of poly condensation increases, the sol becomes viscous and solidifies. The

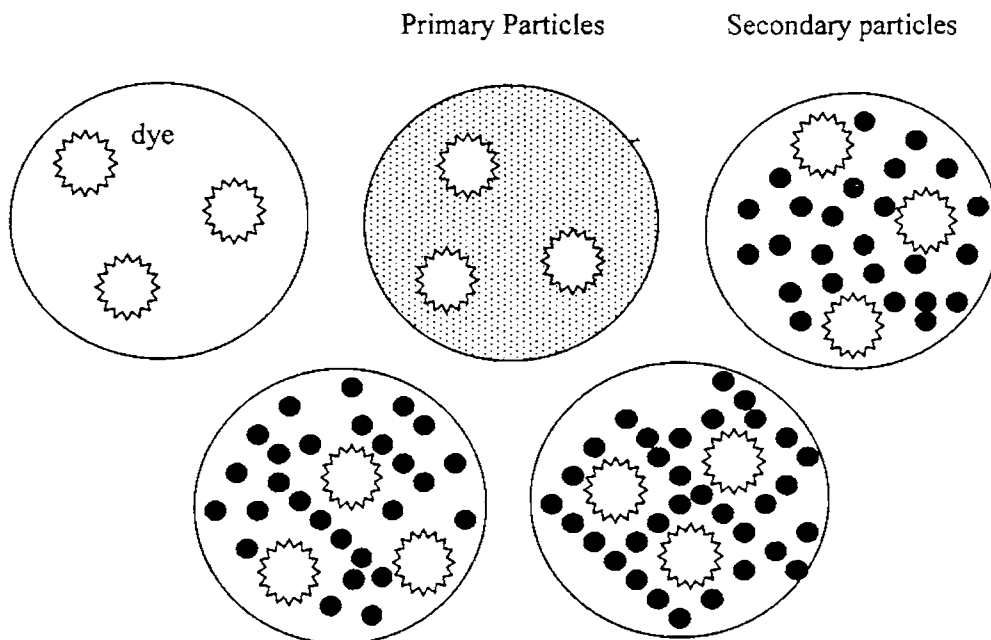


Figure 5.3: Dye encapsulation in sol-gel matrix

process continuous during aging and a porous matrix is formed around the dye molecule, trapping it inside. The large surface area and ultrafine pores of the gel make the dye accessible to small diffusing analyte species (ammonia in the present case), which react with the dye and change its optical properties. The rigid cage structure of the xerogel restricts translational motion of the dye molecules and in addition, dye aggregation is prevented as the individual dye molecules exist in separate cages [54]

as shown in figure 5.3. Entrapment of sol-gel matrices is independent of the functionalities of the dye. Moreover, physical entrapment is functionally non-invasive and preserves the integrity and directional homogeneity of the dye surface microstructure. Another notable property of these hybrid materials is its refractive index, which is specifically important in the development of optical waveguides. Generally, the refractive index of these composites is low because of the low density of the sol gel material. These features of the organically modified sol gel matrix enable this technology to be utilized for various fiber optic chemical sensing applications.

5.3. Unclad EWFS for Ammonia gas detection

5.3.1. Introduction

The advantages of sol gel derived thin films may be combined with those of optical fibers or waveguide to produce intrinsic evanescent wave sensors. As explained in chapter 2, when light is guided through an optical fiber, the evanescent field, which extends to the surrounding region decays exponentially with distance from the core-cladding interface. If the cladding of a certain region of the fiber is removed and that region is coated with an organic dye entrapped sol gel thin film, the degree of the evanescent wave interaction is dependant on the refractive index of the coating material. The evanescent wave – sol gel approach provides a very attractive route to chemical sensors, demanding only a simple dip coating of the required waveguide substrate. Because the interrogating light remains guided, no focusing or collection optics is required in the sensing region and considerable miniaturization is feasible. Furthermore, the versatility of the sol gel process enables the optimization of the sensor parameters viz. sensitivity, response time, signal to noise ratio etc. by the control of sol gel film properties such as coating length, thickness and porosity.

5.3.2. Experimental

5.3.2.1. Preparation of the sensing Element

A 35cm length of plastic clad silica fiber of 200 μ m core diameter and 0.22 numerical aperture is used for making the sensor element. The jacket and cladding of the fiber are removed from a length 8cm of the middle portion of the fiber. Then, the uncladded region is coated with porous SiO₂ matrix in which an ammonia sensitive dye is embedded by using sol gel technology.

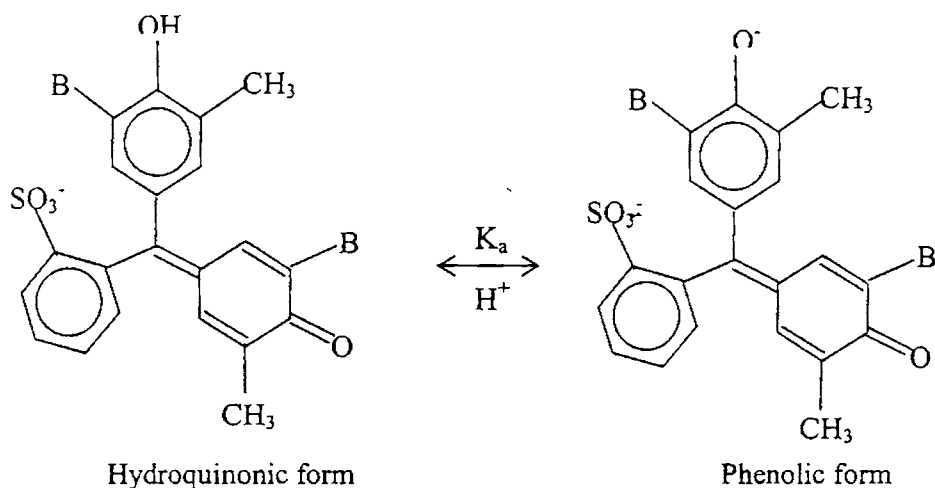


Figure 5.4. Equilibrium of two protonated forms of BCP

TEOS is used as the precursor for the sol preparation since the refractive index of the porous silica film produced is less than that of the fiber core. The ammonia sensitive dye used in the present case is bromocresol purple (BCP), which is chemically more stable and is more resistant to oxidation than other indicators. BCP exists in three different forms out of which two are important and are shown in figure 5.4. The phenolic form predominates in basic conditions, where as hydroquinonic form is dominant in low acid concentrations. A schematic diagram of the sol-gel technique for the fabrication of the sensitive layers on the middle unclad portion of the fiber is shown in the figure 5.5.

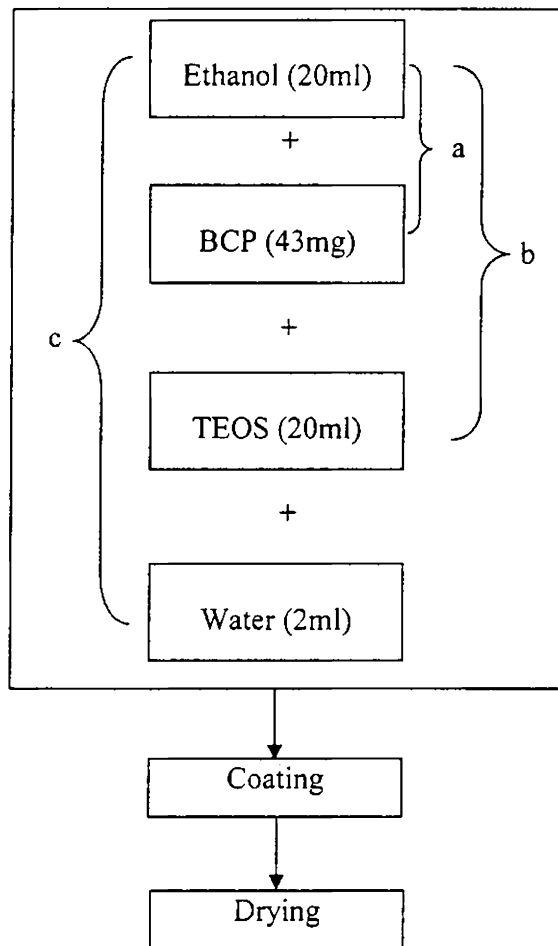


Figure 5.5: Schematic diagram of the sol gel technique for the deposition of sensitive layer.

a: stirred for 5 minutes: , b: stirred for 10 minutes: , c: stirred for 15 minutes:

TEOS, anhydrous ethanol, water and the indicator dye are mixed in the molar ratio $1:4:1:10^{-4}$ at room temperature with the help of a magnetic stirrer. Ethanol acts as a common solvent for TEOS and water. The porous silica is coated on the unclad portion of the fiber using the dip coating technique with the aid of a microprocessor controlled stepper motor. Since the drawing speed of the fiber from the sol is directly proportional to the thin film thickness, we use an optimum speed of 100mm/minute

and a thin film thickness of approximately 200nm for a single layer is obtained. Multilayer sol gel coating is used in the present investigation because multiple sol gel coating enhances the sensitivity of the sensor [34]. The second layer is coated over the first one only after the complete curing of the first one and the third layer is coated in the same fashion. A schematic representation of a two layer sol-gel coating on a multimode fiber is shown in figure 5.6. The coated fiber is then kept for two weeks so that the dye gets stabilized in the gel matrix. It is then washed in water to remove the excess and unbound dye. The fabricated sensitive layers proved to be resistant against dilute acids, alkaline solutions and organic solvents such as acetone or alcohol.

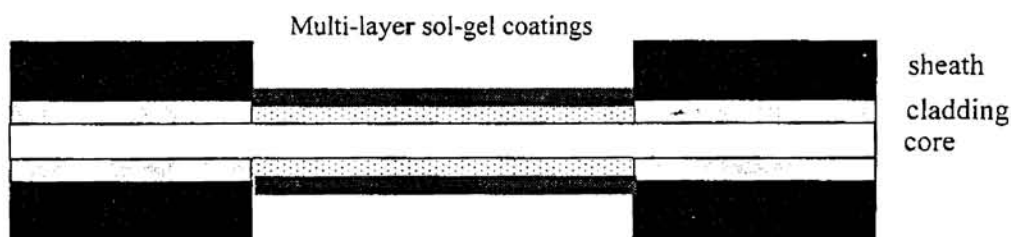


Figure 5.6. Two layer sol gel coatings on a multimode fiber

5.3.2.2. Optical arrangement for sensor characterization

A schematic diagram of the experimental set up used to characterize the ammonia gas sensor is shown in figure 5.7. The laser emission at 600nm from a diode laser is coupled to the optical fiber using a microscope objective having almost the same numerical aperture as that of the fiber. The light intensity at the output of the fiber is detected using an optical power meter (Metrologic 45-545), which in turn is interfaced to a computer. All the measurements are carried out using a Lab-VIEW set-up.

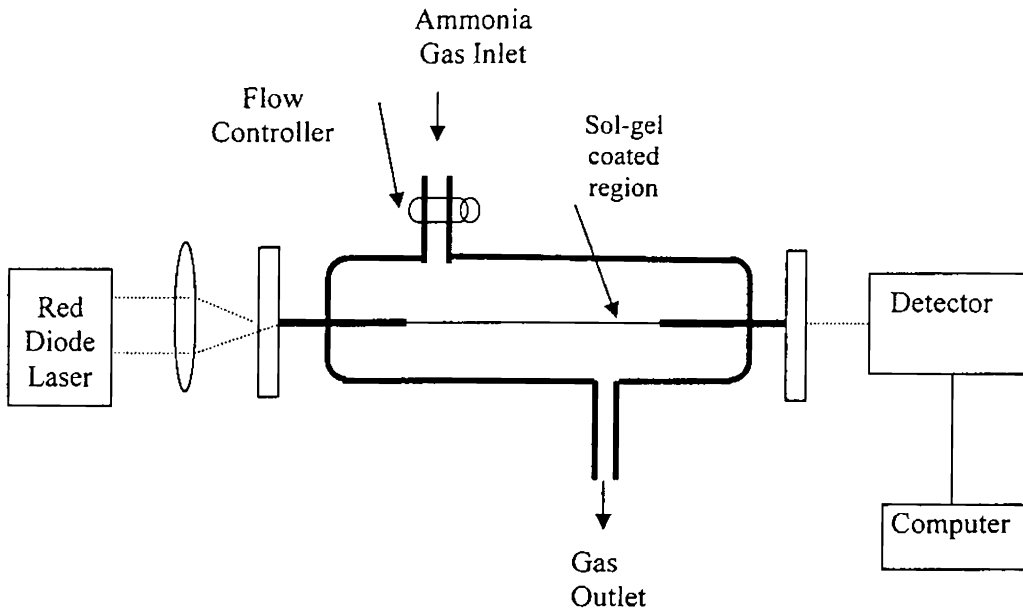


Figure 5.7: Schematic diagram of the experimental setup

5.3.3. Results and discussions

Figure 5.8 displays the absorption spectra of BCP dye doped in multi layer sol-gel thin film coated over a glass substrate under two different environments; before and just after ammonia gas exposure. During the exposure of ammonia gas, depending on the concentration of ammonia, the ammonia sensitive dye changes its colour from yellow to blue. The change in colour leads to an attenuation of the guided light at this wavelength or near to this wavelength. The maximum absorption peak is at 596nm and hence a diode laser emitting near this wavelength is used to power the present sensor.

Here also, the fundamental equation that deals with evanescent wave sensing by conventional unclad fiber is applicable. That is,

$$\frac{P_{out}}{P_{in}} = \frac{1}{N} \sum_{v=1}^N \exp(-\alpha \eta_v C l) \quad (5.6)$$

where P_{out} is the output power, P_{in} is the input power of the fiber, N is the total number of modal groups where each value of N represents a group of modes having the same penetration depth, α is the molar absorption coefficient, η_v is the modal fractional power in the cladding for v^{th} core mode and l is the interaction length of the evanescent field with the absorbing species of concentration C .

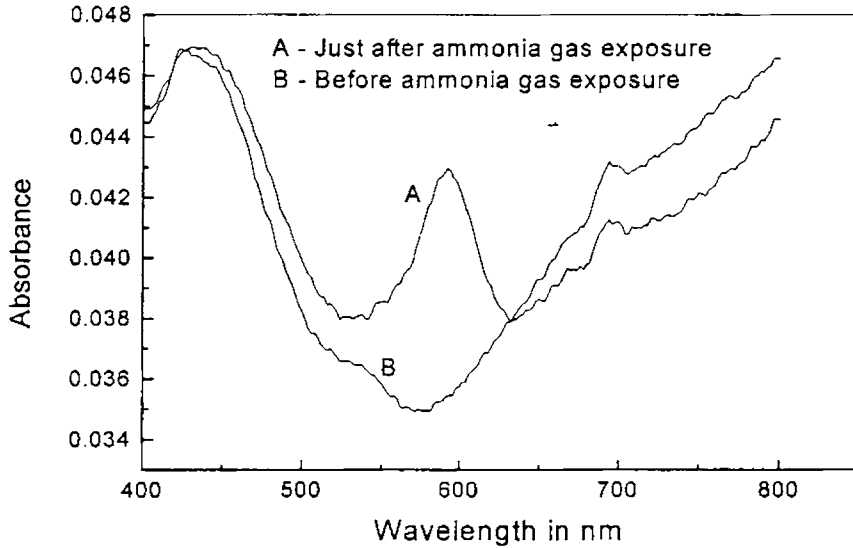


Figure 5.8: Absorption spectra of Bromocresol Purple entrapped in porous SiO₂ matrix

When light from red diode laser is launched into the fiber placed in the sensor cell, the evanescent wave penetrates into the surrounding medium (ammonia gas). Depending on the concentration of ammonia, the ammonia sensitive dye, BCP, entrapped in the multi layer sol-gel thin film on the fiber changes its color from yellow to blue and hence evanescent wave absorption increases at the operating

wavelength. The attenuation of the guided light due to the absorption of its evanescent part in the sensitive layers is pictorially illustrated in figure 5.9.

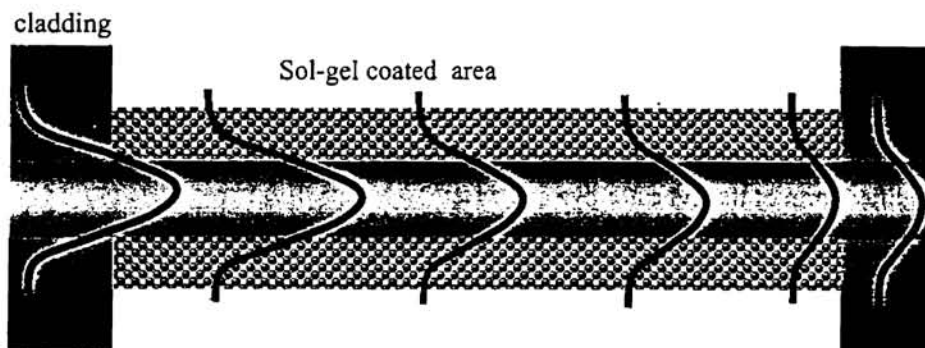


Figure 5.9: Light propagation through sol gel coated fiber

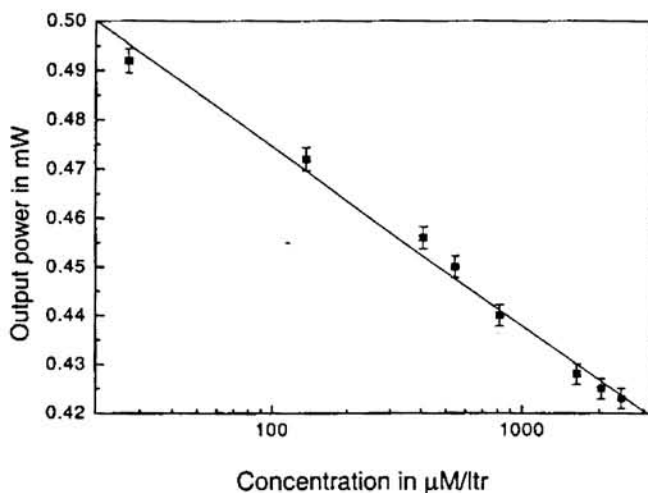
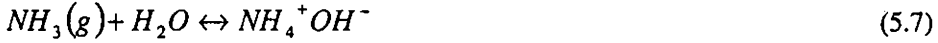


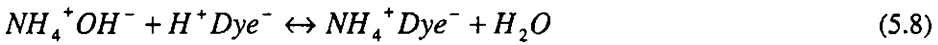
Figure 5.10. Variation of the ammonia sensor output with various concentrations of ammonia gas.

The variation of the sensor output with various concentrations of ammonia gas is shown in Figure 5.10. The curve clearly shows that the present instrument can

measure the ammonia concentration even from 0.027 to 2.04 mM/Ltr. The suggested reaction sequence of ammonia with the indicator dye is a reversible deprotonation of the dye [33]. The reaction can be divided into three steps. The first step is the reaction of gaseous ammonia with water to ammonia hydroxide



The second step is the deprotonation of the dye by ammonium hydroxide to a modified form of the indicator dye and water



The last step is the back reaction to the primary dye and ammonia

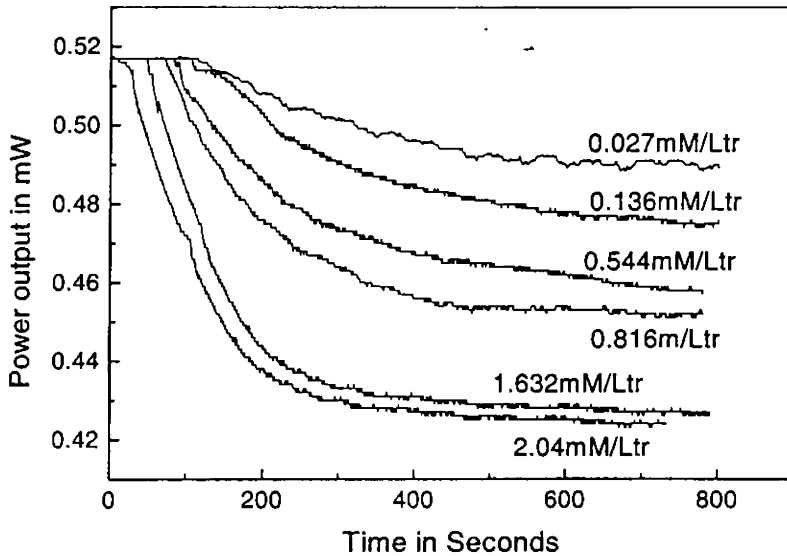


Figure 5.11. Response of the sensor element to different concentrations of ammonia gas

Figure 5.11 shows the response of the sensor element to different concentrations of ammonia gas recorded using Lab-VIEW. It is observed that during the ammonia flow

the sensor output decreases and after some time (approximately 3 minutes) it reaches a steady state value depending on the concentration of the ammonia gas. The reversible nature of the sensing element is also studied and is shown in figure 5.12. In this figure, the graph corresponding to each concentration of ammonia gas has three regions; A, B and C. A and C regions correspond to the sensor output before and after ammonia gas exposure whereas region B represents the sensor output during ammonia gas exposure. From the reversible response curve of the ammonia sensor it is seen that for each concentration of ammonia gas, the sensor output decreases from region A during ammonia gas exposure and reaches a steady state region B after a few minutes (approximately 8 minutes) [55]. Then, if we stop the ammonia flow the sensor output increases and reaches almost the starting region A, which is due to the reverse reaction of the indicator dye. This reversible nature of the sensing element eliminates the difficulty of replacing the sensing fiber after each measurement.

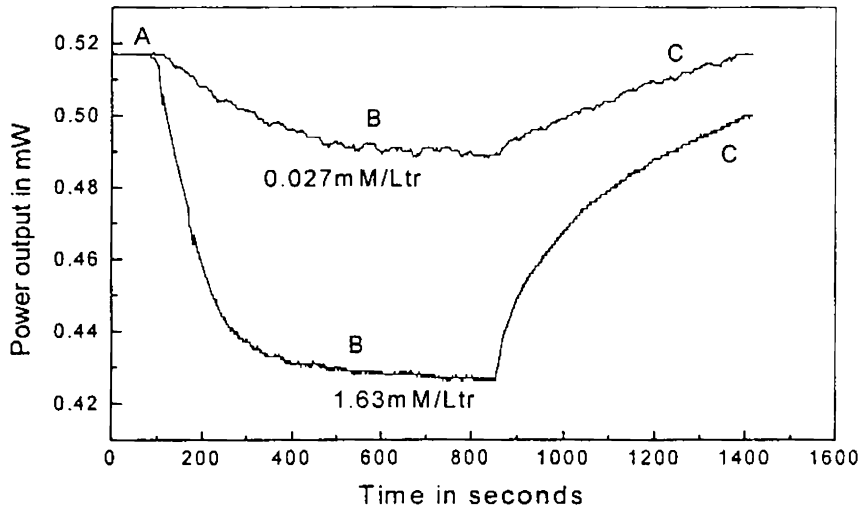


Figure 5.12. Reversible response of the ammonia sensor

5.4. LPG in multimode fiber for Ammonia gas detection

Long period gratings (LPGs) are a relatively new class of fiber optic devices that act to couple light from the propagating fiber mode to cladding modes, producing a series of attenuation bands in the fiber transmission spectrum. The resonance wavelengths of the attenuation are sensitive to local environment experienced by the fiber. Hence, in this section, the studies on the evanescent wave absorption on long period grating (LPG) in multimode optical fibers to detect ammonia gas is discussed. The theory, principle and fabrication of evanescent wave LPG sensors are explained in detail in chapter 4 and hence are not included here.

Long periodic gratings are written in an unjacketed multimode, PCS fiber (200/380 μm) by point-by-point method with UV irradiation (single shot 355nm) from a pulsed Nd – YAG laser (Spectra Physics GCR-170) operated in the Q – switched mode. This LPG region, which has a length of 10mm and periodicity of

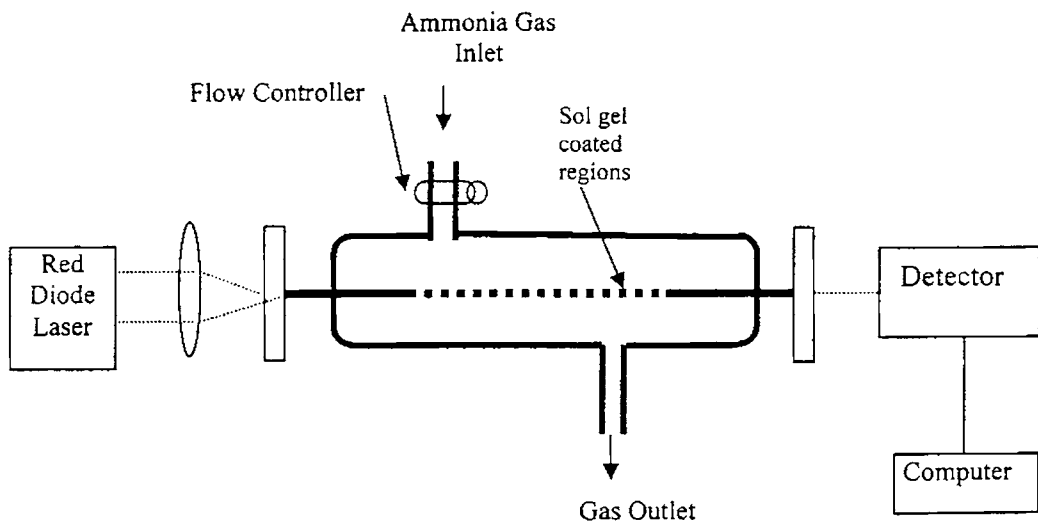


Figure 5.13: Schematic diagram of the experimental setup

100 μm , acts as the sensing region. This area is coated with layers of porous SiO_2 matrix in which an ammonia sensitive dye BCP is embedded by using sol-gel

technology as discussed in section 5.3.2.1. of this chapter. A schematic diagram of the experimental set up that is used to characterize the ammonia gas sensor is shown in figure 5.13, which is the same as Figure 5.7 except for the sensing fiber. The sensing element is introduced into the glass tube through the holes provided at the sides so that grating region of the fiber is within the glass tube and remains straight.

Just as in the case of unclad evanescent wave fiber optic ammonia gas sensor, light from a red diode laser is launched into the fiber placed in the sensor cell. The evanescent wave in the LPG region, penetrate the cladding and escapes into the surrounding medium (ammonia gas). The ammonia sensitive dye, BCP, entrapped in the multi-layer sol-gel thin film on the fiber reversibly changes its color from yellow to blue and hence evanescent wave absorption takes place which increases with increase in concentration of ammonia. Figure 5.14 shows the variation of the sensor output with various concentrations of ammonia gas. It is seen that the dynamic range

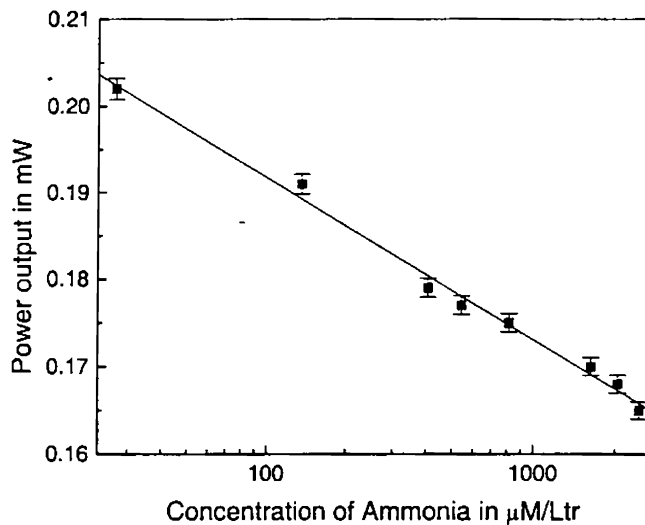


Figure 5.14. Response of the LPG ammonia sensor with different concentrations of ammonia gas

of the sensor is from 0.027 to 2.04 mM/Ltr, which is the same as that of unclad EWFS [56]. It is also observed that during the ammonia flow the sensor output decreases and after some time reaches a steady state value depending on the concentration of the ammonia gas. At this stage if the ammonia flow is stopped, the sensor output increases and reaches almost to the original value recorded before ammonia gas exposure. This reveals the reversibility of the sensor. The response time and the recovery time of this sensor are approximately 3 and 8 minutes respectively, which are same as that in the case of the unclad EWFS discussed in the previous section. However, the main attraction of the present sensor is that the sensing length is only 1 cm, which is very small compared with that of the conventional evanescent wave approach.

References

1. A. C. Stern, R. W. Boubel, C. B. Turner and D. L. Fox, *Fundamentals of Air Pollution*, Academic Press 1984
2. M. Maseini and C. Cremisini, *Anal. Chim. Acta* 92,277(1977).
3. W. N. Opdycke, S. J. Parks, and M. E. Meyerhoff, *Anal. Chim. Acta* 155,11(1983).
4. Y. Fraticelli and M. E. Meyerhoff *Anal. Chem.* 53, 992(19981).
5. I.L. Marr, *Environmental Chemical Analysis*, Intern. Text book Co., Glasgow, 1983.
6. R. Kummel and S. Papp, *Umweltchemie*, VEB DVG, Leipzig 1988.
7. E.E. Hardy, D.J. David, N.S. Kapani, and F.C. Unterleitner, *Nature* 257, 666 (1975).
8. D.J. David, M.C. Willson, and D.S Ruffin, *Anal. Lett.* 9,389 (1976).
9. T.A. Orofino, D.J. Dand, and E.E. Hardy, Forth joint conference on sensing environmental pollutants, New Orleans, La., 1977.
10. J.F. Giuliani, H. Wohltjen, and N.L. Jarvis, *Optics. Lett.* 8,1 (1983).
11. Beyler. L.L, Ferrara. J.A, MacCheeney. J.B, *Proc. Conf."OFS 88"*, New Orleans (1988)pp. 369-372.
12. M.R. Shahriari, Q. Zhou, and G.H. Sigel, *Optics. Lett.* 13,5 (1988).
13. N. Nakano, A. Yamamoto, Y. Kobayashi and K. Nagashima, *Analyst*, 118, 1539 (1993).
14. N. Nakano, A. Yamamoto, Y. Kobayashi and K. Nagashima, *Analyst*, 119, 2009 (1994).
15. T. Pal, A. Pal, G.H. Miller and T. Vo- Dinh, *Anal. Chim. Acta*, 263, 175 (1992)
16. N. Nobuo Nakano, Ken Sugata, and Kunio Nagashima, *Anal. Chim. Acta*, 302, 201 (1995).
17. M. Brie, R. Turcu, C. Neamtu, and S. Pruneanu, *Sens. Actuators B*, 37, 119 (1996)
18. S. A. Krutovertsev, S. I. Sorokin, A.V. Zorin, Y.A. Letuchy and O.Y. Antonova, *Sens. Actuators B*, 7, 492 (1992)
19. A. L Kukla, Y. M. Shirshov and S. A. Piletsky, *Sens. Actuators B*, 37, 135 (1996).
20. Zhe Jin, Yongxuan Su and Yixiang Duan, *Sens. Actuators B*, 72, 75 (2001).
21. B D MacCraith, V Ruddy, C Potter, B O' Kelly, J F McGlip, *Elect. Lett.* 22, 1247 (1991).
22. J Y Ding, M R Shahriari and C H Siger, *Jun. Elec. Lett.* 27, 1560 (1991).
23. C Gagnadre, M Billon, S Thuillier, *Elec. Lett.* 34, 1991 (1998)
24. C Gojon, B Durealt, N Hovanian and C Guizard, *Sens. Act. B*, 38-39, 154 (1997).
25. C A Browne, D H Tarrant, M S Olteanu, J W Muulens and E L Chronister, *Anal. Chem.* 68. 2289 (1996).

26. S McCulloch and D Uttamchandani, IEE Proc.-Sci.Meas. Technol. 144, 241 (1997).
27. A Lobnik and M Cajlakovic, Sens. Act. B, 3682, 1 (2000).
28. B D MacCraith, G O'Keefe, C McDonagh, A K McEvoy, J F McGilp, B O' Kelly, J D O'Mahony, M Cavanagh, Opt. Engg. 33, 3861 (1994).
29. M K Krihak and M R Shahriari, Elec. Lett. 32, 240 (1996).
30. A K McEvoy, C McDonagh, B D MacCraith, Analyst, 121, 785 (1996).
31. A Lobnik and O S Wolfbeis, Sens. Act. B, 51, 203 (1998).
32. O Lev, B I Kuyavskaya, Y Sacharov, C Rottman, Kuselman, D Anvir, M Ottolenghi, Proc. SPIE, 1716 (1982).
33. R Klein, E Voges, Sens. Act. B 11, 221 (1993).
34. S Thomas Lee, Jose Gin, V. P. N. Nampoori, C. P. G. Vallabhan, N. V. Unnikrishnan and P. R. Radhakrishnan, Pure and Appl. Optics A, 3, 355 (2001).
35. C. J. Brinker and G. W. Scherer, Solgel Science, Academic Press, New York, 1990.
36. S. Sakka, K. Aoki, H. Kozuka and J. Yamaguchi, J. Mat. Syt. Proc.,2,305(1994)
37. S. Sakka, K. Aoki, H. Kozuka and J. Yamaguchi, J.mater.sci., 28,4607(1993)
38. D. G. Chen, B. G. Potter and J. H. Simmmons, J. Non-Cryst. Solids, 178, 135(1994)
39. S. Shibata, J. Non-Cryst. Solids, 178, 272(1994)
40. L.C. Klein, Solgel Technology for Thin films , Fibers, Performs, Electronics and Specialty Shapes, Noyse, Park Ridge, N J, 1988.
41. D. Avnir, D. Levi and R. Reisfeld, J. Phys.Chem.,88,5956(1984)
42. D. Avnir, V. R. Kaufman and R. Reisfeld, J. Non-Cryst.Solids,74,395(1985)
43. R. Gvishi and R. Reisfld, J. Non-Cryst.Solids, 128,69(1991)
44. J. McKiernan, J. Pouxviel, B. Dunn and J. I. Zink, J. Phys. Chem.,93,2129(1989)
45. J. Y. Ding, M. R. Shahryari and G. H. Sigel, Electron. Lett., 27.1560(1991)
46. P. W. Wong and J. D. Mackenzie, MRS Symp. Proc.,346(1994)
47. J.Livage and c.Sanches, J. Non -Cryst. Solids, 145, 11(1992).
48. C.Sanches and F. Ribot, New J. Chem., 18,1007(1994)
49. R. I. Iller, The Chemistry of Silica, Willey, NewYork, 1979
50. L. C. Klain, Sol-gel Optics, Processing and applications, Kluwer Academic, Boston, MA, 1994
51. L. D. Landau and B.G. Levich, Acta. Physiochim. URSS, 17, 42(1942)
52. L.E. Scriven, Physics and applications of dip coating and spin coating, BetterCeramic through chemistry,111,Mater.Res.Soc.Pittsburg,PA,1988,717-729.
53. D. Mac Craith, G. O' Keeffe, c.McDonagh and A. K. McEvoy, El.Ltr,30,888(1994)

54. D. A. Avinir, V .R. Kaufman and R. Reisfeld, *J. Non-Cryst. Solids*, 74,395(1985).
55. Suresh Kumar, Abraham V. S, C P G Vallabhan, V P N Nampoori and P Radhakrishnan, *Proc. SPIE*, 5280-108(2003)
56. Suresh Kumar, Abraham V. S, C P G Vallabhan, V P N Nampoori and P Radhakrishnan, *Proc. SPIE*, 5279-61 (2003).



Chapter 6

CONCLUSIONS

Conclusions

Accurate measurement of chemical species in water as well as in air has acquired great practical significance because of the toxic effects these can cause to humans. Development of simple and sensitive, low cost, portable sensors capable of direct measurement of environmental pollution are of considerable interest in this context. Optical fiber technology offers several advantages for chemical sensing over conventional methods and hence it is worthwhile to investigate the feasibility of this method to the above problem of pollution monitoring. The present thesis gives a detailed account on the design, fabrication and implementation of various sensitive and low cost fiber optic sensors for the detection of certain environmental pollutants such as dissolved ammonia, nitrite and chromium in water as well as for the detection of ammonia gas in air. Variety of techniques such as evanescent waves, microbending and long period grating are employed for the design of various sensors developed. The sensors developed for the trace detection of water pollutants are highly sensitive and can measure the pollutants even from parts per billion ranges of concentration.

Design, development and fabrication of evanescent wave fiber optic sensors for the trace detection of certain dissolved pollutants in water such as ammonia, nitrite and chromium are discussed in chapter 2. A comparative study of the developed evanescent wave sensors has been carried out with the commonly used spectrophotometric method. According to drinking water standards of World Health Organisation, the maximum limit of chromium allowed in water is 50ppb and drinking water should be free of ammonia and nitrites. Experimental results reveal that spectrophotometric method has a lower detection limit of 800ppb, 60ppb and 200ppb respectively for ammonia, nitrite and chromium content in water, which are well above the permissible limit of these contaminants in water. The evanescent wave fiber optic sensors are highly sensitive in the lower ranges of concentration of the contaminants especially in the parts per billion ranges. The minimum detectable limit of these sensors using LED sources is 100ppb, 4ppb and 10ppb respectively for

ammonia, nitrite and chromium respectively. Another interesting feature of EWFS is its logarithmic response, which enables the sensor to provide a large dynamic range.

Both laser based and LED based sensors are developed. Eventhough the laser based sensor offers many advantages due to the unique properties of the laser source, LED based EWFS is found to be more useful due to several attractive features such as simplicity, compactness, low cost nature as well as the use of the inexpensive electronic and optoelectronic components in the sensor. Moreover, in order to eliminate undue signals at the sensor output due to power supply variations, thermal noise of the source especially from LEDs, etc., all developed LED based sensors use reference fiber. In addition to all these factors, the Lab VIEW based measurement at the detection side enhances the accuracy and reliability of the data acquisition. The developed sensor can also be used to measure many other contaminants in water by simply replacing the LEDs in accordance with the absorption spectra of the selected species. In conclusion, the developed evanescent wave sensors show superior performance in terms of lower detection limits of the contaminants in water, dynamic range, size, cost, etc. compared to commonly used spectrophotometric method. Moreover, EWFS is highly sensitive in the lower ranges of concentration of the contaminants in water and hence suited for monitoring drinking water quality.

Normally, the water near to fertilizer plants and industries are highly polluted and contains various types of pollutants. Hence, for the trace detection of these pollutants simultaneously, an LED based EWFS is developed, which detect pollutants such as nitrites and chromium. Moreover, with slight modifications in the LEDs switching side and detector part of the electronic circuits, these devices can be used for the simultaneous measurement of many contaminants in water

In normal optical fiber applications, microbends cause undesirable effects such as signal degradation, signal loss, etc., but the same microbend is effectively utilized in the design of fiber optic microbend chemical sensors for the trace detection of pollutants in water, which is explained in chapter 3. Two distinct detection

schemes, core mode detection and cladding mode detection are employed in these types of sensors and they provide more reliable and accurate measurements. The fiber used in these sensors is low cost plastic fiber, which reduces the system cost considerably. Moreover, the sensitivity and dynamic range of the developed sensor is better than that of unclad EWFS.

The very recent development of UV written fiber grating has resulted in a variety of important technological advances in the field of fiber optic sensors. Long period gratings (LPGs) are a relatively new class of fiber optic devices that act to couple light from the propagating fiber mode to cladding modes, producing a series of attenuation bands in the fiber transmission spectrum. The resonance wavelengths of attenuation are sensitive to local environment surrounding the fiber grating. Hence, it is worthwhile to apply this technology in chemical sensing applications such as pollution monitoring, etc. In chapter 4, the design, performance and characterization of a sensitive evanescent wave chemical sensor by creating long period grating on a multimode step index fiber is discussed. A comparative study with a conventional unclad EWFS reveals that the length of the sensing element is only 10mm, but the dynamic range is as good as that of a conventional unclad evanescent wave sensor with a sensing length of 120mm. Moreover, the double detection scheme, core mode detection and cladding mode detection, of the sensor enables more reliable and accurate measurements. A fuel level sensor based on refractive index sensitivity of long periodic grating in multimode optical fiber is also constructed, which is sensitive, reliable and compact. Moreover, due to the use of inexpensive optoelectronic components the cost of the system is very much reduced. The same system can also be used for measuring refractive index and level sensing of various liquids.

The design, development and characterization of two different types of fiber optic sensors, based on unclad evanescent wave fiber optic sensor (EWFS) and long period grating (LPG) EWFS, for the detection of toxic ammonia gas are explained in chapter 5. Sol-gel technology is used in both these cases for

6905

immobilizing a reversible ammonia sensitive dye on the unclad or LPG region of the fiber. The concentration of ammonia gas can be determined by measuring the absorption at a given wavelength. The developed sensors are very sensitive and can measure even trace amounts of ammonia gas. The dynamic range of the sensors is from 0.027 to 2.04 mM/Ltr. Moreover, the sensing element of both the sensors shows reversible nature, which eliminates the difficulty of replacing the sensing fiber after each measurement. The response time and the recovery time of both the sensor are approximately 3 and 8 minutes respectively. However, the main attraction of the LPG based sensor is that the sensing length is only 1cm, which is very small compared with that of the conventional evanescent wave approach. In conclusion, both the sensors are reversible and have good dynamic range and fast response. The techniques described are also relevant to the detection of a wide range of other gases.

Suggestions for future studies

With the advancement in microelectronic and optoelectronic industry, the sensors presented in the thesis can convert to more compact and portable form. With the utilization of microcontrollers, the sensors developed for simultaneous detection of nitrite and chromium content in water can be modified to a fully automated system for the simultaneous detection of several contaminants. Moreover, distributed sensing strategy of optical fibers can be incorporated in the multi contaminant detection scheme, which will reduce the cost and size of the sensor considerably.

The sensors developed for ammonia gas detection, employed laser as the source of radiation. But these sensors can be developed into a more compact and cost effective form by the usage of super-bright LEDs. Moreover, the same technique can be extended for the detection of other toxic gases in air by employing proper dyes.

